Science
AAAS

Supplementary Materials for

Pathogen-sugar interactions revealed by universal saturation transfer analysis

Charles J. Buchanan *et al*.

Corresponding authors: James H. Naismith, naismith@strubi.ox.ac.uk; Andrew J. Baldwin, andrew.baldwin@chem.ox.ac.uk; Benjamin G. Davis, ben.davis@rfi.ac.uk

Science **377**, eabm3125 (2022)
DOI: 10.1126/science.abm3125

The PDF file includes:

Other Supplementary Material for this manuscript includes the following:

Supplementary Methods

*Synthesis of 9-BPC-6'-Sialyllactose (**6**).*

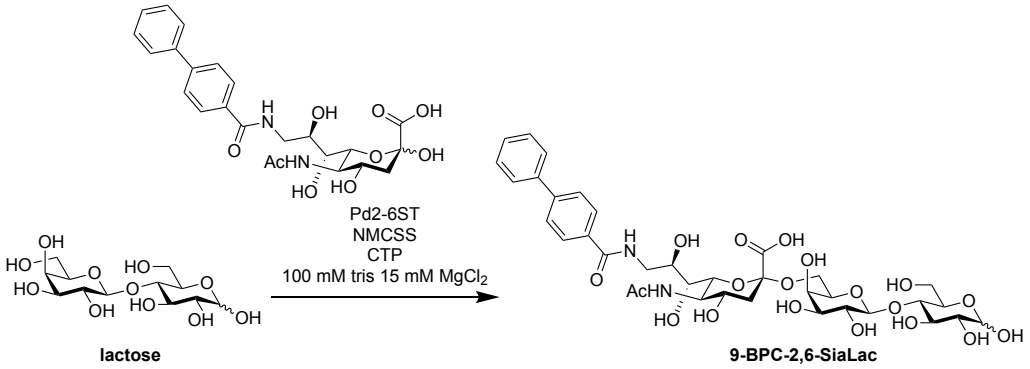

Precursor BPC-Neu5Ac was synthesized using an adapted procedure (*81*). To a solution of 9-amino-Neu5Ac (*82, 83*) (100 mg, 0.324 mmol) in H_2O/MeOH (7 mL, 1:9) was added biphenyl-4-carbonyl chloride (105.4 mg, 0.497 mmol) and DIPEA (226 µL, 1.297 mmol, 0.742 g/mL) and allowed to stir at rt. TLC analysis showed completion after 4 h, at which point the solvent was removed under vacuum. The residue was resuspended in H_2O and lyophilised and then purified via column chromatography (EtOAc:IPA:H_2O- 4:2:1) to yield BPC-Neu5Ac as a white solid (139.7 mg, 88.2%); α:β 1:10; LRMS: m/z (ES-) 487 (100%, $[M-H]^-$); HRMS: m/z (ES+) calculated for $C_{24}H_{29}N_2O_9$ $[M+H]^+$ 489.1868; observed 489.1869; M.P.= 197-203 °C (decomp.); IR ν_{max} 3272 (OH), 1612 (CO-amide), 1553 (COO^-), 1486, 1426, 1375, 1313, 1234, 1152, 1127, 1077, 1034, 944, 896, 854, 781, 746, 695; ^{1}H NMR (400 MHz, MeOD) δ 7.96 – 7.88 (2H, m, ArH), 7.75 – 7.69 (2H, m, ArH), 7.69 – 7.63 (2H,m, ArH), 7.50 – 7.42 (2H,m, ArH), 7.41 – 7.35 (1H, m, ArH), 4.03 (1H, t, *J* = 9.2 Hz, H-6), 4.00 – 3.93 (2H, m, H-4, H-5), 3.87 (1H, ddd, *J* = 9.0, 7.1, 3.2 Hz, H-8), 3.80 (1H, dd, *J* = 13.8, 3.3 Hz, H-9), 3.52 (1H, dd, *J* = 13.7, 7.1 Hz, H-9), 3.40 (1H, dd, *J* = 8.9, 1.0 Hz, H-7), 2.14 (1H, dd, *J* = 12.7, 4.3 Hz, H-3_{eq}), 1.96 (3H, s, $NCOCH_3$), 1.90 (1H, dd, *J* = 12.6, 10.7 Hz, H-3_{ax}); ^{1}H NMR (600 MHz, D_2O) δ 7.93 – 7.88 (2H, m, ArH), 7.86 – 7.82 (2H, m, ArH), 7.82 – 7.77 (2H, m, ArH), 7.62 – 7.56(2H, m, ArH), 7.54 – 7.48 (2H, m, ArH), 4.09 – 4.03 (2H, m, H-4, H-6), 4.00 – 3.93 (2H, m, H-8, H-5), 3.81 (1H, dd, *J* = 14.1_{9-9}, 3.1_{9-8} Hz, H-9), 3.58 (1H, dd, *J* = 14.1_{9-9}, 7.4_{9-8} Hz, H-9), 3.54 (1H, dd, *J* = 9.0_{9-8}, 1.2_{7-6} Hz, H-7), 2.25 (1H, dd, *J* = 12.9_{3-3}, 4.9_{3-4} Hz, H-3_{eq}), 2.03 (3H, s, $NCOCH_3$), 1.87 (1H, t, *J* = 12.9_{3-3}, H-3_{ax}). ^{13}C NMR (101 MHz, MeOD) δ 174.11 (CO), 170.03 (CO), 145.02 (ArC), 140.41 (ArC), 133.27 (ArC), 129.35 (ArCH), 128.44 (ArCH), 128.38 (ArCH), 127.38 (ArCH), 127.33 (ArCH), 97.37 (C-2) 73.56 (C-6), 71.26 (C-7), 70.45 (C-8), 67.70 (C-4), 53.38 (C-5), 44.08 (C-9), 40.98 (C-3), 22.28 ($NCOCH_3$).

To generate Pd2,6ST enzyme, plasmid pET15b-Pd2,6ST (10 ng/µL) (from Prof. Xi Chen – UC Davis) was transformed in chemically competent XL-10 gold *E. coli* cells (Agilent) and plated on LB-agar with ampicillin. Single colonies were picked, cultured in LB medium containing ampicillin (100 mg/mL) and plasmid DNA was purified using QIAprep® Spin Miniprep Kit. As per the suppliers instructions. Plasmid copied were isolated and checked by Sanger sequencing prior to use. The resulting plasmid was transformed into BL21 gold (DE3) cells and plated onto LB-agar with ampicillin. A single colony was picked and cultured in LB media containing Ampicillin (100 mg/mL) and allowed to shake in a stirring incubator at 37 °C. The flask was removed when OD_{600} ~ 0.8 at which point protein expression was induced with IPTG (0.1 mM) and further incubated for 24 h at 20 °C. Cells were harvested by centrifugation (Fiberlite F10BCI-6x500Y, 8000 rpm, 4 °C, 10 min) and the pellets collected and stored at -20 °C. The pellet was then dissolved in lysis buffer (30 mL, pH 7.4, 100 mM Tris–HCl, 0.1% Triton X-100) followed by the addition of 2 compete inhibitor tablets and 2 mg of chicken egg lysozyme and was then sonicated (5x 30 s pulses- 1 min pause between pulses), centrifuged (J25.50, 20000 rpm, 4 °C, 20 min), filtered through a 0.2 µm syringe filter and subjected to purification on an AKTA Purifier FPLC using a HisTrap column (5 mL) pre-equilibrated with 25 mM Tris, 500 mM NaCl, 25 mM imidazole, pH 7.4. Elution was performed over a gradient to 25 mM Tris, 500 mM NaCl, 250 mM imidazole, pH 7.4. Fractions containing Pd2,6ST were combined and subjected to dialysis in PBS buffer (2 h, 2 h, overnight).

To generate NmCSS enzyme, a plasmid (NmCSS-Pet23b 9.4 ng/μL, see relevant gene of interest nucleotide sequence below) was transformed into chemically competent XL-10 gold *E. coli* cells (Agilent) and plated on LB-agar with ampicillin. Single colonies were picked, cultured in LB medium containing ampicillin (100 mg/mL) and plasmid DNA was purified using QIAprep® Spin Miniprep Kit. As per the supplier's instructions. Plasmid copies were isolated and checked by Sanger sequencing prior to use. The resulting plasmid was transformed into BL21 gold (DE3) cells and plated onto LB-agar with ampicillin. A single colony was picked and cultured in LB media containing Ampicillin (100 mg/mL) and allowed to shake in a stirring incubator at 37 °C. The flask was removed when OD_{600} ~ 0.8 at which point protein expression was induced with IPTG (0.5 mM) and further incubated for 4 h at 37 °C. Cells were harvested by centrifugation (JLA 9.1000, 8000 rpm, 4 °C, 20 min) and the pellet collected and stored at -20 °C. The pellet was then dissolved in lysis buffer (30 mL, 25 mM tris, 500 mM, NaCl and 25 mM imidazole, pH 7.4) followed by the addition of 2 compete inhibitor tablets and 2 mg of chicken egg lysozyme and was then sonicated (5x 30 s pulses- 1 min pause between pulses), centrifuged (J25.50, 20000 rpm, 4 °C, 20 min), filtered through a 0.2 μm syringe filter and subjected to purification on an AKTA Purifier FPLC using a HisTrap column (5 mL) pre-equilibrated with 25 mM Tris, 500 mM NaCl, 25 mM imidazole, pH 7.4. Elution was performed over a gradient to 25 mM Tris, 500 mM NaCl, 250 mM imidazole, pH 7.4. Fractions containing NmCSS were combined and subjected to dialysis in PBS buffer (1.5 h, 2 h, overnight).

[NmCSS nucleotide sequence:
ATGATGGAAAAACAAAATATTGCGGTTATACTTGCGCGCCAAAACTCCAAAGGATTGCCATTAAAAAATCTCCGGAAAATGAATG
GCATATCATTACTTGGTCATACAATTAATGCTGCTATATCATCAAAGTGTTTTGACCGCATAATTGTTTCGACTGATGGCGGGTTAA
TTGCAGAAGAAGCTAAAAATTTCGGTGTCGAAGTCGTCCTACGCCCTGCAGAGCTGGCCTCCGATACAGCCAGCTCTATTTCAGGT
GTAATACATGCTTTAGAAACAATTGGCAGTAATTCCGGCACAGTAACCCTATTACAACCAACCAGTCCATTACGCACAGGGGCTCA
TATTCGTGAAGCTTTTTCTCTATTTGATGAGAAAATAAAAGGATCCGTTGTCTCTGCATGCCCAATGGAGCATCATCCACTAAAAAC
CCTGCTTCAAATCAATAATGGCGAATATGCCCCCATGCGCCATCTAAGCGATTTGGAGCAGCCTCGCCAACAATTACCTCAAGCATT
TAGGCCTAATGGTGCAATTTACATTAATGATACTGCTTCACTAATTGCAAATAATTGTTTTTTTATCGCCCCAACCAAACTTTATATTA
TGTCTCATCAAGACTCTATCGATATTGATACTGAGCTTGATTTACAACAGGCAGAAAACATTCTTAATCACAAGGAAAGCCTCGAGC
ACCACCACCACCACCACTGA]

For the synthesis of **6** itself, lactose (30 mg, 0.087 mmol, 1 eq), BPC-Neu5Ac (48 mg, 0.0974 mmol, 1.12 eq) and CTP disodium salt (92 mg, 1.74 mmol, 2 eq) were dissolved in buffer 100 mM Tris, 15 mM $MgCl_2$ pH 8.5, 8.39 mL- to give achieve a final concentration of 10 mM with respect to the lactose acceptor. Pd2,6ST enzyme (261 μL, 1.2 wt%, 1.38 mg/mL) and NmCSS enzyme (107.4 μL, 1 wt %, 2.73 mg/mL) were added to the reaction and the mixture shaken at 37 °C. After 22 h the reaction mixture was concentrated *in vacuo* and then purified via column chromatography (EtOAc:IPA:H_2O 3:2:1→2.5:2:1 and then EtOAc:IPA:H_2O: 4:2:1). Fractions containing the desired compound were concentrated, redissolved in water and lyophilised to yield the product as a white powder (17.7 mg, 0.0218 mmol, 25%) – Note: the reaction conversion was very high, however the yield is reflective of difficult isolation of the product. **LRMS:** m/z (ES-) 811 $[M-H]^-$; **HRMS**: m/z (ESI-): calc. for $C_{36}H_{47}O_{19}N_2$ $[M-H]^-$ 811.2779, found 811.2773; **^{1}H NMR** (400 MHz, D_2O) δ 7.90 (2H, d, *J* = 8.5 Hz, ArH), 7.82 (2H, d, *J* = 8.3 Hz, ArH), 7.80 – 7.71 (2H, m), 7.61 – 7.53 (2H, m), 7.53 – 7.45 (1H, m), 5.16 (0.4H, d, *J* = 3.8 Hz, H-1a (alpha)), 4.63 (1H, d, *J* = 8.0 Hz, H-1a (beta)), 4.41 (1H, d, *J* = 7.8 Hz, H-1b), 4.09 (1H, ddd, *J* = 8.8, 7.2, 3.2 Hz, H-8c), 4.04 – 3.48 (m, 16H), 3.35 – 3.26 (1H, m, H-2a (beta)), 2.73 (1H, dd, J = 12.4, 4.7 Hz, H-3c_{eq}), 2.02 (3H, s, $NCOCH_3$), 1.77 (1H, t, *J* = 12.2 Hz, H-3c_{ax}).

*Synthesis of Heparin Tetrasaccharides (**7, 8**).*

Heparin sodium salt (UFH, 100mg) was dissolved in heparinase-1 (Hep-1) preparations in 100mM Tris Acetate, 5Mm $Ca(OAc)_2$, pH 6.8 to achieve a final concentration of 30 mg/mL UFH and 1.5mg/mL Hep-1-SUMO. The reaction was incubated in a water bath at 28°C and terminated after 36hrs by heating at 95 ˚C for 5 min. Upon centrifugation (2000g, 2min), the supernatant was filtered using a 0.2μm filter (Regenerated Cellulose, Sartorius) and lyophilised to yield a mixture of heparin oligosaccharides as a foam. These were then fractionated based on their degree of polymerisation on a Superdex Peptide 10/300 column (GE-Healthcare), following a procedure adapted from ref. (*84, 85*). Briefly, the column was equilibrated before each run with 2CV of 0.5M $(NH_4)_2CO_3$ and the elution was monitored at 232nm. Sample application (100uL injection per run, ~10mg in sugar

content) was followed by an isocratic elution with 0.5M $(NH_4)_2CO_3$ at a flow rate of 0.6mL/min. The fraction collector was set to collect 1mL fractions until well-resolved peaks were detected; at that point, fractionation was manually controlled and tetrasaccharide-containing fractions from sequential chromatographic runs were pooled together and subjected to serial lyophilisation rounds. Approximately 15mg of heparin tetrasaccharides were recovered upon removal of the volatile salt; these were further analysed with strong anion exchange HPLC on a SAX Propac PA1 column (9x250mm, Thermo Scientific) using H_2O, pH 3.5 as solvent A and 2M NaCl (HPLC grade) pH 3.5 as solvent B. The column was equilibrated with solvent A for 30min prior to sample application (500uL injection per run, 10mg/mL) and the target oligosaccharides were eluted following a linear gradient from 30% to 70% solvent B over 180min, at a flow rate of 1mL/min. Fractions corresponding to the same retention times were pooled, neutralized with saturated $NaHCO_3$ (HPLC grade) and lyophilized. Desalting was performed on an AKTA Purifier system (GE healthcare) by connecting three 5mL HiTrap Desalting columns (GE Healthcare) in a row. Elution with water was performed at a flow rate of 6mL/min and monitored at 232nm; UV absorbing fractions were pooled and lyophilized to yield the pure target tetrasaccharides.

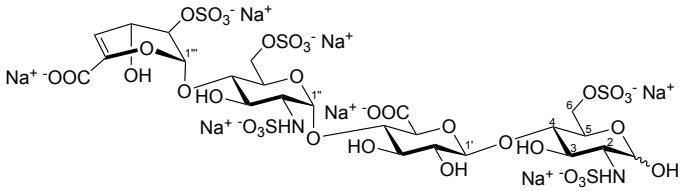

Compound **7**. White solid. ^{1}H NMR (700 MHz, D_2O) δ 5.91 (dd, $J_{4''',3'''}$ 4.7 Hz, $J_{4''',2'''}$ 1.4 Hz, 1H, H-4'''), 5.50 (d, $J_{1'',2''}$ 3.8 Hz, 1H, H-1''), 5.43 (d, $J_{1''',2'''}$ 2.6 Hz, 1H, H-1'''), 5.39 (d, $J_{1\alpha,2\alpha}$ 3.5 Hz, 1H, H-1α), 4.55 (m, 1H, H-2'''), 4.52 (d, $J_{1',2'}$ 8.0 Hz, 1H, H-1'), 4.29 – 4.26 (m, 3H, H-6a'', 6a, 6b), 4.25 (dd, $J_{3''',4'''}$ 4.8 Hz, $J_{3''',2'''}$ 2.1 Hz, 1H, H-3'''), 4.13 (dd, $J_{6b'',6a''}$ 11.3 Hz, $J_{6b'',5''}$ 2.0 Hz, 1H, H-6b''), 4.08 (ddd, $J_{5,4}$ 9.7 Hz, $J_{5,6a}$ 4.2 Hz, $J_{5,6b}$ 2.7 Hz, 1H, H-5), 3.91 (ddd, $J_{5'',4''}$ 10.1 Hz, $J_{5'',6a''}$ 4.2 Hz, $J_{5'',6b''}$ 2.2 Hz, 1H, H-5''), 3.79 – 3.70 (m, 4H, H-3', H-4', H-5', H-4''), 3.68 – 3.59 (m, 2H, H-4, H-3), 3.56 (dd, $J_{3'',2''}$ 10.6 Hz, $J_{3'',4''}$ 8.8 Hz, 1H, H-3''), 3.31 (dd, $J_{2',3'}$ 9.5 Hz, $J_{2',1'}$ 7.9 Hz, 1H, H-2'), 3.23 (dd, $J_{2'',3''}$ 10.6 Hz, $J_{2'',1''}$ 3.8 Hz, 1H, H-2''), 3.20 (dd, $J_{2\alpha,3\alpha}$ 10.2 Hz, $J_{2\alpha,1\alpha}$ 3.6 Hz, 1H, H-2), 2.97 (dd, $J_{2\beta,3\beta}$ 10.0 Hz, $J_{2\beta,1\beta}$ 8.4 Hz, H-2β). ^{13}C NMR (176 MHz, D_2O) δ 169.3 (C-6''' - COOH), 160.2 (C-6' – COOH), 144.8 (C-5'''), 106.0 (C-4'''), 102.1 (C-1'), 97.7 (C-1''), 97.1 (C-1'''), 91.0 (C-1), 78.8 (C-4), 78.0 (C-4''), 77.5 (C-4'), 76.4, 75.9 (C-3',5'), 74.5 (C-2'''), 72.9 (C-2'), 69.53 (C-3''), 69.3 (C-3), 68.7 (C-5''), 68.1 (C-5), 66.7 (C-6), 66.1 (C-6''), 62.8 (C-3'''), 57.6 (C-2), 57.5 (C-2''). Data consistent with previous reports[4]. LRMS m/z (ESI-): Found 535.5 $[M-2H]^{2-}$; HRMS: m/z (ESI-) calc. for $C_{24}H_{36}N_2O_{35}S_5^{2-}$ $[M-2H]^{2-}$ 535.9857, found 535.9858.

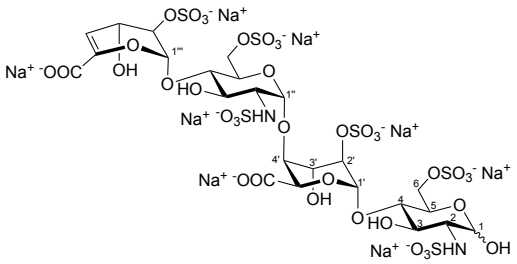

Compound **8**. White solid. ^{1}H NMR (700 MHz, D_2O) δ 5.91 (dd, $J_{4''',3'''}$ 4.8 Hz, $J_{4''',2'''}$ 1.4 Hz, 1H, H-4'''), 5.43 (d, $J_{1''',2'''}$ 1.9 Hz, 1H, H-1'''), 5.38 (dd, J 3.6, 1.7 Hz, 2H, H-1α, H-1''), 5.13 (d, $J_{1',2'}$ 3.4 Hz, 1H, H-1'), 4.67 (d, $J_{5',4'}$ 3.0 Hz, 1H, H-5'), 4.62 (d, $J_{1\beta,2\beta}$ 8.3 Hz, 0.1H, H-1β), 4.55 (m, 1H, H-2'''), 4.30 (dd, $J_{6a,6b}$ 11.4 Hz, $J_{6a,5}$ 4.9 Hz, 1H, H-6a), 4.27 (dd, $J_{6b'',6a''}$ 10.7 Hz, $J_{6b'',5''}$ 1.6 Hz, 1H, H-6b''), 4.25 – 4.21 (m, 3H, H-6b, H-2', H-3'''), 4.18 (dd, $J_{6a'',6b''}$ 11.3 Hz, $J_{6a'',5''}$ 2.0 Hz, 1H, H-6a''), 4.12 (dd, $J_{3',2'}$ 6.7 Hz, $J_{3',4'}$ 3.9 Hz, 1H, H-3'), 4.07 – 4.02 (m, 2H, H-4', H-5), 3.97 (m, 1H, H-5''), 3.75 (at, J 9.5 Hz, 1H, H-4''), 3.67 (at, J 9.4 Hz, 1H, H-4), 3.62 (dd, $J_{3,2}$ 10.4 Hz, $J_{3,4}$ 8.9 Hz, 1H, H-3), 3.55 (dd, $J_{3'',2''}$ 10.6 Hz, $J_{3'',4''}$ 8.8 Hz, 1H, H-3''), 3.22 (dd, $J_{2'',3''}$ 10.6 Hz, $J_{2'',1''}$ 3.6 Hz, 1H, H-2''), 3.18 (dd, $J_{2\alpha,3}$ 10.3 Hz, $J_{2\alpha,1\alpha}$ 3.6 Hz, 1H, H-2α), 2.97 (dd, $J_{2\beta,3}$ 10.1 Hz, $J_{2\beta,1\beta}$ 8.4 Hz, H-2β, 0.1H). ^{13}C NMR (176 MHz, D_2O) δ 174.4 (C-6' – COOH), 169.2 (C-6''' – COOH), 144.8 (C-5'''), 105.8 (C-4'''), 99.4 (C-1'), 97.2 (C-1'''), 96.5 (C1''), 91.0 (C-1), 78.1 (C-4''), 76.9 (C-4), 76.6 (C-2'), 76.3 (C-4'), 74.4 (C-

2'''), 69.7 (C-5'), 69.6 (C-3'), 69.5 (C-3''), 69.4 (C-3), 68.8 (C-5''), 68.4 (C-5), 67.0 (C-6), 66.2 (C-6''), 62.7 (C-3'''), 57.9 (C-2), 57.6 (C-2''). Data consistent with previous reports[4]. LRMS m/z (ESI-): Found 575.5 $[M-2H]^{2-}$; HRMS: m/z (ESI-) calc. for $C_{24}H_{36}N_2O_{38}S_6^{2-}$ $[M-2H]^{2-}$ 575.9641, found 575.9651.

Synthesis of (Tri-iodobenzamide)ethyl 2,3-Sialo-trisaccharide (**9**).

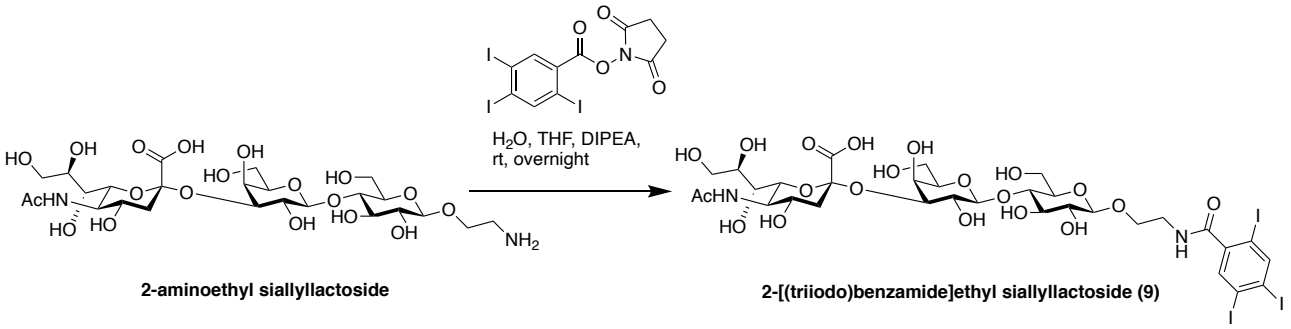

A solution of 2-aminoethyl siallyllactoside (20 mg, 30 μmol) (prepared as per Lee *et al* (*86*)) and *N*,*N*-di*iso*propylethylamine (10.4 μL, 60 μmol) in H_2O (5 mL) and a solution of 2,3,5-triiodobenzoic acid NHS ester (70 mg, 60 μmol, 50%, prepared as per Blum *et al* (*87*)) and *N*,*N*-di*iso*propylethylamine (10.4 μL, 60 μmol) in THF (5 mL) were combined and stirred overnight at rt. The solution was concentrated and could be purified in batches by flash chromatography (EtOAc:IPA:H_2O, 4:2:1). R_f = 0.26 (EtOAc:IPA:H_2O, 4:2:1). ^{1}H NMR (400 MHz, D_2O) δ 8.47 (1H, d, *J* = 2.0 Hz, ArH), 7.71 (1H, d, *J* = 2.0 Hz, ArH), 4.56 (1H, d, *J* = 7.9 Hz), 4.53 (1H, d, *J* = 7.8 Hz), 4.16 – 4.04 (2H, m), 4.01 – 3.54 (20H, m), 3.37 (1H, t, *J* = 8.5 Hz, 1H), 2.77 (1H, dd, *J* = 12.4, 4.6 Hz, $H3_{eq}$), 2.05 (3H, s, NAc), 1.81 (1H, t, *J* = 12.0 Hz, $H3_{ax}$). HRMS (ES-): *m*/*z* calculated for $C_{32}H_{44}N_2O_{20}I_3$ $[M-H]^-$ 1156.9642. Found: 1156.9627.

*Synthesis of SiaLac-IME (**10**) Reagent for SPR Chip Generation*

To generate PmST enzyme, plasmid (PmST-Pet23a 5.6 ng/μL, see relevant gene of interest nucleotide sequence below) was transformed in chemically competent XL-10 gold *E. coli* cells (Agilent) and plated on LB-agar with ampicillin. Single colonies were picked, cultured in LB medium containing ampicillin (100 mg/mL) and plasmid DNA was purified using QIAprep® Spin Miniprep Kit. As per the suppliers instructions. Plasmid copied were isolated and checked by Sanger sequencing prior to use. The resulting plasmid was transformed into BL21 gold (DE3) cells and plated onto LB-agar with ampicillin. A single colony was picked and cultured in LB media containing Ampicillin (100 mg/mL) and allowed to shake in a stirring incubator at 37 °C. The flask was removed when OD_{600} ~ 0.8 at which point protein expression was induced with IPTG (0.5 mM) and further incubated for 4 h at 37 °C. Cells were harvested by centrifugation (JLA 9.1000, 8000 rpm, 4 °C, 20 min) and the pellet collected and stored at -20 °C. The pellet was then dissolved in lysis buffer (30 mL, 25 mM tris, 500 mM, NaCl and 25 mM imidazole, pH 7.4) followed by the addition of 2 compete inhibitor tablets and 2 mg of chicken egg lysozyme and was then sonicated (5x 30 s pulses- 1 min pause between pulses), centrifuged (J25.50, 20000 rpm, 4 °C, 20 min), filtered through a 0.2 μm syringe filter and subjected to purification on an AKTA Purifier FPLC using a HisTrap column (5 mL) pre-equilibrated with 25 mM Tris, 500 mM NaCl, 25 mM imidazole, pH 7.4. Elution was performed over a gradient to 25 mM Tris, 500 mM NaCl, 250 mM imidazole, pH 7.4. Fractions containing PmST were combined and subjected to dialysis in PBS buffer (1.5 h, 2 h, overnight).

[PmST nucleotide sequence:

ATGAAAACAATCACGCTGTATTTAGATCCTGCCTCCTTACCGGCATTAAATCAGCTGATGGACTTTACGCAAAATAATGAAGATAAA
ACACATCCACGTATTTTTGGTCTTTCTCGCTTTAAAATCCCTGACAACATTATTACACAGTATCAAAATATCCATTTCGTCGAACTCAA

AGATAATCGTCCCACTGAAGCACTTTTTACGATTTTAGATCAATACCCTGGTAACATTGAGTTAAATATACACTTAAATATTGCTCAT
TCCGTTCAATTAATTCGTCCGATTTTGGCATATCGTTTTAAACATTTAGATCGTGTATCAATTCAGCAGTTAAATCTTTATGACGATG
GCTCAATGGAATATGTTGATTTAGAAAAAGAAGAAAATAAAGATATTTCCGCAGAAATTAAGCAAGCAGAAAAACAACTTTCTCAC
TATTTGCTTACTGGCAAAATAAAATTTGATAACCCAACTATTGCTCGTTATGTCTGGCAATCCGCGTTCCCAGTAAAATATCATTTTT
TAAGTACAGACTATTTTGAAAAAGCCGAATTTTTACAACCACTAAAAGAATATTTAGCAGAAAATTATCAAAAAATGGACTGGACT
GCTTACCAACAGCTGACTCCAGAACAGCAAGCATTCTACTTAACATTGGTAGGCTTCAATGACGAAGTCAAGCAGTCGCTAGAAGT
GCAACAAGCTAAATTTATCTTTACCGGCACGACAACTTGGGAAGGAAATACCGATGTGCGAGAATACTACGCACAGCAACAACTTA
ATTTACTTAATCACTTTACCCAAGCTGAGGGCGATTTATTTATTGGTGATCATTATAAAATCTACTTTAAAGGGCATCCTAGAGGTG
GTGAAATTAATGACTACATTCTGAACAATGCTAAAAATATCACCAATATCCCTGCCAATATTTCCTTTGAAGTATTGATGATGACAG
GCTTATTACCTGATAAAGTGGGTGGTGTTGCAAGTTCACTGTATTTCTCCTTACCAAAAGAAAAAATTAGCCATATTATTTTCACATC
GAATAAACAAGTGAAAAGCAAAGAAGATGCGCTAAATAATCCGTATGTTAAGGTCATGCGTCGTTTAGGTATAATTGACGAATCA
CAAGTCATCTTTTGGGACAGTTTAAAACAGTTGGGTGGAGGTCTCGAGCACCACCACCACCACCACTGA]

To generate the IME precursor, cyanomethyl β-D-galactopyranosyl-(1→4)-1-thio-β-D-glucopyranoside (200 mg, 503.3 μmol, the final concentration is 10 mM, prepared as per Alexander et al (*88*)) was dissolved in fresh ammonium carbonate (50.33 mL, 100 mM, containing 20 mM $MgCl_2$, pH = 8.5) buffer in conical flask, *N*-acetylneuraminic acid (163.4 mg, 528.4 μmol), cytidine-5'-triphosphate disodium salt (663.1 mg, 1.258 mmol), CMP-sialic acid synthetase (42.34 μL, 2.5 μg per mg substrate, 11.81 mg/mL in PBS buffer, *NmCSS*), and 2,3-sialyltransferase (41.48 μL, 3.0 μg per mg substrate, 14.465 mg/mL in PBS buffer, *PmST*) were added, the resulting mixture was incubated at 37 °C/200rpm. After 2 to 3 h, the reaction was quenched by adding equal volume of cold ethanol (200 mL). The proteins and insoluble precipitates were removed by centrifugation, the supernatant was concentrated in vacuum, the crude residue was purified by flash column chromatography (H_2O–*i*PrOH–EtOAc, 1:2:3 to 1:2:2) followed by size exclusion chromatography (LH20, CH_3OH–H_2O, 1:1), the combined fractions were concentrated, lyophilized in water, yielding cyanomethyl (5-acetamido-3,5-dideoxy-D-glycero-α-D-galacto-non-2-ulopyranosylonic acid)-(2→3)-β-D-galactopyranosyl-(1→4)-1-thio-β-D-glucopyranoside (331 mg, 96%) as a white powder: R_f = 0.61 (H_2O–*i*PrOH–EtOAc, 1:2:2); mp 169 – 170 °C; [a]25 − 19.1 (*c* 1.00, H_2O); FT-IR (film): ν_{max} = 3017, 2349, 1612, 1108, 1030, 618 cm^{-1}; ^1H NMR (700 MHz, D_2O): δ 4.78 (d, $J_{1,2}$ = 10.0 Hz, 1H, H-1), 4.57 (d, $J_{1',2'}$ = 7.8 Hz, 1H, H-1′), 4.14 (dd, $J_{2',3'}$ = 9.9 Hz, $J_{3',4'}$ = 3.2 Hz, 1H, H- 3′), 4.02 (dd, $J_{5',6'a}$ = 2.2 Hz, $J_{6'a,6'b}$ = 12.5 Hz, 1H, H-6′a), 3.98 (app d, $J_{3',4'}$ = 3.1 Hz, 1H, H- 4′), 3.92−3.59 (m, 17H), 3.50 (dd, $J_{1,2}$ = 9.7 Hz, $J_{2,3}$ = 9.0 Hz, 1H, H-2), 2.78 (dd, $J_{3''eq,4''}$ = 4.7 Hz, $J_{3''ax,3''eq}$ = 12.5 Hz, 1H, H-3″eq), 2.05 (s, 3H, C*H*$_3$CONH), 1.82 (t, $J_{3''ax,4''}$ = 12.3 Hz, $J_{3''ax,3''eq}$ = 12.3 Hz, 1H, H-3″ax) *ppm*; ^{13}C NMR (175 MHz, D_2O) δ 175.0 (CH_3*C*ONH), 173.9 ($J_{C1'',H3''ax}$ = 4.7 Hz, *C*OOH, *C*-1″), 118.6 (SCH_2*C*N), 102.6 (*C*-1′), 99.8 (*C*-2″), 84.4 (*C*-1), 78.9, 77.7, 75.6, 75.5 (*C*-3′), 75.2, 72.9, 71.8, 71.7 (*C*-2), 69.4 (*C*-2′), 68.3, 68.1, 67.5 (*C*-4′), 62.6 (*C*-9″), 61.0 (*C*-6), 60.0 (*C*-6′), 51.7, 39.6 (*C*-3″), 22.0 (*C*H_3CONH), 14.5 (S*C*H_2CN) *ppm*; HRMS (ESI): *m*/*z* calcd for $C_{25}H_{40}N_2NaO_{18}S$ $[M+Na]^+$ 711.1889. Found: 711.1887.

The IME precursor was activated to SiaLac IME reagent **10** as follows. To a stirred solution of trisaccharide (6.89 mg, 10 μmol) in dry CH_3OH (480 μL) was added CH_3ONa solution (20 μL, 0.5 M in dry CH_3OH), the resulting mixture was stirred at room temperature for 4 days. The cloudy solution was then concentrated and dried in high vacuum, giving a mixture of starting material (50%) and the desired imidate (50%): R_f = 0.47 (H_2O–*i*PrOH–EtOAc, 1:2:2); ^1H NMR (400 MHz, CD_3OD): δ 4.59 (d, $J_{1,2}$ = 9.7 Hz, H^1-1), 4.43 (d, $J_{1',2'}$ = 7.8 Hz, H^1-1′), 4.42 (d, $J_{1',2'}$ = 9.7 Hz, H^7-1′), 4.35 (d, $J_{1,2}$ = 7.8 Hz, H^7-1), 4.06−3.24 (m, 23H), 2.85 (dd, dd, $J_{3''eq,4''}$ = 2.4 Hz, $J3_{''ax,3''eq}$ = 12.2 Hz, 1H, H^1-3″eq & H^7-3″eq), 2.00 (s, 3H, C*H*$_3$CONH for 1 and 7), 1.74−1.69 (m, 1H, H^1-3″ax & H^7-3″ax) *ppm*; ^{13}C NMR (100 MHz, CD_3OD): δ 175.5 (CH_3*C*ONH), 174.9 (*C*OOH, *C*-1″), 173.0 (*C*(NH)OCH_3), 118.6 (SCH_2*C*N), 105.0 (C^1-1′ & C^7-1′), 101.1 (C^1-2″ & C^7-2″), 86.6 (C^7-1), 85.2 (C^1-1), 80.8, 80.7, 80.62, 80.58, 77.79, 77.76, 77.6, 77.1, 74.9, 74.1, 73.0, 70.8, 70.1, 69.4, 69.0, 64.6, 62.7, 62.1, 62.0, 53.9, 42.1 (C^1-3″ & C^7-3″), 22.6 (*C*H_3CONH) *ppm*; HRMS (ESI): *m*/*z* calcd for $C_{26}H_{45}O_{19}N_2S$ $[M+H]^+$ 721.2327. Found: 721.2332.

NMR Methods Tables.

Table S8: NMR Experiment Conditions and Parameters

Sample:	Ligand concentration / µM	Protein concentration / µM	On-resonance frequency / ppm	Total acquisition time	Used in
BSA + Tryp	**1000**	**5**			
STD			5.44	13.4hrs	Fig 1 D, E i) & F i)
STD 10 ms Gaussian duration			5.44	6.7hrs	
STD 25 ms Gaussian duration			5.44	6.7hrs	
STD 50 ms Gaussian duration			5.44	6.7hrs	
BSA + Tryp	**200**	**5**			
STD			5.44	13.4hrs	Fig 1 E ii) & F ii)
BSA + Tryp	**40**	**5**			
STD			5.44	13.4hrs	Fig 1 E iii) & F iii)
BSA	**None**	**5**			
1D				12.5hrs	
STD			5.44	13.4hrs	Fig 1D, E i-iii) & Fi-iii)
WT HA	**None**	**1**			
STD			5.44	8.7hrs	Fig 2 B, C & D
WT HA + 3-SiaLac 2	**1000**	**1**			
STD			5.44	8.7hrs	Fig 2 B, C & D
ΔRBS HA	**None**	**1**			
STD			5.44	8.7hrs	Fig 2 B, C & D
ΔRBS HA + 3-SiaLac 2	**1000**	**1**			
STD			5.44	8.7hrs	Fig 2 B, C & D
3-SiaLac 2	**1000**	**None**			
STD			5.44	8.7hrs	Fig 2 B, C & D
SPIKE	**None**	**1.5**			
1D				12.5hrs	
STD			5.44	8.7hrs	
SPIKE + Neu5Ac 1	**200**	**1.5**			
STD			5.44	8.7hrs	
SPIKE + 9-azido-Neu5Ac 4	**200**	**1.5**			
STD			5.44	8.7hrs	
SPIKE + BPC-Neu5Ac 5	**200**	**1.5**			
STD			5.44	8.7hrs	Fig 3 G i)
SPIKE + 6-SiaLac 3	**200**	**1.5**			
STD			5.44	2.5hrs	Fig 3 D ii)
STD			5.44	9.83hrs	Fig 3 D ii)
SPIKE + 3-SiaLac 2	**200**	**1.5**			
STD			5.44	2.5hrs	

STD			5.44	9.83hrs	
STD			5.44	8.7hrs	Fig 4 A
SPIKE + BPC-6-SiaLac 6	**200**	**1.5**			
STD			5.44	8.7hrs	Fig 3 G ii)
SPIKE	**None**	**6**			
STD			5.44	8.7hrs	Fig S8, 3 A i), B, D & G
STD			8.00	7.8hrs	
STD var freq 1			List1	29.3hrs	
SPIKE + 3-SiaLac 2	**2000**	**6**			
STD			5.44	8.7hrs	Fig 4 A, 3 B, D & G
STD var freq 2			List2	14.1hrs	
SPIKE + 3-SiaLac 2	**1000**	**6**			
STD			5.44	8.7hrs	Fig 4 A, S6 & S8
STD			8.00	7.8hrs	Fig S6 & S8
STD var freq 3			List3	14.7hrs	
SPIKE + 3-SiaLac 2	**60**	**6**			
STD			5.44	8.7hrs	Fig 4 A
SPIKE + 3-SiaLac 2	**12**	**6**			
STD			5.44	8.7hrs	
Neu5Ac 1	**1000**	**None**			
1D				1 minute	
3-SiaLac 2	**1000**	**None**			
1D				1 minute	
STD			5.44	8.7hrs	Fig 4 A, S6 & S8
STD			8.00	7.8hrs	Fig S6 & S8
STD var freq 2			List2	14.1hrs	
STD var freq 3			List3	14.7hrs	
6-SiaLac 3	**1000**	**None**			
1D				1 minute	
STD			5.44	8.7hrs	
STD			8.00	7.8hrs	
BPC-6-SiaLac 6	**500**	**None**			
1D				18 minutes	
9-azido-Neu5Ac 4	**1000**	**None**			
1D				1 minute	
BPC-Neu5Ac 5	**1000**	**None**			
1D				1 minute	
B.1.1.7-SPIKE	**None**	**6**			
STD			8.00	7.8h	Fig 5 D
B.1.1.7-SPIKE + 3-SiaLac 2	**2000**	**6**			
STD			8.00	7.8h	Fig 5 D

B.1.617.2-SPIKE STD	**None**	**6**	8.00	7.8hrs	Fig 5 D
B.1.617.2-SPIKE + 3-SiaLac 2 STD	**200**	**6**	8.00	7.8hrs	Fig 5 D
B.1.617.2-SPIKE + 3-SiaLac 2 STD	**1000**	**6**	8.00	7.8hrs	Fig 5 D
3-SiaLac 2 STD	**1000**	**None**	8.00	7.8hrs	Fig 5 D
B.1.1.529-SPIKE STD	**None**	**6**	8.00	7.8hrs	Fig 5 D
B.1.1.529-SPIKE + 3-SiaLac 2 STD	**200**	**6**	8.00	7.8hrs	Fig 5 D
B.1.1.529-SPIKE + 3-SiaLac 2 STD	**1000**	**6**	8.00	7.8hrs	Fig 5 D
3-SiaLac 2 STD	**1000**	**None**	8.00	7.8hrs	Fig 5 D

Table S9: NMR Experiment Conditions and Parameters

Sample:	Ligand concentration / µM	Protein concentration / µM	On-resonance frequency / ppm	Total acquisition time	Used in
Tryp STD var freq 4	**1000**	**None**	List 4	19.2hrs	Fig S7
BSA STD var freq 4	**None**	**5**	List 4	19.2hrs	Fig S7
BSA STD	**None**	**10**	5.44	7.9hrs	
BSA + Tryp STD var freq 4	**1000**	**5**	List 4	19.2hrs	Fig S7
BSA + Tryp STD	**25**	**10**	5.44	11.9hrs	
SPIKE + Neu5Ac 1 STD	**2000**	**3**	8.00	7.9hrs	
SPIKE STD	**None**	**3**	-1.00	7.9hrs	Fig 5 A & B
Heparin B STD	**500**	**None**	-1.00	7.9hrs	Fig 5 A
Heparin C	**500**	**None**			

STD			-1.00	7.9hrs	Fig 5 B
SPIKE + Heparin B	**500**	**3**			
STD			-1.00	7.9hrs	Fig 5 A
SPIKE + Heparin C	**500**	**3**			
STD			-1.00	7.9hrs	Fig 5 B
SPIKE B.1.351	**None**	**6**			
STD			-1.00	7.9hrs	Fig 5 D
STD			5.44	7.9hrs	
3-SiaLac 2	**1000**	**None**			
STD			-1.00	7.9hrs	Fig 5 D
SPIKE B.1.351 + 3-SiaLac 2	**60**	**6**			
STD			-1.00	7.9hrs	Fig 5 D
SPIKE B.1.351 + 3-SiaLac 2	**200**	**6**			
STD			-1.00	7.9hrs	Fig 5 D
SPIKE B.1.351 + 3-SiaLac 2	**1000**	**6**			
STD			-1.00	7.9hrs	Fig 5 D
SPIKE B.1.351 + 3-SiaLac 2	**2000**	**6**			
STD			-1.00	7.9hrs	Fig 5 D

Table S10: NMR Experiment Conditions and Parameters

Sample:	Ligand conc. / µM	Protein conc. / µM	Nanobody conc. / µM	On-resonance frequency / ppm	Total acquisition time	Used in
SPIKE	**None**	**6**	**None**			
STD				8.00	7.9hrs	Fig 5 E i) & F
3-SiaLac 2	**2000**	**None**	**None**			
STD				8.00	7.9hrs	Fig 5 E & F
C5 Nanobody	**None**	**None**	**6**			
STD				8.00	7.9hrs	
SPIKE + 3-SiaLac 2	**2000**	**6**	**None**			
STD				8.00	7.9hrs	Fig 5 E i) & F
SPIKE + C5 Nanobody	**None**	**6**	**6**			
STD				8.00	7.9hrs	Fig 5 E ii) & F
SPIKE + 3-SiaLac 2 + C5 Nanobody	**2000**	**6**	**6**			
STD				8.00	7.9hrs	Fig 5 E ii) & F

3-SiaLac 2 + C5 Nanobody	**2000**	**None**	**6**			
STD				8.00	7.9hrs	Fig 5 E ii) & F

Table S11: NMR Experiment Conditions and Parameters

Sample:	Ligand concentration / µM	Protein concentration / µM	On-resonance frequency / ppm	Total acquisition time	Used in
SPIKE	**None**	**6**			
STD			8.00	7.2hrs	Fig 3 E, F, S9 A & B
SPIKE + Neu5Ac 1	**2000**	**3**			
STD			5.44	7.2hrs	Fig 3 E, F i), F ii) & S9 A
SPIKE + 9-Azido-Neu5Ac 4	**2000**	**3**			
STD			5.44	7.2hrs	Fig 3 F iii), F iv) & S9 B
Neu5Ac 1	**2000**	**None**			
STD			5.44	7.2hrs	Fig 3 F i), F ii) & S9 A
Neu5Ac 1	**5000**	**None**			
STD			5.44	7.2hrs	
9-Azido-Neu5Ac 4	**2000**	**None**			
STD			5.44	7.2hrs	Fig 3 F iii), F iv) & S9 B

Cryo EM Data Table.

Table S12: **Cryo-EM data collection, refinement and validation statistics**

	Spike_ ethylbenzamide-triiodo siallyllactose _C1 (EMDB-14154)	Spike_ ethylbenzamide-triiodo siallyllactose_C3 (EMDB-14152) (PDB 7QUR)	Spike_native_C1 (EMDB-14155)	Spike_native_C3 (EMDB-14153) (PDB 7QUS)
Data collection and processing				
Microscope Voltage (kV)	300	300	300	300
Camera	K2	K2	K2	K2
Magnification	165,000	165,000	165,000	165,000
Pixel size (Å/pixel)	0.82	0.82	0.82	0.82
Total electron exposure (e–/Å^2)	60; 61	60; 61	57; 60	57; 60
Number of frames collected during exposure	50; 50	50; 50	50; 50	50; 50
Micrographs used (no.)	5492; 8284	5492; 8284	6618; 6067	6618; 6067
Defocus range (μm)	-0.8 ~ -2.4	-0.8 ~ -2.4	-0.8 ~ -2.4	-0.8 ~ -2.4
Automation software	SerialEM	SerialEM	SerialEM	SerialEM
Energy filter slit width	20	20	20	20
Symmetry imposed	C1	C3	C1	C3
Total extracted particles (no.)	5,419,671	5,419,671	4,508,794	4,508,794
Final particles (no.)	312,018	312,018	551,582	551,582
Map resolution (Å)	2.44	2.27	2.49	2.39
FSC threshold	0.143	0.143	0.143	0.143
Map sharpening *B* factor (Å^2)	-87.9	-89.4	-103.7	-110.2
Model Refinement				
Initial model used (PDB code)		7JJI		7JJI
Model resolution (Å)		2.3		2.4
FSC threshold		0.143		0.143
Model composition				
Non-hydrogen atoms		27174		26742
Protein residues		3303		3303
Ligands		75		69
Waters		282		0
Model data correlation				
CC(mask)		0.87		0.85
CC(box)		0.73		0.70
CC(peaks)		0.72		0.71
CC(volume)		0.86		0.82
CC(ligand)		0.65		0.66
B factors (Å^2)				
Protein residues		55		52
Ligand		79		70
Water		49		-
R.m.s. deviations				
Bond lengths (Å)		0.002		0.002
Bond angles (°)		0.51		0.46
Validation				
MolProbity score		1.55		1.67
Clashscore		4.9		5.5
Poor rotamers (%)		1.0		1.5
Ramachandran plot				
Favored (%)		96.0		96.4
Allowed (%)		3.9		3.5
Disallowed (%)		0.1		0.2

Nucleotide Sequences of Novel Spike Variants of Concern Used

Alpha Spike BAP	ATGTTCGTGTTCCTGGTGCTGCTGCCTCTGGTGAGCAGCCAGTGCGTGAATCTGACCACCAGAACCCAGCTGCCTCCTGCCTACAC CAATAGCTTCACCAGAGGAGTTTATTATCCCGATAAGGTGTTCAGAAGTAGTGTATTACATAGTACCCAGGACCTGTTCCTACCTTT CTTCAGTAACGTGACCTGGTTCCACGCCATCAGCGGCACCAATGGCACCAAGAGATTCGACAATCCTGTGCTGCCTTTCAATGACG GCGTGTACTTCGCCAGCACCGAGAAGAGCAATATCATCAGAGGCTGGATCTTCGGCACCACCTTGGATTCCAAGACTCAGAGCCT GCTGATTGTAAACAACGCTACAAATGTGGTGATCAAGGTGTGCGAGTTCCAGTTCTGCAATGACCCTTTCCTGGGTGTTTATCATA AGAACAACAAGAGCTGGATGGAGAGCGAGTTCCGCGTATATTCGTCGGCTAATAATTGCACCTTCGAGTACGTGAGCCAGCCTTT CCTGATGGACCTGGAGGGCAAGCAGGGCAATTTCAAGAATCTGAGAGAGTTCGTGTTCAAGAATATCGACGGCTACTTCAAGATC TACAGCAAGCACACACCCATTAATCTGGTGAGAGACCTGCCTCAGGGCTTCAGCGCCCTGGAGCCTCTGGTGGACCTGCCTATCG GCATCAATATCACCAGATTCCAGACCCTGCTGGCCCTGCACAGATCATATCTTACACCAGGCGATTCGTCAAGCGGTTGGACCGCT GGAGCTGCGGCATATTACGTGGGCTACCTGCAGCCTAGAACCTTCCTGCTGAAGTACAATGAGAATGGTACGATAACCGACGCAG TTGATTGTGCCCTGGACCCTCTGAGCGAGACCAAGTGCACCCTGAAGAGCTTCACCGTGGAGAAGGGCATCTACCAGACCAGCAA TTTCAGAGTGCAGCCTACCGAGAGCATCGTGAGATTCCCTAATATCACCAATCTGTGCCCTTTCGGCGAGGTGTTCAATGCCACCA GATTCGCCAGCGTGTACGCATGGAACCGCAAGCGGATAAGCAATTGCGTGGCCGACTACAGCGTGCTGTACAATAGCGCCAGCT TCAGCACCTTCAAATGTTATGGTGTTTCGCCAACAAAGCTGAATGACCTGTGCTTCACCAATGTGTACGCCGACAGCTTCGTGATC AGAGGCGACGAGGTGAGACAGATCGCGCCAGGGCAGACCGGCAAGATCGCCGACTACAATTACAAGCTGCCTGACGACTTCACC GGCTGCGTGATCGCGTGGAACTCTAACAATCTAGATTCGAAAGTTGGAGGCAATTACAATTACCTGTACAGACTGTTCAGAAAGA GCAATCTGAAGCCTTTCGAGAGAGACATCAGCACCGAGATCTACCAGGCCGGCAGCACACCGTGTAATGGCGTGGAGGGCTTCA ATTGCTACTTCCCTCTGCAGAGCTACGGCTTCCAGCCTACCTATGGCGTGGGCTACCAGCCTTACAGAGTGGTGGTGCTGAGCTTC GAGCTGCTGCACGCTCCCGCTACCGTGTGCGGCCCTAAGAAGAGCACCAATCTGGTGAAGAATAAGTGCGTGAATTTCAATTTCA ATGGTCTAACTGGAACGGGCGTGCTGACCGAGAGCAATAAGAAGTTTCTTCCCTTTCAACAATTCGGCAGAGACATCGACGACAC CACAGATGCTGTAAGAGACCCTCAGACCCTGGAGATCCTGGACATCACTCCGTGTAGCTTCGGCGGCGTGAGCGTGATCACACCG GGTACCAATACCAGCAATCAGGTGGCCGTGCTGTACCAGGGCGTGAATTGCACCGAGGTGCCTGTGGCCATCCACGCCGACCAG CTGACTCCCACTTGGAGGGTATATTCCACGGGAAGCAATGTGTTCCAGACCAGAGCCGGCTGCCTGATCGGCGCCGAGCACGTG AATAATAGCTACGAGTGCGACATCCCTATCGGCGCCGGCATCTGCGCCAGCTACCAGACCCAGACCAATAGCCATGGAAGCGCCA GCAGCGTGGCCAGCCAGAGCATCATCGCCTACACCATGAGCCTGGGCGCCGAGAATAGCGTGGCCTACAGCAATAATAGCATCG CCATCCCTATCAATTTCACCATCAGCGTGACCACCGAAATATTACCAGTCTCCATGACCAAGACCAGCGTGGACTGCACCATGTAC ATCTGCGGCGACAGCACCGAGTGCAGCAATCTGCTGCTGCAGTACGGCAGCTTCTGCACCCAGCTGAATAGAGCCCTGACCGGCA TCGCCGTGGAGCAGGACAAGAATACCCAGGAGGTGTTCGCCCAGGTGAAGCAGATCTACAAGACTCCGCCGATCAAGGACTTCG GCGGCTTCAATTTCAGCCAAATACTCCCAGATCCAAGCAAGCCTAGCAAGAGGAGCTTCATCGAGGACCTGCTGTTCAATAAGGT GACCCTGGCCGACGCCGGCTTCATCAAGCAGTACGGCGACTGCCTAGGTGATATTGCGGCAAGAGACCTGATCTGCGCCCAGAA GTTTAACGGTTTGACAGTACTACCTCCTCTGCTGACCGACGAGATGATAGCACAATATACGTCGGCATTGCTCGCTGGCACGATCA CATCGGGCTGGACTTTCGGCGCCGGAGCAGCGTTGCAAATCCCTTTCGCCATGCAGATGGCCTACAGATTCAATGGCATCGGCGT GACCCAGAATGTGCTGTACGAGAATCAGAAGCTGATCGCCAATCAGTTCAATAGCGCCATCGGCAAGATCCAGGACAGCCTGAG CAGCACCGCCAGCGCCCTGGGCAAGCTGCAGGACGTGGTGAATCAGAATGCCCAGGCCCTGAATACCCTGGTGAAGCAGCTGAG CAGCAATTTCGGCGCCATCAGTAGTGTACTCAACGATATCCTGGCCAGACTGGACCCGCCAGAGGCCGAGGTGCAAATTGATCGT CTTATTACTGGCAGACTGCAGAGCCTGCAGACCTACGTGACCCAGCAGCTGATCAGAGCCGCCGAGATCAGAGCCAGCGCCAATC TGGCCGCCACCAAGATGAGCGAGTGCGTGCTGGGCCAGAGCAAGAGAGTGGACTTCTGCGGCAAGGGCTACCACCTGATGAGC TTCCCTCAGAGCGCTCCACATGGCGTGGTGTTCCTGCACGTGACCTACGTGCCTGCCCAGGAGAAGAATTTCACCACCGCACCCGC AATCTGCCACGACGGCAAGGCCCACTTCCCTAGAGAGGGCGTGTTCGTGAGCAATGGCACCCACTGGTTCGTGACCCAGAGAAAT TTCTACGAGCCTCAGATCATCACCACCCACAATACCTTCGTGAGCGGCAATTGCGACGTGGTGATCGGGATAGTCAATAATACTGT CTACGACCCTCTGCAGCCTGAGCTGGACAGCTTCAAGGAGGAGCTGGACAAGTACTTCAAGAATCACACCAGCCCTGACGTGGAC CTCGGTGATATTTCGGGAATCAATGCCAGCGTGGTGAATATCCAGAAGGAAATTGATCGGCTCAACGAAGTGGCCAAGAATCTG AATGAGAGCCTGATCGACCTGCAGGAGCTGGGCAAGTACGAGCAGGGATCAGGTTATATTCCTGAAGCTCCAAGAGATGGGCAA GCTTACGTTCGTAAAGATGGCGAATGGGTATTACTTTCTACCTTTTTAAGCTTGCTGAATGACATATTCGAGGCCCAGAAGATTGA ATGGCATGAGAAACATCACCATCACCATCACTAATAA
Beta Spike BAP	ATGTTCGTGTTCCTGGTGCTGCTGCCTCTGGTGAGCAGCCAGTGCGTGAATTTCACCACCAGAACCCAGCTGCCTCCTGCCTACAC CAATAGCTTCACCAGAGGAGTTTATTATCCCGATAAGGTGTTCAGAAGTAGTGTATTACATAGTACCCAGGACCTGTTCCTACCTTT CTTCAGTAACGTGACCTGGTTCCACGCCATCCACGTGAGCGGCACCAATGGCACCAAGAGATTCGCCAATCCTGTGCTGCCTTTCA ATGACGGCGTGTACTTCGCCAGCACCGAGAAGAGCAATATCATCAGAGGCTGGATCTTCGGCACCACCTTGGATTCCAAGACTCA GAGCCTGCTGATTGTAAACAACGCTACAAATGTGGTGATCAAGGTGTGCGAGTTCCAGTTCTGCAATGACCCTTTCCTGGGTGTTT ATTATCATAAGAACAACAAGAGCTGGATGGAGAGCGAGTTCCGCGTATATTCGTCGGCTAATAATTGCACCTTCGAGTACGTGAG CCAGCCTTTCCTGATGGACCTGGAGGGCAAGCAGGGCAATTTCAAGAATCTGAGAGAGTTCGTGTTCAAGAATATCGACGGCTAC TTCAAGATCTACAGCAAGCACACACCCATTAATCTGGTGAGAGGCCTGCCTCAGGGCTTCAGCGCCCTGGAGCCTCTGGTGGACC TGCCTATCGGCATCAATATCACCAGATTCCAGACCCTGCACATATCATATCTTACACCAGGCGATTCGTCAAGCGGTTGGACCGCT GGAGCTGCGGCATATTACGTGGGCTACCTGCAGCCTAGAACCTTCCTGCTGAAGTACAATGAGAATGGTACGATAACCGACGCAG TTGATTGTGCCCTGGACCCTCTGAGCGAGACCAAGTGCACCCTGAAGAGCTTCACCGTGGAGAAGGGCATCTACCAGACCAGCAA TTTCAGAGTGCAGCCTACCGAGAGCATCGTGAGATTCCCTAATATCACCAATCTGTGCCCTTTCGGCGAGGTGTTCAATGCCACCA GATTCGCCAGCGTGTACGCATGGAACCGCAAGCGGATAAGCAATTGCGTGGCCGACTACAGCGTGCTGTACAATAGCGCCAGCT TCAGCACCTTCAAATGTTATGGTGTTTCGCCAACAAAGCTGAATGACCTGTGCTTCACCAATGTGTACGCCGACAGCTTCGTGATC AGAGGCGACGAGGTGAGACAGATCGCGCCAGGGCAGACCGGCAATATCGCCGACTACAATTACAAGCTGCCTGACGACTTCACC GGCTGCGTGATCGCGTGGAACTCTAACAATCTAGATTCGAAAGTTGGAGGCAATTACAATTACCTGTACAGACTGTTCAGAAAGA GCAATCTGAAGCCTTTCGAGAGAGACATCAGCACCGAGATCTACCAGGCCGGCAGCACACCGTGTAATGGCGTGAAGGGCTTCA ATTGCTACTTCCCTCTGCAGAGCTACGGCTTCCAGCCTACCTATGGCGTGGGCTACCAGCCTTACAGAGTGGTGGTGCTGAGCTTC GAGCTGCTGCACGCTCCCGCTACCGTGTGCGGCCCTAAGAAGAGCACCAATCTGGTGAAGAATAAGTGCGTGAATTTCAATTTCA ATGGTCTAACTGGAACGGGCGTGCTGACCGAGAGCAATAAGAAGTTTCTTCCCTTTCAACAATTCGGCAGAGACATCGCCGACAC CACAGATGCTGTAAGAGACCCTCAGACCCTGGAGATCCTGGACATCACTCCGTGTAGCTTCGGCGGCGTGAGCGTGATCACACCG GGTACCAATACCAGCAATCAGGTGGCCGTGCTGTACCAGGGCGTGAATTGCACCGAGGTGCCTGTGGCCATCCACGCCGACCAG CTGACTCCCACTTGGAGGGTATATTCCACGGGAAGCAATGTGTTCCAGACCAGAGCCGGCTGCCTGATCGGCGCCGAGCACGTG AATAATAGCTACGAGTGCGACATCCCTATCGGCGCCGGCATCTGCGCCAGCTACCAGACCCAGACCAATAGCCCTGGAAGCGCCA GCAGCGTGGCCAGCCAGAGCATCATCGCCTACACCATGAGCCTGGGCGTCGAGAATAGCGTGGCCTACAGCAATAATAGCATCG

	CCATCCCTACCAATTTCACCATCAGCGTGACCACCGAAATATTACCAGTCTCCATGACCAAGACCAGCGTGGACTGCACCATGTAC ATCTGCGGCGACAGCACCGAGTGCAGCAATCTGCTGCTGCAGTACGGCAGCTTCTGCACCCAGCTGAATAGAGCCCTGACCGGCA TCGCCGTGGAGCAGGACAAGAATACCCAGGAGGTGTTCGCCCAGGTGAAGCAGATCTACAAGACTCCGCCGATCAAGGACTTCG GCGGCTTCAATTTCAGCCAAATACTCCCAGATCCAAGCAAGCCTAGCAAGAGGAGCTTCATCGAGGACCTGCTGTTCAATAAGGT GACCCTGGCCGACGCCGGCTTCATCAAGCAGTACGGCGACTGCCTAGGTGATATTGCGGCAAGAGACCTGATCTGCGCCCAGAA GTTTAACGGTTTGACAGTACTACCTCCTCTGCTGACCGACGAGATGATAGCACAATATACGTCGGCATTGCTCGCTGGCACGATCA CATCGGGCTGGACTTTCGGCGCCGGAGCAGCGTTGCAAATCCCTTTCGCCATGCAGATGGCCTACAGATTCAATGGCATCGGCGT GACCCAGAATGTGCTGTACGAGAATCAGAAGCTGATCGCCAATCAGTTCAATAGCGCCATCGGCAAGATCCAGGACAGCCTGAG CAGCACCGCCAGCGCCCTGGGCAAGCTGCAGGACGTGGTGAATCAGAATGCCCAGGCCCTGAATACCCTGGTGAAGCAGCTGAG CAGCAATTTCGGCGCCATCAGTAGTGTACTCAACGATATCCTGAGCAGACTGGACCCGCCGGAGGCCGAGGTGCAAATTGATCGT CTTATTACTGGCAGACTGCAGAGCCTGCAGACCTACGTGACCCAGCAGCTGATCAGAGCCGCCGAGATCAGAGCCAGCGCCAATC TGGCCGCCACCAAGATGAGCGAGTGCGTGCTGGGCCAGAGCAAGAGAGTGGACTTCTGCGGCAAGGGCTACCACCTGATGAGC TTCCCTCAGAGCGCTCCACATGGCGTGGTGTTCCTGCACGTGACCTACGTGCCTGCCCAGGAGAAGAATTTCACCACCGCACCCGC AATCTGCCACGACGGCAAGGCCCACTTCCCTAGAGAGGGCGTGTTCGTGAGCAATGGCACCCACTGGTTCGTGACCCAGAGAAAT TTCTACGAGCCTCAGATCATCACCACCGACAATACCTTCGTGAGCGGCAATTGCGACGTGGTGATCGGGATAGTCAATAATACTGT CTACGACCCTCTGCAGCCTGAGCTGGACAGCTTCAAGGAGGAGCTGGACAAGTACTTCAAGAATCACACCAGCCCTGACGTGGAC CTCGGTGATATTTCGGGAATCAATGCCAGCGTGGTGAATATCCAGAAGGAAATTGATCGGCTCAACGAAGTGGCCAAGAATCTG AATGAGAGCCTGATCGACCTGCAGGAGCTGGGCAAGTACGAGCAGGGATCAGGTTATATTCCTGAAGCTCCAAGAGATGGGCAA GCTTACGTTCGTAAAGATGGCGAATGGGTATTACTTTCTACCTTTTTAAGCTTGCTGAATGACATATTCGAGGCCCAGAAGATTGA ATGGCATGAGAAACATCACCATCACCATCACTAATAA

Amino Acid Sequences of Spike Variants of Concern Used

Alpha	MFVFLVLLPLVSSQCVNLTTRTQLPPAYTNSFTRGVYYPDKVFRSSVLHSTQDLFLPFFSNVTWFHAISGTN GTKRFDNPVLPFNDGVYFASTEKSNIIRGWIFGTTLDSKTQSLLIVNNATNVVIKVCEFQFCNDPFLGVYHKN NKSWMESEFRVYSSANNCTFEYVSQPFLMDLEGKQGNFKNLREFVFKNIDGYFKIYSKHTPINLVRDLPQG FSALEPLVDLPIGINITRFQTLLALHRSYLTPGDSSSGWTAGAAAYYVGYLQPRTFLLKYNENGTITDAVDCAL DPLSETKCTLKSFTVEKGIYQTSNFRVQPTESIVRFPNITNLCPFGEVFNATRFASVYAWNRKRISNCVADYS VLYNSASFSTFKCYGVSPTKLNDLCFTNVYADSFVIRGDEVRQIAPGQTGKIADYNYKLPDDFTGCVIAWNS NNLDSKVGGNYNYLYRLFRKSNLKPFERDISTEIYQAGSTPCNGVEGFNCYFPLQSYGFQPTYGVGYQPYR VVVLSFELLHAPATVCGPKKSTNLVKNKCVNFNFNGLTGTGVLTESNKKFLPFQQFGRDIDDTTDAVRDPQT LEILDITPCSFGGVSVITPGTNTSNQVAVLYQGVNCTEVPVAIHADQLTPTWRVYSTGSNVFQTRAGCLIGAE HVNNSYECDIPIGAGICASYQTQTNSHGSASSVASQSIIAYTMSLGAENSVAYSNNSIAIPINFTISVTTEILPVS MTKTSVDCTMYICGDSTECSNLLLQYGSFCTQLNRALTGIAVEQDKNTQEVFAQVKQIYKTPPIKDFGGFNF SQILPDPSKPSKRSFIEDLLFNKVTLADAGFIKQYGDCLGDIAARDLICAQKFNGLTVLPPLLTDEMIAQYTSAL LAGTITSGWTFGAGAALQIPFAMQMAYRFNGIGVTQNVLYENQKLIANQFNSAIGKIQDSLSSTASALGKLQD VVNQNAQALNTLVKQLSSNFGAISSVLNDILARLDPPEAEVQIDRLITGRLQSLQTYVTQQLIRAAEIRASANL AATKMSECVLGQSKRVDFCGKGYHLMSFPQSAPHGVVFLHVTYVPAQEKNFTTAPAICHDGKAHFPREGV FVSNGTHWFVTQRNFYEPQIITTHNTFVSGNCDVVIGIVNNTVYDPLQPELDSFKEELDKYFKNHTSPDVDL GDISGINASVVNIQKEIDRLNEVAKNLNESLIDLQELGKYEQGSGYIPEAPRDGQAYVRKDGEWVLLSTFLSL LNDIFEAQKIEWHEKHHHHHH
Beta	MFVFLVLLPLVS/SQCVNFTTRTQLPPAYTNSFTRGVYYPDKVFRSSVLHSTQDLFLPFFSNVTWFHAIHVSG TNGTKRFANPVLPFNDGVYFASTEKSNIIRGWIFGTTLDSKTQSLLIVNNATNVVIKVCEFQFCNDPFLGVYY HKNNKSWMESEFRVYSSANNCTFEYVSQPFLMDLEGKQGNFKNLREFVFKNIDGYFKIYSKHTPINLVRGL PQGFSALEPLVDLPIGINITRFQTLHISYLTPGDSSSGWTAGAAAYYVGYLQPRTFLLKYNENGTITDAVDCAL DPLSETKCTLKSFTVEKGIYQTSNFRVQPTESIVRFPNITNLCPFGEVFNATRFASVYAWNRKRISNCVADYS VLYNSASFSTFKCYGVSPTKLNDLCFTNVYADSFVIRGDEVRQIAPGQTGNIADYNYKLPDDFTGCVIAWNS NNLDSKVGGNYNYLYRLFRKSNLKPFERDISTEIYQAGSTPCNGVKGFNCYFPLQSYGFQPTYGVGYQPYR VVVLSFELLHAPATVCGPKKSTNLVKNKCVNFNFNGLTGTGVLTESNKKFLPFQQFGRDIADTTDAVRDPQT LEILDITPCSFGGVSVITPGTNTSNQVAVLYQGVNCTEVPVAIHADQLTPTWRVYSTGSNVFQTRAGCLIGAE HVNNSYECDIPIGAGICASYQTQTNSPGSASSVASQSIIAYTMSLGVENSVAYSNNSIAIPTNFTISVTTEILPV SMTKTSVDCTMYICGDSTECSNLLLQYGSFCTQLNRALTGIAVEQDKNTQEVFAQVKQIYKTPPIKDFGGFN FSQILPDPSKPSKRSFIEDLLFNKVTLADAGFIKQYGDCLGDIAARDLICAQKFNGLTVLPPLLTDEMIAQYTSA LLAGTITSGWTFGAGAALQIPFAMQMAYRFNGIGVTQNVLYENQKLIANQFNSAIGKIQDSLSSTASALGKLQ DVVNQNAQALNTLVKQLSSNFGAISSVLNDILSRLDPPEAEVQIDRLITGRLQSLQTYVTQQLIRAAEIRASAN LAATKMSECVLGQSKRVDFCGKGYHLMSFPQSAPHGVVFLHVTYVPAQEKNFTTAPAICHDGKAHFPREG VFVSNGTHWFVTQRNFYEPQIITTDNTFVSGNCDVVIGIVNNTVYDPLQPELDSFKEELDKYFKNHTSPDVDL GDISGINASVVNIQKEIDRLNEVAKNLNESLIDLQELGKYEQGSGYIPEAPRDGQAYVRKDGEWVLLSTFLSL LNDIFEAQKIEWHEKHHHHHH
Delta	MFVFLVLLPLVSSQCVNLRTRTQLPPAYTNSFTRGVYYPDKVFRSSVLHSTQDLFLPFFSNVTWFHAIHVSG TNGTKRFDNPVLPFNDGVYFASTEKSNIIRGWIFGTTLDSKTQSLLIVNNATNVVIKVCEFQFCNDPFLDVYY HKNNKSWMESGVYSSANNCTFEYVSQPFLMDLEGKQGNFKNLREFVFKNIDGYFKIYSKHTPINLVRDLPQ GFSALEPLVDLPIGINITRFQTLLALHRSYLTPGDSSSGWTAGAAAYYVGYLQPRTFLLKYNENGTITDAVDC ALDPLSETKCTLKSFTVEKGIYQTSNFRVQPTESIVRFPNITNLCPFGEVFNATRFASVYAWNRKRISNCVAD YSVLYNSASFSTFKCYGVSPTKLNDLCFTNVYADSFVIRGDEVRQIAPGQTGKIADYNYKLPDDFTGCVIAW NSNNLDSKVGGNYNYRYRLFRKSNLKPFERDISTEIYQAGSKPCNGVEGFNCYFPLQSYGFQPTNGVGYQ PYRVVVLSFELLHAPATVCGPKKSTNLVKNKCVNFNFNGLTGTGVLTESNKKFLPFQQFGRDIADTTDAVRD PQTLEILDITPCSFGGVSVITPGTNTSNQVAVLYQGVNCTEVPVAIHADQLTPTWRVYSTGSNVFQTRAGCLI GAEHVNNSYECDIPIGAGICASYQTQTNSRGSASSVASQSIIAYTMSLGAENSVAYSNNSIAIPTNFTISVTTEI LPVSMTKTSVDCTMYICGDSTECSNLLLQYGSFCTQLNRALTGIAVEQDKNTQEVFAQVKQIYKTPPIKDFG GFNFSQILPDPSKPSKRSPIEDLLFNKVTLADAGFIKQYGDCLGDIAARDLICAQKFNGLTVLPPLLTDEMIAQ YTSALLAGTITSGWTFGAGPALQIPFPMQMAYRFNGIGVTQNVLYENQKLIANQFNSAIGKIQDSLSSTPSAL GKLQNVVNQNAQALNTLVKQLSSNFGAISSVLNDILSRLDPPEAEVQIDRLITGRLQSLQTYVTQQLIRAAEIR ASANLAATKMSECVLGQSKRVDFCGKGYHLMSFPQSAPHGVVFLHVTYVPAQEKNFTTAPAICHDGKAHF PREGVFVSNGTHWFVTQRNFYEPQIITTDNTFVSGNCDVVIGIVNNTVYDPLQPELDSFKEELDKYFKNHTS PDVDLGDISGINASVVNIQKEIDRLNEVAKNLNESLIDLQELGKYEQGSGYIPEAPRDGQAYVRKDGEWVLLS TFLGRS
Omicron	MFVFLVLLPLVSSQCVNLTTRTQLPPAYTNSFTRGVYYPDKVFRSSVLHSTQDLFLPFFSNVTWFHVISGTN GTKRFDNPVLPFNDGVYFASIEKSNIIRGWIFGTTLDSKTQSLLIVNNATNVVIKVCEFQFCNDPFLDHKNNKS WMESEFRVYSSANNCTFEYVSQPFLMDLEGKQGNFKNLREFVFKNIDGYFKIYSKHTPIIVREPEDLPQGFS ALEPLVDLPIGINITRFQTLLALHRSYLTPGDSSSGWTAGAAAYYVGYLQPRTFLLKYNENGTITDAVDCALD PLSETKCTLKSFTVEKGIYQTSNFRVQPTESIVRFPNITNLCPFDEVFNATRFASVYAWNRKRISNCVADYSV LYNLAPFFTFKCYGVSPTKLNDLCFTNVYADSFVIRGDEVRQIAPGQTGNIADYNYKLPDDFTGCVIAWNSN KLDSKVSGNYNYLYRLFRKSNLKPFERDISTEIYQAGNKPCNGVAGFNCYFPLKSYSFRPTYGVGHQPYRV VVLSFELLHAPATVCGPKKSTNLVKNKCVNFNFNGLKGTGVLTESNKKFLPFQQFGRDIADTTDAVRDPQTL EILDITPCSFGGVSVITPGTNTSNQVAVLYQGVNCTEVPVAIHADQLTPTWRVYSTGSNVFQTRAGCLIGAEY VNNSYECDIPIGAGICASYQTQTKSHGSASSVASQSIIAYTMSLGAENSVAYSNNSIAIPTNFTISVTTEILPVS MTKTSVDCTMYICGDSTECSNLLLQYGSFCTQLKRALTGIAVEQDKNTQEVFAQVKQIYKTPPIKYFGGFNF SQILPDPSKPSKRSPIEDLLFNKVTLADAGFIKQYGDCLGDIAARDLICAQKFKGLTVLPPLLTDEMIAQYTSAL LAGTITSGWTFGAGPALQIPFPMQMAYRFNGIGVTQNVLYENQKLIANQFNSAIGKIQDSLSSTPSALGKLQD VVNHNAQALNTLVKQLSSKFGAISSVLNDIFSRLDPPEAEVQIDRLITGRLQSLQTYVTQQLIRAAEIRASANL AATKMSECVLGQSKRVDFCGKGYHLMSFPQSAPHGVVFLHVTYVPAQEKNFTTAPAICHDGKAHFPREGV FVSNGTHWFVTQRNFYEPQIITTDNTFVSGNCDVVIGIVNNTVYDPLQPELDSFKEELDKYFKNHTSPDVDL GDISGINASVVNIQKEIDRLNEVAKNLNESLIDLQELGKYEQGSGYIPEAPRDGQAYVRKDGEWVLLSTFLGR S

Supplementary Text

Supplementary Note 1. Discussion of the Classical STD Experiment.

Specifically, in a dynamic binding equilibrium, binding-rebinding cycles repeat during the saturation pulse. Although 'saturation' is not itself a measurable phenomenon, after a pre-set duration the remaining signal on the ligand can be recorded and the difference in signal for each resonance (sometimes called the 'saturation transfer difference') from a reference spectrum used to indicate ligand-protein contact. This magnetization transfer has often been colloquially described in terms of modes of 'saturation transfer' and, indeed, sometimes given an interpreted converse direction of 'saturation transfer' from protein-to-ligand(*24*) although, in practice, signal on the ligand is in fact reduced by this process.

Supplementary Note 2. Discussion of the Utility of uSTA.

'Universal' saturation transfer analysis (uSTA) only requires a series of specific simplified magnetization transfer spectra to be acquired on a protein-only sample, and then with a range of ligand concentrations (**Supplementary Figures S5, S6, S8**). The signal intensity from individual resonances in these spectra are obtained automatically. These are then converted into on and off rates (and K_Ds) via complete theoretical treatment. These can also provide per resonance transfer efficiencies that, when used as constraints to high-level (e.g. HADDOCK) computational modelling environments provide exact structural models. In this way, uSTA analysis provides an automated pipeline from raw NMR free induction decay (FID) signals all the way to protein•ligand structures in a freely available form for the non-expert.

Supplementary Note 3. Analysis and Circumvention of the Current Limits of Classical Methods of 'STD'.

There are significant challenges that prevent classical 'STD' experiments being reliably applied to mammalian-derived proteins to quantitatively survey ligand binding (**Supplementary Figures S6,S8**). Our theoretical analyses (**Supplementary Figure S4**) suggested that many common assumptions or limits that are thought to govern the applicability of magnetization transfer might in fact be circumvented and we set out to devise a complete treatment that might accomplish this (**Supplementary Figures S5,S6,S8**). The result is a series of modifications to classical methods that combine to provide a more general and now quantitative, automated means of analyzing ligand-binding: uSTA (**Supplementary Figure S1**).

First, and perhaps most notably, appreciable transfer of signal can in fact occur for a wider range of timescales and strength of protein•ligand interaction than previously recognised (**Supplementary Figures S2,S4**). The sensitivity of such experiments is strictly independent of chemical exchange, in that the chemical shift difference between the free and bound ligand conformation is not in itself relevant to the mechanism of 'saturation'/magnetization transfer. Instead, such modes are governed by the number of ligands that come into contact with protein

and the cross relaxation between the two – this does not restrict the saturation transfer to the 'fast' exchange regime, as is commonly argued.(*24*) It also means that use of equations based on fast exchange that are typically used to analyze STD data cannot provide a general method. As a result this can lead to very larger errors in extracted K_Ds, depending on the specific association and dissociation rates (**Supplementary Figures S6,8**).

Second, in seeking to precisely quantitate magnetization transfer, our analysis also reveals that it is vital to systematically vary both the protein and the ligand concentration in order to robustly separate exchange parameters from concentration-independent relaxation processes (**Supplementary Figure S4**).(*24, 89*) In this way, forward and backward rates (and K_D) can be consistently obtained via experiments at multiple concentrations coupled with global, complete analyses of cross-relaxation.

Third, as in the case of heavily glycosylated human-derived proteins covered by highly mobile sugars,(*90*) the problems may be greatly exacerbated. The conformational flexibility of these groups is such that their R_2 relaxation rates become extremely short(*90-92*) leading to greatly confounded difference spectra. In conventional STD experiments, using for example the 'group epitope' method,(*30*) relaxation filters are added at the end of an experiment where protein signal is hoped to evenly decay away, ideally leaving only signal from ligands. However, in a protein that contains both mobile modifications as well as mobile disordered regions, such as SARS-CoV-2-spike, this approach is no longer viable since protein signal remains, even after aggressive use of such relaxation filters (**Supplementary Figures S5,S6,S8**). Moreover, relaxation filters inevitably result in reduced overall sensitivity and effects of intra-ligand cross-relaxation via the nuclear Overhauser effect (NOE) and ROE inhibit the elucidation of atom-specific data. In principle, however, relaxation filters would not be necessary at all with reliable extraction of ligand-only signal. We considered that baseline subtraction of residual signal transfer using reference to samples containing only protein could prove possible if methods for precise resonance identification could be developed.

Finally, NMR spectra from biological ligands such as sugars can be extremely complex, containing a large number of multiplets across diverse chemical shifts, each of which can be highly overlapped. Typically only the small number of resonances that are not overlapped are selected for detailed analysis in classical experiments, and so important information characterizing the ligand present in the spectrum cannot be easily extracted. In order to accurately quantify such a spectrum for use in saturation transfer methods, it is necessary to accurately determine the degree of magnetization (and its change) for each and all observed proton resonances. This too would be addressed by precise resonance identification (**Supplementary Figures S5,S6,S8**).

Supplementary Note 4. Detailed Analysis of the Design of uSTA.

STD analysis is a well-used method for studying protein/ligand interactions. It is widely thought to be a 'fast exchange' method, suitable only for weakly binding ligands with fast on/off rates. Quantitative analysis methods for STD data have been proposed based on the assumption that exchange is fast, though the agreement between measured K_Ds from this method of analysis and alternative biophysical methods such as ITC and SPR can diverge by orders of magnitude.

We performed a theoretical analysis (**Supplementary Figure S4**) that suggests that many common assumptions or limits that are thought to govern the applicability of magnetization transfer might in fact be circumvented (see **Supplementary Note 3** for more details) and we set out to devise a more general experiment including pulse sequences as well as a data analysis pipeline that might accomplish this (**Supplementary Figures S5,S6,S8**). The result is 5 modifications that combine to provide a more general and now quantitative, semi-automated means of analyzing ligand-binding: uSTA (**Supplementary Figure S1**, **S5** for abstract, **S8** for improvements). Overall, the uSTA package provides a mechanism for semi-automatically analyzing protein/ligand interactions using NMR that is more general, sensitive and accurate than previously available methods.

First, in order to completely and quantitatively determine kinetic factors associated with binding (k_{on}, k_{off}, K_D) via uSTA we considered full aspects of the appropriate spin physics (**Figure 1** and **Supplementary Figure S2**). In brief, initially, the protein and ligand resonances are initially at equilibrium (**Figure 1A, grey**). Magnetization transfer experiments(*22*) move spin systems inside the protein that are within the bandwidth of the excitation 'pulse 'out of equilibrium (**Figure 1A** and **Supplementary Figure S2**). These resonances then cross-relax with adjacent spins in the protein (spin-diffusion), which results in wide-ranging sets of spin systems within the protein that are effectively out of equilibrium. During this period, previously free ligand binds the protein and the ligand-protein cross relax via the nuclear Overhauser effect (magnetization is passed from ligand that is initially at equilibrium to out- of-equilibrium spin systems in the protein).

Modelling the degree to which signal has passed between the ligand and protein is complex; transfer depends on ligand binding kinetics k_{on} and k_{off} (and hence K_D) and the intrinsic cross-relaxation rates, which depend on the tumbling time of the complex (see **Figure 1A** and **Supplementary Figure S4** and **Methods** for mathematical analysis). A model for this signal transfer suitable for fitting to data has therefore not, to our knowledge, been addressed to date. However, these factors would, in principle, be straightforward to accommodate in theoretical analyses of the transfer, using comprehensive numerical approaches. In this approach, all relevant interactions could be fully and hence quantitatively described by modified Bloch-McConnell equations. Indeed, Bloch-McConnell approaches prove successful in other protein NMR methods involving dynamic processes such as CEST(*26, 27*) or DEST.(*28*) Although it is more parametrically complex to analyze such magnetization transfer data using this formalism, all that would be required, in principle, is calculation(*93*) of the ratio of signal loss before and after the

saturation pulse for each and every identified resonance, as well as the total concentration of protein and ligand (**Supplementary Figure S5, S6, S8**).

In this way, the theoretical description of the experiment would allow calculation of the expected transfer of signal with varying k_{ex} and K_D values (see **Methods**), where concentration dependent factors of biological significance, k_{on}, K_D, can be rigorously numerically disentangled from concentration independent factors such as relaxation rates. We demonstrated the effectiveness of the analysis by demonstrating that the BSA•Trp (**Figure 1**), and the SPIKE•sialoside K_Ds (**Figure 3**) derived from NMR, and from ITC/SPR respectively are essentially identical. The uSTA analysis in addition to a K_D provides 'true' in solution k_{on}, k_{off} as well as an atomic resolution description of the ligand binding that allows us to determine binding poses of the ligands, and identify precisely which anomeric form of the sialosides (alpha or beta configurations of Sia) are binding with the protein.

This approach has similarity in principle to the CORCEMA method (*69*), where a protein structure is taken and all inter-proton distances are calculated to estimate how relaxation will evolve over the protein and between ligand and protein. As the matrices obtained for this calculation are extremely large, this is not an effective method for data analysis, as the calculation extremely expensive if used for optimization, and the rates obtained for cross relaxation in this way are known to be insufficiently accurate to describe the evolution of magnetization throughout a dynamic protein. For example, NOE intensities are not considered reliable indicators of distance in protein structure calculations for precisely the same reason. In our approach, we treat the system as both protein and ligand existing in 2 states, free and bound, which means we have effectively 4 spin states to consider, which can be represented as a 13 x 13 evolution matrix in the Bloch-McConnell equation. Here, the various relaxation rates are parameterized by relevant tumbling rates and geometric factors. This might appear to be a poor model for such a complicated system as a protein. Our confidence in the method comes primarily from our observation that the K_Ds we obtain through fitting are consistent with those obtained using orthogonal methods. We rationalize its success from the fact that we are not seeking to get accurate descriptions of the intrinsic relaxation processes within the protein that are inherently complicated – we are instead trying to numerically separate the concentration dependent factors that tell us about binding interactions (k_{ex}, K_D) from the concentration-independent factors that will govern the relaxation in the system which we merely need to approximately parameterize. Like when using 2-state models in analyzing protein dynamics via CEST/DEST/CPMG NMR experiments, our 2-state model here appears to strike an excellent balance between simplicity, and capturing the essential physics of the system in a manner that allows us to obtain useful biological data (k_{on}, k_{off}, K_D).

Second, central to this process is precise resonance identification and accurate extraction of signal intensity from all resonances. This was made possible by the design of a Bayesian computational method(*31*) to detect ligand and protein resonances in the 'raw' (unperturbed/reference) spectral data, even when complex and/or obscured by competing signals

(see **Figure 1B** and **Supplementary Figures S5, S6, S8**). By this method, spectra could be automatically reduced to a series of constituent peaks and intensities (**Figure 1B,D**).(*94, 95*) Resonances in the NMR spectrum can be described as a convolution between peak shape and a set of weighted delta functions (a 'delta matrix', see **Figure 1B** and **Methods**), and an algorithm developed previously for analyzing mass spectrometry data, Unidec (*31*) was used to iteratively determine the location of the 'true 'peaks.

The uSTA algorithm allows automatic detection of resonances returning a set of unique delta functions that describe peak positions and intensities, and a 'simulated' spectrum that allows a user to immediately visually verify the success of the calculation through comparison to the original 'raw' data. This process was executed simultaneously for two acquired spectra (excitation pulse on and 'off '(at -38ppm ppm, termed '1D' in figures)) in order to exactly and precisely determine not only peak positions, but also the change in intensity due to magnetization transfer (**Figure 1C**).

The effectiveness of the uSTA algorithm was measured via overlapped 1D spectra (see **Figures 1B, 1D, 3D, 4A** for examples – see also overlaps in all subsequent uSTA analyses and **Supplementary Table S7**) – the success of uSTA was immediately evident from comparison of raw data and algorithmically-derived spectra that were essentially identical in all cases. The peak positions identified by the algorithm mapped well to the locations established using conventional, manual NMR assignments (see **Methods**). Importantly, this enabled signal intensity determination in the background of other confounding resonances (**Supplementary Figure S5, S6, S8**). Moreover, those background resonances themselves could also be similarly analyzed. In this way, the two contributing components to signal intensity found in all magnetization transfer experiments (i.e. protein (P) and ligand (L)) were therefore determined and precisely dissected. Such precise determination of all contributions and consequent intensity changes upon magnetization transfer enabled a detailed quantitative analysis via uSTA by revealing signals that would be otherwise 'hidden '(**Figure 1**). The intensity from each multiplet was summed via scalar coupling, and the uSTA pipeline calculates transfer efficiencies on a per resonance, not a per multiplet basis.

Thirdly, we make adjustments to the experimental protocol that differ from the standard STD and 'epitope mapping' methodology (*30*). In the case of mammalian proteins covered in highly flexible glycans, it is not possible to simply remove signals from protein using a 'relaxation filter'. A period in the pulse sequence where magnetization is held and resonances with a large R_2 from the protein decay to zero, aiming to leave only ligand resonances in the final spectrum. As these flexible residues with low R_2s are directly attached to the protein, they have a very strong STD response on their own. Moreover, during the 'relaxation filter', magnetization on the ligand is free to cross-relax internally thus making it more challenging to separate protein/ligand binding effects of biological interest from relaxation processes. In uSTA this is addressed simply by removing the relaxation filter, and recording a 'protein only' set of STD spectra that can be used by our software

to baseline subtract. This builds on Saturation Transfer Double Difference (STDD) NMR (*96*), with uSTA enabling automatic deconvolution of the protein contribution (**Supplementary Figure S8**). The result is a simple addition to the method that generalizes its applicability and also increases its sensitivity by removing a segment of the pulse sequence where ligand signal unnecessarily decays.

Fourthly, we introduce a 'ligand subtraction'. When applying the excitation pulse during the saturation transfer process, the objective is to excite protein, but entirely 'miss' ligand. The bandwidth of the pulse ultimately sets the spectral region whereupon excitation is achieved, and so this ultimately sets the spectral 'distance', in ppms, that should separate ligand signals from the centre of the pulse. The action of a signal perfectly rectangular pulse element with well defined B_1 inhomogeneity has an excitation profile that resembles a sinc function, and so no matter where one excites, there is always a risk of small but transient excitation of regions of the ligand, that during a long excitation time can become significant, despite the fact that a simulation of the excitation profile of a 90˚ or 180˚ pulse might give the impression that there has been zero excitation outside the bandwidth of the pulse. We can effectively deal with this small residual excitation using a ligand subtraction (**Supplementary Figures 9 and 10**). We demonstrate that providing one excites in a position that is 2x the expected bandwidth of the pulse, and small residual effects of ligand excitation are subtracted, the final 'transfer efficiency' is invariant to precisely where the excitation is performed. This is physically sensible, and amounts to arguing that internal cross relaxation within the protein is much faster than protein/ligand cross relaxation. Without the ligand subtraction, the small effects of transient ligand excitation can compete with very small saturation transfer efficiencies in remote binding positions in the ligand, resulting in interaction/binding heat maps that are visually no longer identical. Thus, no matter which ppm is excited by an experimentalist, provided the ligand is avoided, the degree of cross relaxation from the ligand to the protein and hence the STD response is invariant to excitation frequency. When simulating the effects of the saturation transfer using the Bloch-McConnell equations, the STD response is highly sensitive to the details of the excitation pulse, and so it is vital to simulate exactly the pulse that was executed by the spectrometer (shape, phase, B_1 field amplitudes and duration).

Finally, we sum signal intensity from the different multiplets coming from a resonance to get true 'resonance' signal intensities, from which transfer efficiencies are calculated. These are represented as true atom specific measurements, and as a $<1/r^6>$ interpolated binding map 'that allows rapid and easy visual inspection of the ligand, that allows comparison of binding poses between sequences of ligands as we show in the text.

All this analysis is handled by our software, that is free to use for academic users. Bruker FIDs for the 'pulse on/pulse off' STD experiment are read-in, automatically processed to get spectra and analyzed. A peak list is provided, for which a user has to manually input an assignment (peak X is associated with resonance Y etc). This information is used to automatically generate the binding maps. If data is provided as a function of concentration, varying both protein

and ligand concentrations, the software allows data fitting using the Bloch-McConnell formalism described to provide k_{on}, k_{off}, K_D values

Supplementary Note 5. Precision of uSTA in Allowing Dissection of Two Binding Modes in Unnatural Hybrid Sugars.

In classical STD, the analysis of hybrid sugars would have been dominated simply by the most potent hydrophobic interaction (with ligand sugar protons lost within glycoprotein sugar responses). In this way, we could demonstrate that such modified ligands bind through *all* portions of their surfaces but a distinct difference of interaction is observed in hybrid ligands: a greater and distinct contact was seen with the hydrophobic moiety than with the carbohydrate moiety. Such is the precision of uSTA, graded binding even within these two portions of the ligand was also determined (see atom-specific scoring). For example in **5**, greatest binding for the hydrophobic moiety was seen at the tip with lowering, graduated binding towards the amide junction at C9. In the sugar portion, despite a quite different contact type, individual gradation was also observed: the C7-C9 sidechain bound most strongly but a clear significant contribution from the NHAc-5 group can also be discerned. Trisaccharide-BPC hybrid sugar **6** (with both hydrophobic BPC-moiety and sugar) was also synthetically generated (**Supplementary Figure S12**) to test the relative dominance of the two most potent moieties identified by uSTA. Interestingly, significantly extended binding interfaces were seen in both moieties, consistent with two modes of binding. In this way, uSTA rapidly allowed the mapping and iterative design of natural and unnatural sugar ligands for SARS-CoV-2-spike and the identification of multiple potential binding modes present in these unnatural variants.

Supplementary Note 6. Full GEN-COVID Consortium Listing.

GEN-COVID Multicenter Study (https://sites.google.com/dbm.unisi.it/gen-covid)

Francesca Montagnani[9,17], Mario Tumbarello[9,17], Ilaria Rancan[9,17], Massimiliano Fabbiani[17], Elena Bargagli[18], Laura Bergantini[18], Miriana D'Alessandro[18], Paolo Cameli[18], David Bennett[18], Sabino Scolletta[19], Federico Franchi[19], Federico Anedda[19], Simona Marcantonio[19], Maria Antonietta Mazzei[20], Susanna Guerrini[20], Edoardo Conticini[21], Luca Cantarini[21], Bruno Frediani[21], Danilo Tacconi[22], Chiara Spertilli Raffaelli[22], Marco Feri[23], Alice Donati[23], Raffaele Scala[24], Luca Guidelli[24], Genni Spargi[25], Marta Corridi[25], Cesira Nencioni[26], Leonardo Croci[26], Gian Piero Caldarelli[27], Davide Romani[28], Paolo Piacentini[28], Maria Bandini[28], Elena Desanctis[28], Silvia Cappelli[28], Anna Canaccini[29], Agnese Verzuri[29], Valentina Anemoli[29], Manola Pisani[29], Agostino Ognibene[30], Alessandro Pancrazzi[30], Maria Lorubbio[30], Massimo Vaghi[31], Antonella D'Arminio Monforte[32], Federica Gaia Miraglia[32], Mario U. Mondelli[33,34], Marco Vecchia[33], Stefania Mantovani[33], Raffaele Bruno[33,34], Marcello Maffezzoni[35], Massimo Girardis[36], Sophie Venturelli[36], Stefano Busani[36], Andrea Cossarizza[37], Andrea Antinori[38], Alessandra Vergori[38], Arianna Emiliozzi[38], Stefano

Rusconi[39,40], Matteo Siano[40], Arianna Gabrieli[40], Agostino Riva[39,40], Daniela Francisci[41], Elisabetta Schiaroli[41], Andrea Tommasi[41], Pier Giorgio Scotton[42], Francesca Andretta[42], Sandro Panese[43], Stefano Baratti[43], Renzo Scaggiante[44], Francesca Gatti[44], Saverio Giuseppe Parisi[45], Francesco Castelli[46], Eugenia Quiros-Roldan[46], Melania Degli Antoni[46], Isabella Zanella[47,48], Matteo Della Monica[49], Carmelo Piscopo[49], Mario Capasso[50,51], Roberta Russo[50,51], Immacolata Andolfo[50,51], Achille Iolascon[50,51], Giuseppe Fiorentino[52], Massimo Carella[53], Marco Castori[53], Giuseppe Merla[50,54], Gabriella Maria Squeo[54], Filippo Aucella[55], Pamela Raggi[56], Rita Perna[56], Matteo Bassetti[57,58], Antonio Di Biagio[57,58], Maurizio Sanguinetti[59,60], Luca Masucci[59,60], Alessandra Guarnaccia[59], Serafina Valente[61], Alex Di Florio[61], Francesca Mari[8,9,12], Mirella Bruttini[8,9,12], Ilaria Meloni[8,9], Susanna Croci[8,9], Gabriella Doddato[8,9], Flavia Privitera[8,9], Loredaria Adamo[8,9], Viola Bianca Serio[8,9], Enrica Antonili[8,9], Mirjam Lista[8,9], Giada Beligni[8,9], Debora Maffeo[8,9], Elena Pasquinelli[8,9], Kristina Zguro[9], Giulia Brunelli[9], Rossella Tita[12], Maria Antonietta Mencarelli[12], Caterina Lo Rizzo[12], Anna Maria Pinto[12], Francesca Ariani[8,9,12], Marco Mandalà[62], Alessia Giorli[62], Lorenzo Salerni[62], Patrizia Zucchi[63,] Pierpaolo Parravicini[63], Elisabetta Menatti[64], Tullio Trotta[65], Ferdinando Giannattasio[65], Gabriella Coiro[65], Fabio Lena[66], Gianluca Lacerenza[66], Cristina Mussini[67], Enrico Martinelli[69], Luisa Tavecchia[70], Lia Crotti[71,72,73,74,75], Gianfranco Parati[71,72], Roberto Menè[71,72], Maurizio Sanarico[76], Francesco Raimondi[77], Alessandra Stella[77], Filippo Biscarini[78], Tiziana Bachetti[79], Maria Teresa La Rovere[80], Maurizio Bussotti[81], Serena Ludovisi[82], Katia Capitani[9,83], Chiara Gabbi[84], Simona Dei[85], Sabrina Ravaglia[86], Rosangela Artuso[87], Elena Andreucci[87], Giulia Gori[87], Angelica Pagliazzi[87], Erika Fiorentini[87], Antonio Perrella[88], Francesco Bianchi[9,88], Paola Bergomi[89], Emanuele Catena[89], Riccardo Colombo[89], Sauro Luchi[90], Giovanna Morelli[90], Paola Petrocelli[90], Sarah Iacopini[90], Sara Modica[90], Silvia Baroni[91], Giulia Micheli[92], Marco Falcone[93], Giusy Tiseo[93], Chiara Barbieri[93], Tommaso Matucci[93], Davide Grassi[94], Claudio Ferri[94], Franco Marinangeli[95], Francesco Brancati[96], Antonella Vincenti[97], Valentina Borgo[97], Stefania Lombardi[97], Mirco Lenzi[97], Massimo Antonio Di Pietro[98], Francesca Vichi[98], Benedetta Romanin[98], Letizia Attala[98], Cecilia Costa[98], Andrea Gabbuti[98], Marta Colaneri[99], Patrizia Casprini[100], Cristoforo Pomara[101], Massimiliano Esposito[101], Lucrezia Galasso[102], Michele Cirianni[102], Roberto Leoncini[9,102], Marco Antonio Bellini[103], Alessio Bellucci[104].

17. Department of Medical Sciences, Infectious and Tropical Diseases Unit, Azienda Ospedaliera Universitaria Senese, Siena, Italy
18. Unit of Respiratory Diseases and Lung Transplantation, Department of Internal and Specialist Medicine, University of Siena, Italy
19. Dept of Emergency and Urgency, Medicine, Surgery and Neurosciences, Unit of Intensive Care Medicine, Siena University Hospital, Italy
20. Department of Medical, Surgical and Neuro Sciences and Radiological Sciences, Unit of Diagnostic Imaging, University of Siena, Italy

21. Rheumatology Unit, Department of Medicine, Surgery and Neurosciences, University of Siena, Policlinico Le Scotte, Italy
22. Department of Specialized and Internal Medicine, Infectious Diseases Unit, San Donato Hospital Arezzo, Italy
23. Department of Emergency, Anesthesia Unit, San Donato Hospital, Arezzo, Italy
24. Department of Specialized and Internal Medicine, Pneumology Unit and UTIP, San Donato Hospital, Arezzo, Italy
25. Department of Emergency, Anesthesia Unit, Misericordia Hospital, Grosseto, Italy
26. Department of Specialized and Internal Medicine, Infectious Diseases Unit, Misericordia Hospital, Grosseto, Italy
27. Clinical Chemical Analysis Laboratory, Misericordia Hospital, Grosseto, Italy
28. Dipartimento di Prevenzione, Azienda USL Toscana Sud Est, Italy
29. Dipartimento Tecnico-Scientifico Territoriale, Azienda USL Toscana Sud Est, Italy
30. Clinical Chemical Analysis Laboratory, San Donato Hospital, Arezzo, Italy
31. Chirurgia Vascolare, Ospedale Maggiore di Crema, Italy
32. Department of Health Sciences, Clinic of Infectious Diseases, ASST Santi Paolo e Carlo, University of Milan, Italy
33. Division of Clinical Immunology - Infectious Diseases, Department of Medicine, Fondazione IRCCS Policlinico San Matteo, Pavia, Italy
34. Department of Internal Medicine and Therapeutics, University of Pavia, Italy
35. University of Pavia, Pavia, Italy
36. Department of Anesthesia and Intensive Care, University of Modena and Reggio Emilia, Modena, Italy
37. Department of Medical and Surgical Sciences for Children and Adults, University of Modena and Reggio Emilia, Modena, Italy
38. HIV/AIDS Department, National Institute for Infectious Diseases, IRCCS, Lazzaro Spallanzani, Rome, Italy
39. III Infectious Diseases Unit, ASST-FBF-Sacco, Milan, Italy
40. Department of Biomedical and Clinical Sciences Luigi Sacco, University of Milan, Milan, Italy
41. Infectious Diseases Clinic, “Santa Maria” Hospital, University of Perugia, Perugia Italy
42. Department of Infectious Diseases, Treviso Hospital, Local Health Unit 2 Marca Trevigiana, Treviso, Italy
43. Clinical Infectious Diseases, Mestre Hospital, Venezia, Italy.
44. Infectious Diseases Clinic, ULSS1, Belluno, Italy
45. Department of Molecular Medicine, University of Padova, Italy
46. Department of Infectious and Tropical Diseases, University of Brescia and ASST Spedali Civili Hospital, Brescia, Italy
47. Department of Molecular and Translational Medicine, University of Brescia, Italy;

48. Clinical Chemistry Laboratory, Cytogenetics and Molecular Genetics Section, Diagnostic Department, ASST Spedali Civili di Brescia, Italy
49. Medical Genetics and Laboratory of Medical Genetics Unit, A.O.R.N. "Antonio Cardarelli", Naples, Italy.
50. Department of Molecular Medicine and Medical Biotechnology, University of Naples Federico II, Naples, Italy
51. CEINGE Biotecnologie Avanzate, Naples, Italy
52. Unit of Respiratory Physiopathology, AORN dei Colli, Monaldi Hospital, Naples, Italy
53. Division of Medical Genetics, Fondazione IRCCS Casa Sollievo della Sofferenza Hospital, San Giovanni Rotondo, Italy
54. Laboratory of Regulatory and Functional Genomics, Fondazione IRCCS Casa Sollievo della Sofferenza
55. Department of Medical Sciences, Fondazione IRCCS Casa Sollievo della Sofferenza Hospital, San Giovanni Rotondo, Italy
56. Clinical Trial Office, Fondazione IRCCS Casa Sollievo della Sofferenza Hospital, San Giovanni Rotondo, Italy
57. Department of Health Sciences, University of Genova, Genova, Italy
58. Infectious Diseases Clinic, Policlinico San Martino Hospital, IRCCS for Cancer Research Genova, Italy
59. Microbiology, Fondazione Policlinico Universitario Agostino Gemelli IRCCS, Catholic University of Medicine, Rome, Italy
60. Department of Laboratory Sciences and Infectious Diseases, Fondazione Policlinico Universitario A. Gemelli IRCCS, Rome, Italy
61. Department of Cardiovascular Diseases, University of Siena, Siena, Italy
62. Otolaryngology Unit, University of Siena, Italy
63. Department of Internal Medicine, ASST Valtellina e Alto Lario, Sondrio, Italy
64. Study Coordinator Oncologia Medica e Ufficio Flussi Sondrio, Italy
65. First Aid Department, Luigi Curto Hospital, Polla, Salerno, Italy
66. Department of Pharmaceutical Medicine, Misericordia Hospital, Grosseto, Italy.
67. Infectious Diseases Clinics, University of Modena and Reggio Emilia
69. Department of Respiratory Diseases, Azienda Ospedaliera di Cremona, Cremona, Italy
70. U.O.C. Medicina, ASST Nord Milano, Ospedale Bassini, Cinisello Balsamo (MI), Italy
71. Istituto Auxologico Italiano, IRCCS, Department of Cardiovascular, Neural and Metabolic Sciences, San Luca Hospital, Milan, Italy
72. Department of Medicine and Surgery, University of Milano-Bicocca, Milan, Italy
73. Istituto Auxologico Italiano, IRCCS, Center for Cardiac Arrhythmias of Genetic Origin, Milan, Italy
74. Istituto Auxologico Italiano, IRCCS, Laboratory of Cardiovascular Genetics, Milan, Italy

75. Member of the European Reference Network for Rare, Low Prevalence and Complex Diseases of the Heart-ERN GUARD-Heart
76. Independent Data Scientist, Milan, Italy
77. Scuola Normale Superiore, Pisa, Italy
78. CNR-Consiglio Nazionale delle Ricerche, Istituto di Biologia e Biotecnologia Agraria (IBBA), Milano, Italy
79. Direzione Scientifica, Istituti Clinici Scientifici Maugeri IRCCS, Pavia, Italy
80. Istituti Clinici Scientifici Maugeri IRCCS, Department of Cardiology, Institute of Montescano, Pavia, Italy
81. Istituti Clinici Scientifici Maugeri IRCCS, Department of Cardiology, Institute of Milan, Italy
82. Fondazione IRCCS Ca' Granda Ospedale Maggiore Policlinico, Milan, Italy
83. Core Research Laboratory, ISPRO, Florence, Italy
84. Department of Biosciences and Nutrition, Karolinska Institutet, Stockholm, Sweden
85. Health Management, Azienda USL Toscana Sudest, Tuscany, Italy
86. IRCCS C. Mondino Foundation, Pavia, Italy
87. Medical Genetics Unit, Meyer Children's University Hospital, Florence, Italy
88. Department of Medicine, Pneumology Unit, Misericordia Hospital, Grosseto, Italy.
89. Department of Anesthesia and Intensive Care Unit, ASST Fatebenefratelli Sacco, Luigi Sacco Hospital, Polo Universitario, University of Milan, Milan
90. Infectious Disease Unit, Hospital of Lucca, Italy
91. Department of Diagnostic and Laboratory Medicine, Institute of Biochemistry and Clinical Biochemistry, Fondazione Policlinico Universitario A. Gemelli IRCCS, Catholic University of the Sacred Heart, Rome, Italy.
92. Clinic of Infectious Diseases, Catholic University of the Sacred Heart, Rome, Italy
93. Department of Clinical and Experimental Medicine, Infectious Diseases Unit, University of Pisa, Pisa, Italy
94. Department of Clinical Medicine, Public Health, Life and Environment Sciences, University of L'Aquila, Italy
95. Anesthesiology and Intensive Care, University of L'Aquila, L'Aquila, Italy
96. Medical Genetics Unit, Department of Life, Health and Environmental Sciences, University of L'Aquila, L'Aquila, Italy
97. Infectious Disease Unit, Hospital of Massa, Italy
98. Infectious Diseases Unit, Santa Maria Annunziata Hospital, USL Centro, Florence, Italy
99. Division of Infectious Diseases I, Fondazione IRCCS Policlinico San Matteo, Pavia, Italy
100. Laboratory of Clinical Pathology and Immunoallergy, Florence-Prato, Italy
101. Department of Medical, Surgical and Advanced Technologies "G.F. Ingrassia", University of Catania, Catania, Italy
102. Laboratorio Patologia Clinica, Azienda Ospedaliero-Universitaria Senese, Siena, Italy

103. Ambulatory Chronic Polipathology of Siena, Department of Medicine, Surgery and Neurosciences, University of Siena, Siena, Italy
104. Infectious Diseases Unit, Santa Maria Annunziata Hospital, USL Centro, Florence, Italy

Supplementary Figures

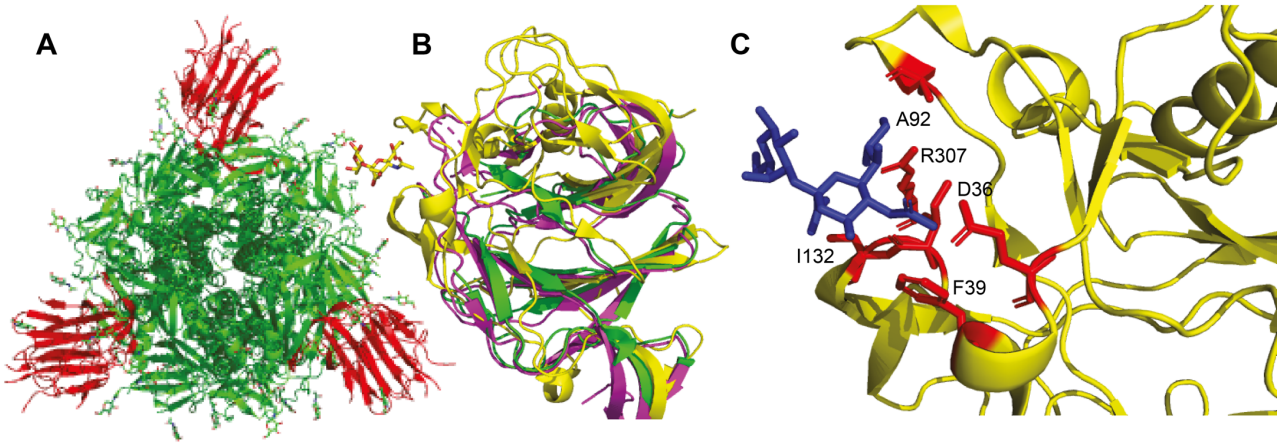

D

```
K0BRG7 K0BRG7_MERS    1  MIHSVFLLMFLLTPTESYVDVGPDSVKSACIEVDIQQTFFDKTWPRP-IDVSKADGIIYP    59
P59594 SPIKE_CVHSA    1  ----MFIFLLFLTLT-S----------GSDLD--RCTTFDDVQAPNYTQHTSSMRGVYYP    43
P0DTC2 SPIKE_SARS2    1  ----MFVFLVLLPLV-S----------SQCVN--LTT--RTQLPPAY--TNSFTRGVYYP    39
                            :*:::.:*  . *          .  ::          *     *   *: **

K0BRG7 K0BRG7_MERS   60  QGRTYSNITITYQGLF-PYQGDHGDMYVYSAGHATGTTPQKLFVANYSQDVKQFANGFVV   118
P59594 SPIKE_CVHSA   44  DEIFRSDTLYLTQDLFLPFYSNVT---GFHTIN-------HT----FGNPVIPFKDGIYF    89
P0DTC2 SPIKE_SARS2   40  DKVFRSSVLHSTQDLFLPFFSNVT---WFHAIHVSGTNGTKR----FDNPVLPFNDGVYF    92
                         :    *.     *.** *: .:      : : :       :     :.: *  * :*. .

K0BRG7 K0BRG7_MERS  119  RIGAAANSTGTVIISPSTSATIRKIYPAFMLGSSVGNFSDGKMGRFFNHTLVLLPDGCGT   178
P59594 SPIKE_CVHSA   90  AATE-----------------KSNVVRGWVFGSTMNNKSQ---------SVIIINNSTNV   123
P0DTC2 SPIKE_SARS2   93  ASTE-----------------KSNIIRGWIFGTTLDSKTQ---------SLLIVNNATNV   126
                                               ::  .:::*:::.. ::         ::::: :. ..

K0BRG7 K0BRG7_MERS  179  LLRAF--YCILEPRSGNHCPAGNSYTSFATYHTPATDCSDGNYNRNASLNSFKEYFNLRN   236
P59594 SPIKE_CVHSA  124  VIRACNFELCDNPFFAVSKPMGT------------------------QTHTMIFDNAFN   158
P0DTC2 SPIKE_SARS2  127  VIKVCEFQFCNDPFLGVYYHKNN---------------------KSWMESEFRVYSSANN   165
                         :::.       :*  .     ..                          .    : .  *

K0BRG7 K0BRG7_MERS  237  CTFMYTYNITEDEILEWFGITQTAQG-VHLFSSRYVDLYGGN---------------MFQ   280
P59594 SPIKE_CVHSA  159  CTFEYISDAFSLDVSEKSGNFKHLREFVFKNKDGFLYVYKGYQPIDVVRDLPSGFNTLKP   218
P0DTC2 SPIKE_SARS2  166  CTFEYVSQPFLMDLEGKQGNFKNLREFVFKNIDGYFKIYSKHTPINLVRDLPQGFSALEP   225
                         *** *  :    ::    *  :  :  *.   . :. :*                :

K0BRG7 K0BRG7_MERS  281  FATLPVYDTIKYYSIIPHSIR---SIQSDRKAW----AAFYVYKLQPLTFLLDFSVDGYI   333
P59594 SPIKE_CVHSA  219  IFKLPLGINITNFRAILTAFS------PAQDIWGTSAAAYFVGYLKPTTFMLKYDENGTI   272
P0DTC2 SPIKE_SARS2  226  LVDLPIGINITRFQTLLALHRSYLTPGDSSSGWTAGAAAYYVGYLQPRTFLLKYNENGTI   285
                         :  **:  .*. :  :             . *    **::*  *:* **:*.:. :* *
```

Supplementary Figure S1. Homology Analyses. A) The N-terminal domain of the SARS-CoV-2 spike protein (green, 6vxx). The N-terminal domain comprises the first 280 residues (red). **B**) The structural homology of MERS (yellow, 6q06), sars-cov1 (magenta, 5x58) and sars-cov2 (green, 6vxx) spike proteins in this region is partial. The C-terminal domains show substantial similarities, but the N-terminus show substantial differences. **C**) The interaction between Gal-Sia and MERS NTD. The interaction can be largely attributed to 5 amino acid residues with the NAc binding F39, I132 and D36, and the glycerol arm binding to A92 and R307. D) Sequence homology of the N-terminal domains of MERS, SARS-CoV-1 and SARS-CoV-2 using BLASTP. Substantial differences between the three proteins are observed. The five key residues for sialic acid binding in MERS are indicated. These all fall within regions in SARS-CoV-1 and SARS-CoV-2 that differ substantially from MERS, thus rendering the likelihood of generating a reliable homology model exceedingly unlikely.

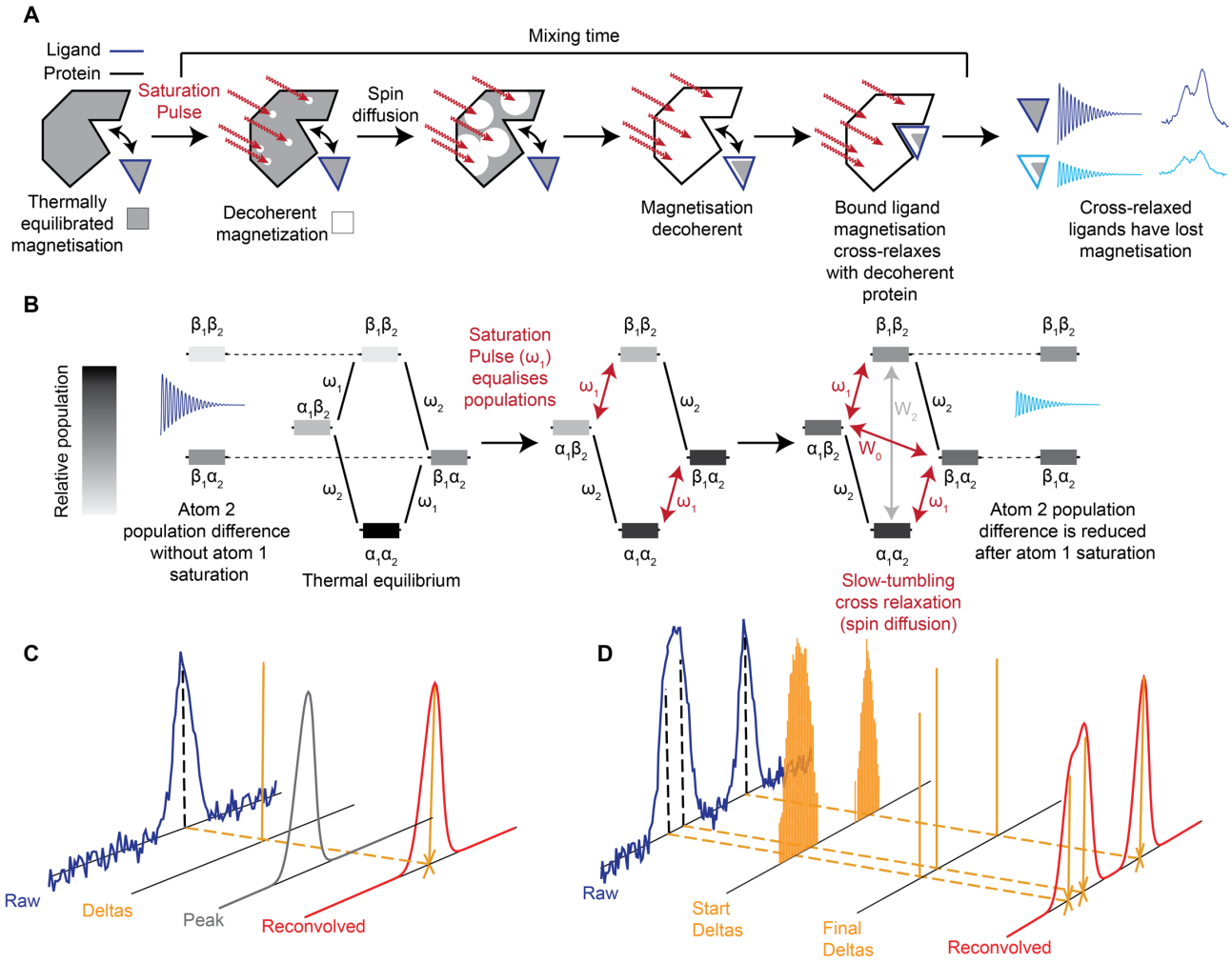

Supplementary Figure S2: Schematic Representation of the Classical STD Experiment and the Deconvolution Approach.
A): A 'saturation pulse' is applied to a protein and ligand mixture that covers a specific but narrow range of ppm frequencies selected to avoid excitation of the ligand. The nuclei excited in the protein will have specific spatial locations within the protein, for example methyl groups or aromatics. Spins in the protein that have been excited will cross-relax with their neighbours, aiming to restoring the initially excited spins to equilibrium. This process continues during the period in which the excitation pulse is applied and the net magnetisation on each spin within the protein is gradually reduced to zero, a process termed ‘spin diffusion’. The rate of the many interior cross relaxations increases as tumbling time of the protein decreases. When a ligand binds rigidly to the protein, intermolecular cross-relaxation can occur if adjacent spins in the protein have been knocked out of equilibrium by either the initial excitation, or spin diffusion. The action will be to transfer unperturbed longitudinal magnetisation from the ligand to partially restore the now unequilibrated longitudinal magnetization on the various spins of the protein. After the mixing time, the quantity of magnetization on the ligand is detected, following a 90˚ pulse. The action of the saturation pulse therefore is to reduce the magnetisation on the ligand in a manner that depends on the on and off rates, the various tumbling times of ligand and protein that govern intrinsic (R_1/R_2) and cross (intra/inter) relaxation and the details of the saturation pulse. A 'build-up curve' follows the amount of lost signal from the ligand versus the duration of the mixing time. These processes can be effectively modelled using modified Bloch-McConnell equations and by recording 'build-up curves' at a range of varying ligand and protein concentrations, and fitting them to an appropriate model based on the modified Bloch-McConnell equations (see methods) concentration independent

effects such as relaxation rates, and concentration dependent effects, such as binding, can be separated, as is demonstrated in this article.
B): The details of the experiment can be understood with a series of single spin energy level illustration. Initially, protein and ligand spins are thermally equilibrated. The application of a saturation pulse at ω1 (always chosen to be a protein spin) induces coherence between the a and b spin states, and with sustained application will eventually equalises populations in the two α1 to β1 transitions (the transition becomes 'saturated', net magnetisation for the spin in the ensemble has gone to zero). In our slowly-tumbling protein, the W0 cross-relaxation pathway is most efficient, providing a path to move magnetization from the state closes to equilibrium (ligand) to the state furthest from equilibrium (protein), here pushing population from the β1α2 state to the α1β2. The combination of continuous application of saturation pulse and cross-relaxation (both intra to ligand and inter within the protein) lowers the population differences between the interacting spin states. This is the nuclear Overhauser effect (NOE). The rate for cross relaxation, both inter and intra depends on the tumbling time of the complex, and the distance between the spins. If atom 2 is a nearby protein spin, we are interrogating part of intra-protein cross relaxation or spin diffusion, if atom 2 is a bound ligand spin, we are interrogating intermolecular cross-relaxation. These complex processes can be well accounted for in a simple two spin model as described in the methods. Our analysis is validated in this work by demonstrating that fitted K_Ds using our picture returns values that are equal to those obtained by independent means, together with the on and off rates.
C),D): Schematic of process for automatically quantifying the signal intensities in NMR spectra using deconvolution. The analysis determined the number of peaks that can give rise to the signal and return a simulated spectrum by convolving these with a peak shape function. Precise peak positions and their intensities are returned, which can be attributed to single protons observed in a spectrum.

A In a sample containing both protein and ligand....

1. An NMR spectrum is recorded, the spectrum is dominated by signals from the ligand.

2. An NMR spectrum is recorded, as for (1), but with excitation specifically in spectral regions that only contain protein, with no signal from ligand. Signal is transferred from the ligand onto the protein, trying to restore protein magnetisation back to equilibrium, after it has been pertrubed by the selective pulse.

3. The difference spectrum reveals signal pass from the ligand to the protein, which indicates transient formation of a complex

4. This is quantified as a 'transfer efficiency' which allows for rigorous comparison between data from different ligand atoms that can be discerned in the spectrum.

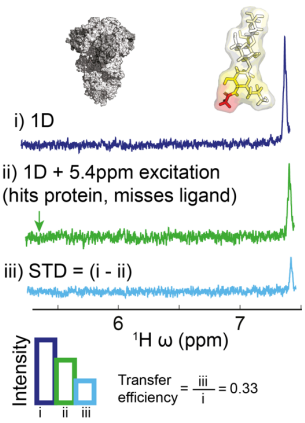

B

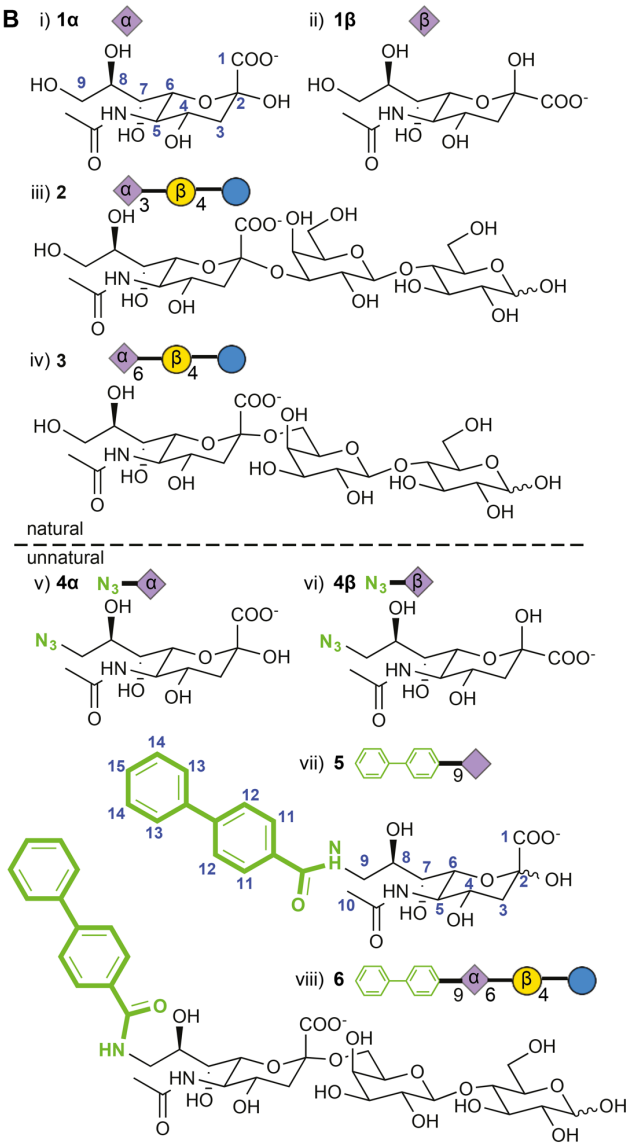

C

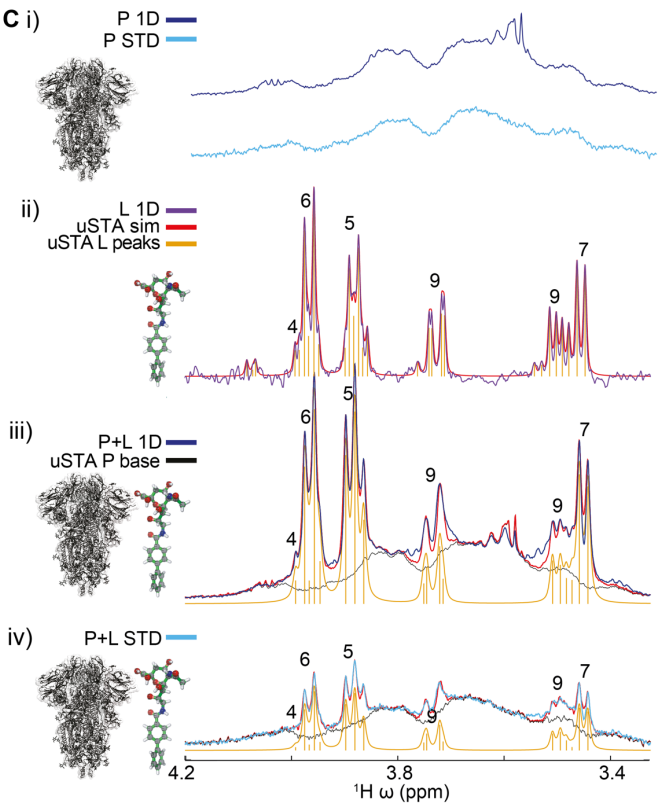

D

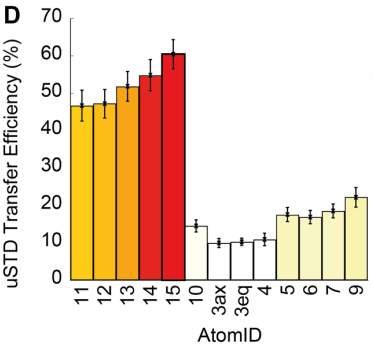

E

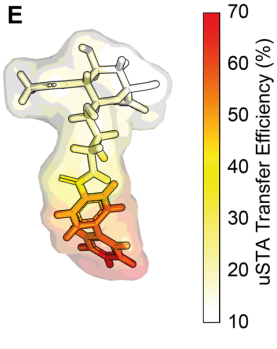

F

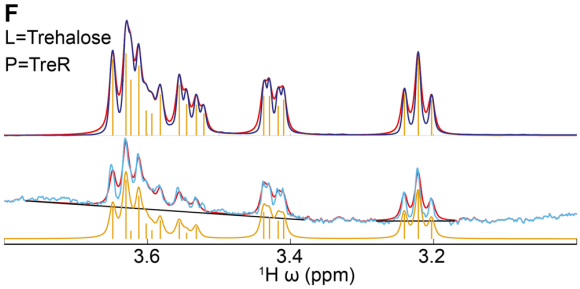

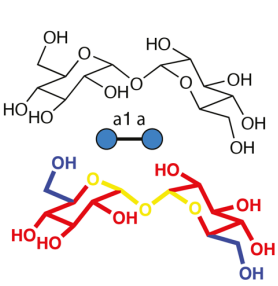

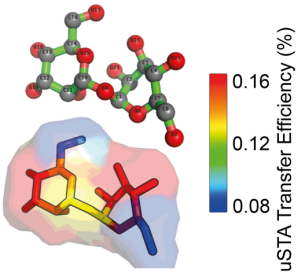

Supplementary Figure S3. A Summary of the Workflow in a Classical NMR STD Experiment and Application of uSTA to Spike•Sugar-hybrid 5 and TreR•Tre systems.
A): When the protein is selectively excited, its magnetisation is pushed far from its equilibrium value. When a ligand binds the protein when in this state, cross relaxation occurs where signal from the ligand moves onto the protein, effectively trying to restore the protein to equilibrium. By comparing the intensity of ligand resonances with, and without the selective excitation, the quantity of magnetisation that has been transferred can be determined, which indicates binding. In order to compare accurately between different atoms in the same spectrum, the degree of transferred magnetisation needs to be expressed relative to the initial magnetisation. This ratio is referred to in this work as the 'transfer efficiency', which can be physically interpreted as a fraction of magnetisation from an atom on the ligand that has moved onto the protein. Increasing the power and the duration of the selective excitation will increase this signal. The specific transfer efficiency will depend on the proximity of the ligand atom and the protein when the complex forms, the overall correlation time of the complex, and the chemical kinetics of the complex formation, the on and the off rate. With the uSTA method, these factors are all treated rigorously using the Bloch-McConnell equations in order to ascertain a reliable K_D.
B): A panel of natural, unnatural and hybrid variant sialoside sugars **1-6** was used to probe interaction between sialic acid moieties and spike. Unnatural variations (**4-6**, green) allowed mapping of C7-C9 side-chain interactions in the sialoside whilst use of extended sugars probed differing cell-surface glycan structures
C): Application of the uSTA workflow (**Supplementary Figure S6**) to SARS-CoV-2-spike protein (shown in detail for **5**, see also **Figures 1,2**) i) The 1D ^{1}H-NMR of SARS-CoV-2-spike protein shows considerable signal in the glycan-associated region despite protein size, indicative of mobile internal glycans in spike protein. This effectively masks traditional analyses, as without careful subtraction of the protein's contributions to the spectrum (**Supplementary Figure S8**), the ligand cannot be effectively studied. The uSTA process of: ii) ligand peak assignment and deconvolution → iii) p + L peak assignment and deconvolution → iv) application to p + L STD yields precise atom-specific transfer efficiencies (**Supplementary Figure S6**). Note how in ii) individual multiplet components, have been assigned (yellow); the back-calculated deconvolved spectrum (red) is an extremely close match for the raw data (purple). In iii) the spectrum is a complex superposition of the ligand spectrum (and protein only yet uSTA again accurately deconvolves the spectrum revealing the contribution of protein only (black) and the ligand peaks (yellow). Using these data, uSTA analysis of the STD spectrum in iv) pinpoints ligand peaks and signal intensities.
D),E): Using these intensities, atom-specific transfer efficiencies can be determined with high precision and reveal in hybrid **5** the details of both the unnatural BPC moiety and the natural sialicacid moiety. Although the aromatic BPC dominates the interaction for the unnatural ligand **5**, the subtleties of the associated sugar contribution in this ligand can nonetheless be determined (**Supplementary Figure S5,S6,S8**).
F): Application of the same uSTA workflow allows precise determination of even weakly binding sugar ligand trehalose (Glc-α1,1α-Glc) to E. coli trehalose repressor TreR. Again, the uSTA allows determination of transfer efficiencies with atom-specific precision.

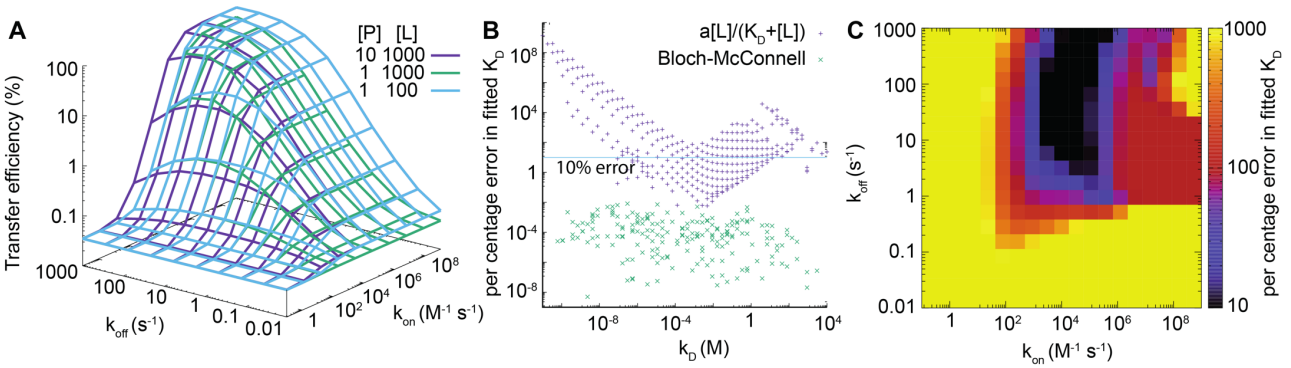

Supplementary Figure S4. Modelling of Current STD Dependencies/Methods. A) The region of validity of the saturation transfer experiment is wider than has been realised, and that by taking both variable protein and ligand concentrations, the two rates, k_{on} and k_{off}, can be numerically separated from the concentration independent factors that describe the relaxation processes. Transfer efficiency from the saturation transfer experiment was simulated using the Bloch-McConnell equations (see **Methods**) using parameters optimised for the alpha3/spike interaction that describe the concentration independent relaxation effects (t_G 2.5 ns, t_E 85 ns, $r_{IS}P$ 1.6 A, $r_{IS}I$=3.1 A, r_{IS}(mix) 2.4 A, *fac* 18) simulated using a Gaussian pulse train of peak B_1 field of 200 Hz with each element running for 50 ms for a total duration of 5 s, as utilised in the experiments, as a function of k_{on} and k_{off} for various protein and ligand concentrations (specified on figure, units of μM). The specific value of the parameters that affect relaxation alter the expected transfer efficiency, but fitting data with varying protein and ligand concentration is able to uniquely determine on and off rates. Experimentally, the ability to measure a transfer efficiency depends on the specific signal to noise, which can always be increased with more scans. In this work, we reliably determine transfer efficiencies on the order of 0.5%. At this sensitivity level, k_{on} needs to exceed 100 M^{-1} s^{-1}, and k_{off} needs to exceed 0.1 s^{-1}. Above these limits, the transfer efficiency is increases with increasing on and off rates. Above these limits, suitable combinations of ligand and protein concentration can give sufficiently different values of transfer efficiency at different mixing times to enable the concentration independent intrinsic relaxation rates to be reliably separated from the concentration dependent parameters that describe the protein/ligand interaction, k_{on} and k_{off} during numerical fitting. Notably, we obtain two physically sensible limits from these simulations. With high k_{off}, the transfer efficiency becomes independent of ligand concentration (green and blue converge), whereas at high k_{on}, the transfer efficiency becomes independent of the overall protein to ligand ratio, L/P (purple and blue converge). In a general case, determining errors in the fitting parameters is sufficient to tell a user whether or not they are well defined. If insufficient ligand/protein concentration dependence has been sampled to accurately determine k_{on} and k_{off}, the numerical uncertainties in these parameters obtained from a bootstrapping procedure will be large.

B) It has been previously proposed that an approximate treatment can be applied to reliably obtain K_D values.(*24, 97*) Applications of this method have resulted in K_D values being significantly underestimated, by orders of magnitude or more, suggesting limitations in this approach.(*98*) By using this approach to fit simulated data, we establish that this method has a very narrow region where it can be considered effective. As has been argued previously,(*97*) a Bloch-McConnell treatment that covers the chemical kinetics and the relaxation processes, exactly as we perform in this work, is the method by which saturation transfer data should be analysed, and with appropriate choices of protein and ligand concentrations, is expected to yield accurate exchange parameters for the range of on and off rates described in (A). In brief, the method described by Angelo et al. determines the initial gradient of the build-up curve. These values are then followed versus ligand concentration to create an isotherm, which is fitted to $A[L]/(K_D+[L])$ to obtain K_D values. Here, we perform this analysis by simulating isotherms with 10 ligand concentrations spaced between 10 μM and 1 mM for a wide range of pairs of K_D and k_{off}. The simulated data is fitted according to the protocol described above, and the per centage error in the fitted K_D versus the simulated K_D is obtained. This fitting method is shown to be effective only in a narrow window of parameter space (black, errors below 10%). These points are roughly described by a locus centred on 50 μM K_D and an off rate of 10 s^{-1}. In the cases encountered in this work, the off rate is determined to be in the

vicinity of 0.1 s^{-1}, a region of parameter space where the expectation for reliable parameters using this method is expected to give, at a minimum errors of 1,000 %. Fundamentally, the assumptions that underpin this method requires that the saturation transfer is proportional to the percentage of bound complex, and the proportionality constant is itself independent of protein/ligand combination. This is reliable only for a narrow region of parameter space. The differences shown here, between 'actual' and 'fitted' K_D demonstrate that 'non-specific binding' is not required to explain the discrepancy.(*98*) The fitting methods described in this work using the Bloch-McConnell equations do not need to make assumptions about the binding regime and provide a reliable and rigorous method to obtain parameters such as k_{on}, k_{off} and K_D.

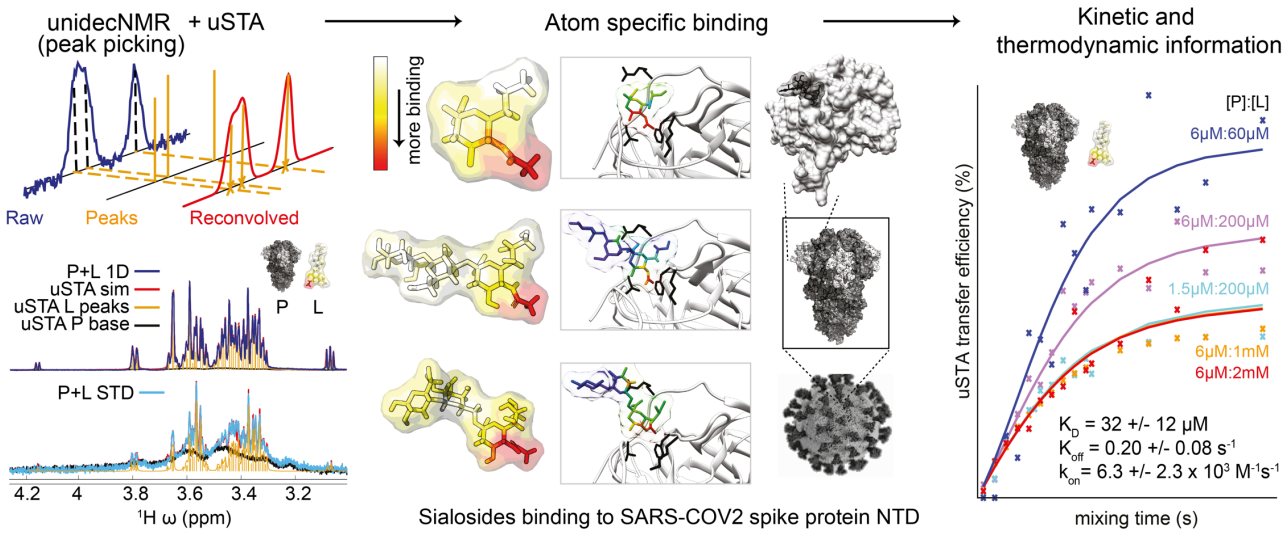

Supplementary Figure S5. The uSTA Concept.

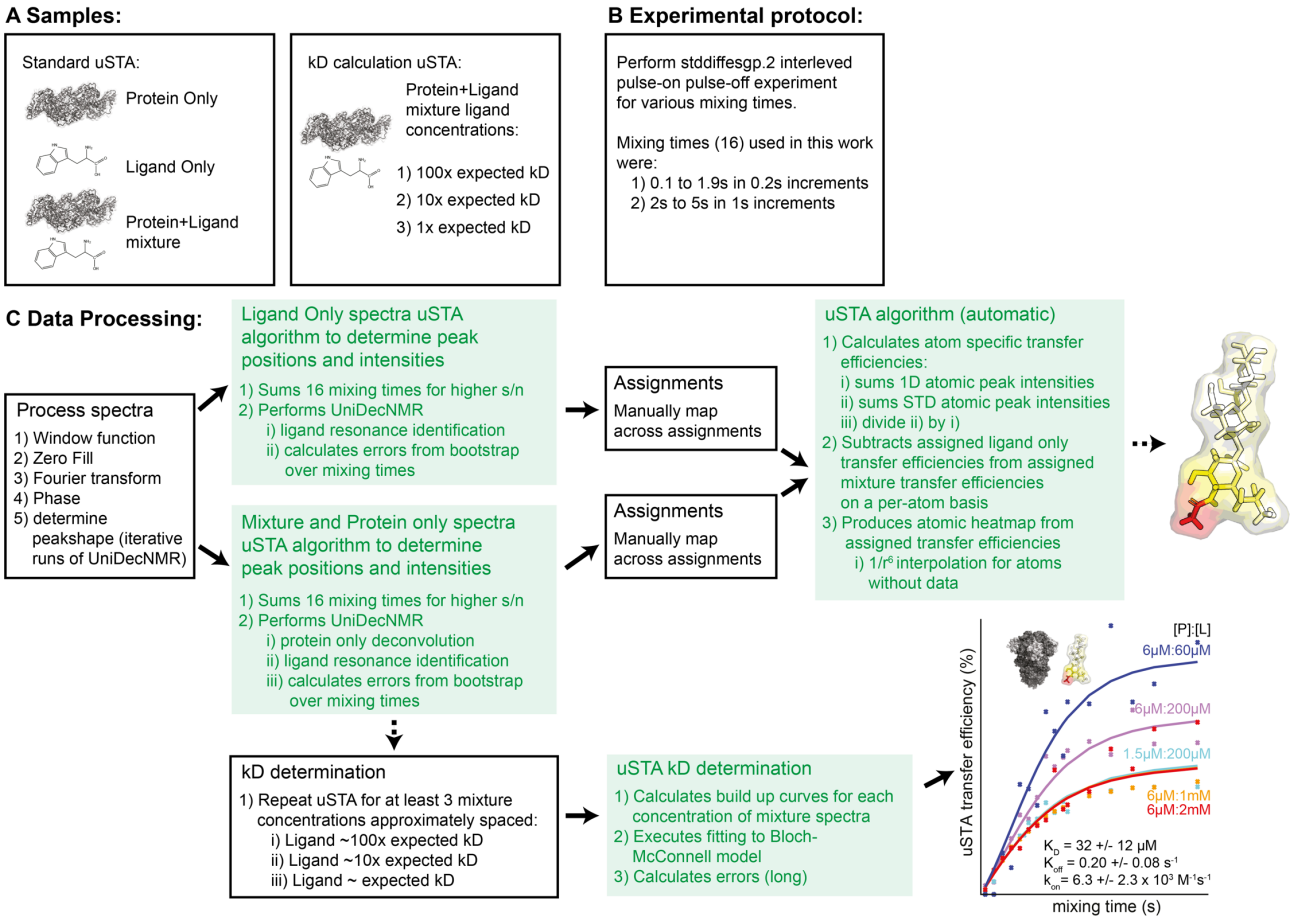

Supplementary Figure S6. Workflow of uSTA. Flowchart describing the specific samples required for a uSTA analysis, and the data processing steps involved. The boxes with a white inlay are the parts that require manual intervention, and the boxes in green show the automated analysis by the uSTA pipeline including figure generation.

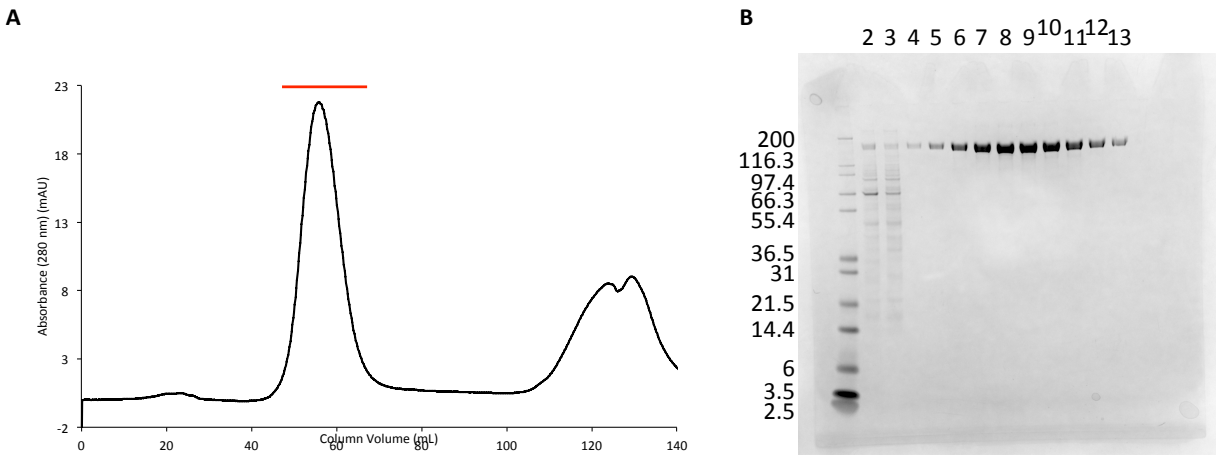

Supplementary Figure S7. Preparation and Purification of SARS-CoV-2 Spike Protein-BAP. **A**: Gel filtration (Superdex S200, GE Life Sciences) profile of Spike-BAP following elution from Ni resin. Elution volume 56.7 mL. Red line denoted fractions analyzed on SDS-PAGE. **B**: SDS-PAGE analysis of Spike-BAP purification. 1 - Mark 12 ladder (labels in kDa); 2 - Load onto Ni column; 3 - Flow through from Ni; 4 - Gel filtration fraction A3; 5 - Gel filtration fraction A4; 6 - Gel filtration fraction A5; 7 - Gel filtration fraction A6; 8 - Gel filtration fraction A7; 9 - Gel filtration fraction A8; 10 - Gel filtration fraction A9; 11 - Gel filtration fraction A10; 12 - Gel filtration fraction A11; 13 - Gel filtration fraction A12. Fractions A3 to A12 were pooled and concentrated to a final volume of 1.6 mL at 7.91 μM.

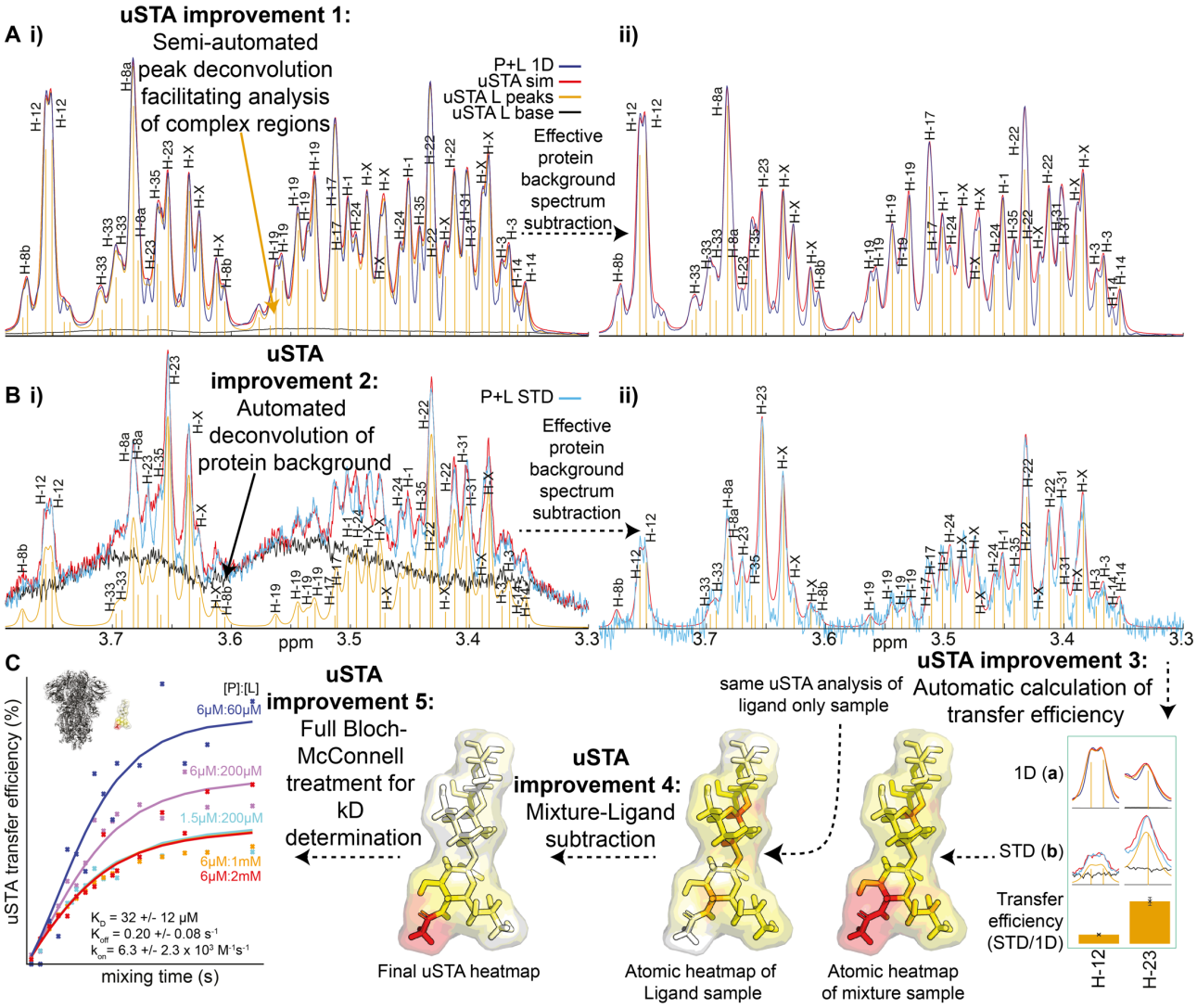

Supplementary Figure S8. Advantages of the uSTA Pipeline, Emphasising Specific Advantages Over A More Conventional Analysis. The UnidecNMR algorithm allows for highly efficient and automated peak detection, including the ability to subtract the protein background. The analysis when combined with a manual assignment of the individual resonances directly computes the transfer efficiencies which when combined with ligand-only data, provide a heat map of the molecule of interest. Finally, where data are available with variable protein/ligand concentrations, the method computes a K_D via a model using the Bloch-McConnell equations.

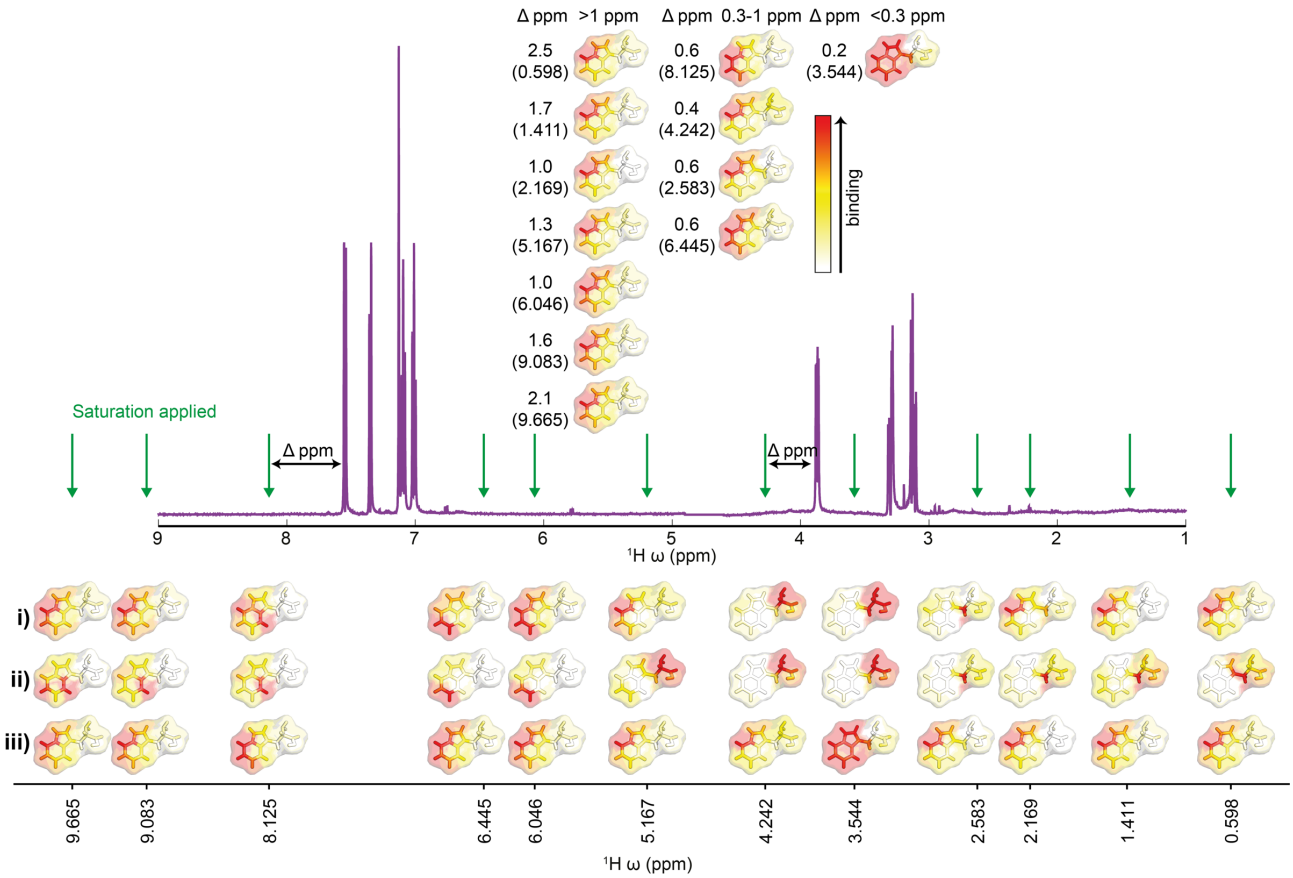

Supplementary Figure S9. The Importance and Reliability of Ligand Subtraction when Calculating uSTA Surfaces [BSA•Trp Examples]. The interaction between BSA and tryptophan was examined while varying the excitation frequency of the saturation pulse. The observed uSTA surface without making a ligand correction was found to vary slightly depending on precisely where (green) the excitation pulse was applied (i). However, an analogous result was observed for a sample containing purely ligand (ii). Subtracting the ligand-only contributions produced highly consistent heatmaps (iii) when the excitation was further than 1 ppm from a ligand resonance (excitation distance is denoted here as Δ ppm). This is because the excitation bandwidth to 95% of the Gaussian pulse cascade with a B1 field of 200 Hz should be ca. 0.3ppm at 600MHz. While this pulse has a narrow bandwidth, there will be some small perturbations to the ligand outside of the expected range. When ligand concentration is much higher than protein, the transfer efficiency due to this residual ligand excitation is constant, and so to a reasonable first approximation we can correct the measurement by subtracting the apparent transfer efficiency measured on the ligand-only sample. As can be seen in the figure, when exciting > 1ppm from the ligand using a pulse whose bandwidth is 0.3 ppm, the final ligand corrected uSTA heat map obtained is invariant to excitation frequency. This implies that the cross relaxation within the protein is highly efficient, as we would expect owing to the high proton density and slow tumbling of the protein, occurring on a timescale faster than the rate require for cross relaxation between ligand and protein. Provided the ligand only results are subtracted from the mixture, and excitation occurs > 1ppm from a ligand resonance, the final surface is largely invariant of the specific excitation frequency, and while it is desirable to move to outside of the bandwidth of the excitation pulse it is important to note that one may still have small residual excitation effects that are well accounted for by ligand subtraction. It is desirable to excite the protein in an area where the spectral density is high (ie overlapping with an area where the protein NMR spectrum shows significant intensity) to maximise the degree of saturation in the protein.

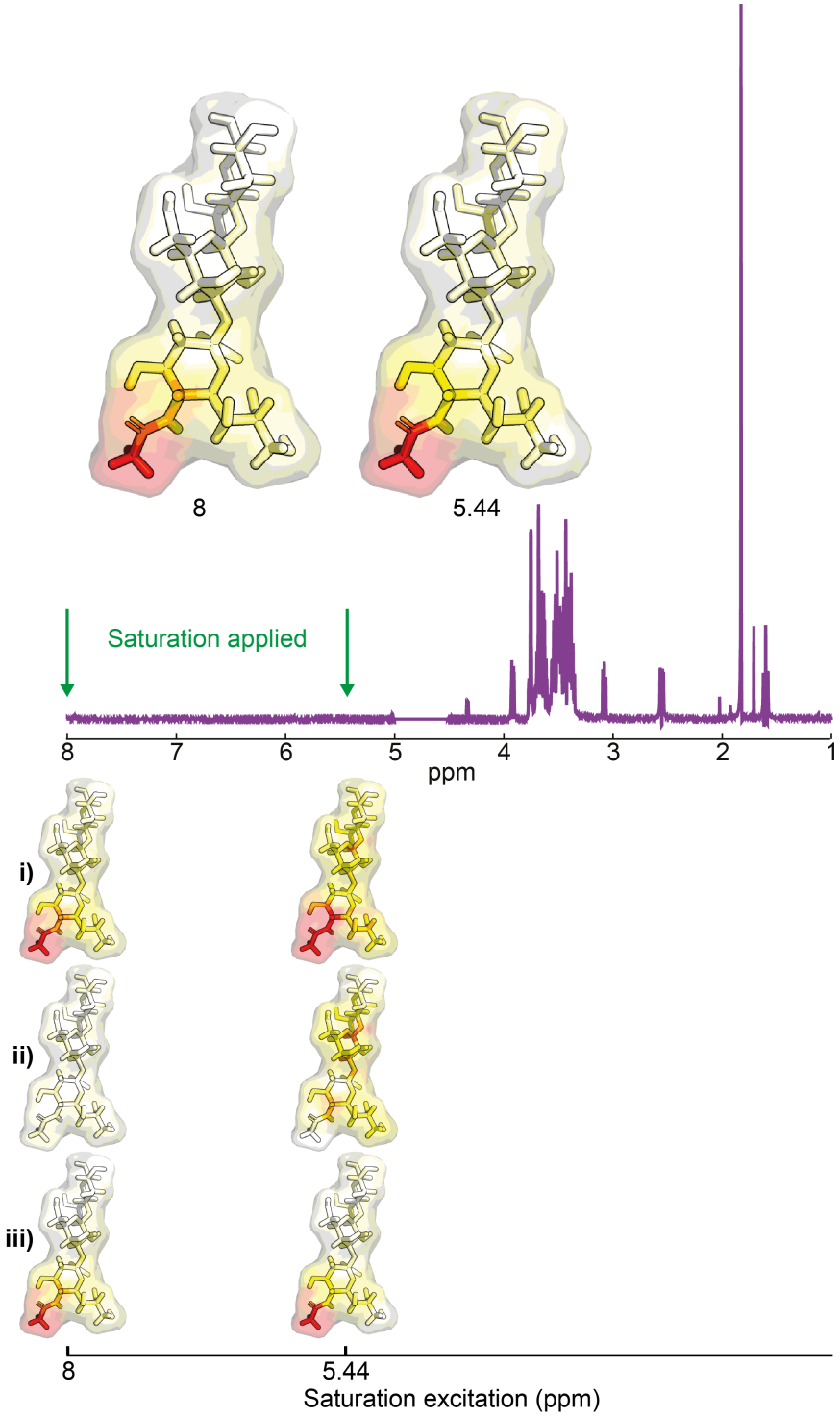

Supplementary Figure S10. The Importance and Reliability of Ligand Subtraction when Calculating uSTA Surfaces [SARS-CoV-2 Spike examples]. The variation of the uSTA surface depending on excitation frequency. uSTA surfaces for **2** were calculated before **(i)** and after **(iii)** subtracting the ligand-only contribution **(ii)**, exciting at 8 ppm (2.7 ppm from a ligand resonance) and at 5.4 ppm (0.3 ppm form a ligand resonance). After subtracting the ligand contributions, the final surfaces are highly similar, a result mirroring our findings for BSA and tryptophan (**Supplementary Figure S9**). Provided one excites >1ppm from a ligand residue with a saturation pulse with this bandwidth and applies the ligand subtraction, the uSTA data will be invariant of excitation location.

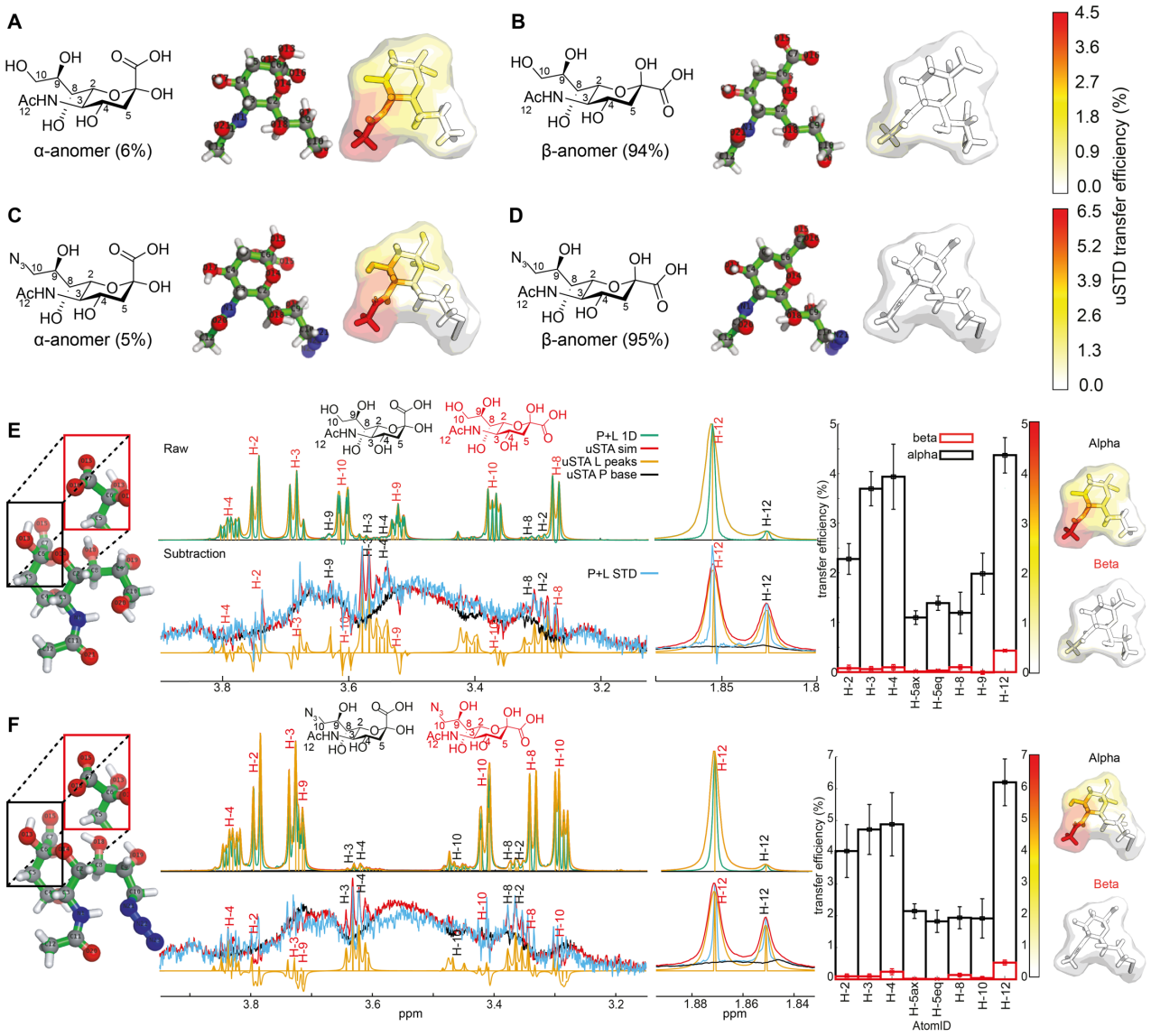

Supplementary Figure S11. uSTA Observes Stereochemical Discrimination in Binding even within Dominated Sugar Ligand Equilibria.

In the spectra of sialic acid (**1**) and azido-sialic acid (**4**), both α and β anomeric forms could be readily identified, with the overall population being dominated by the β form (94 and 95%, respectively). Even despite this strong population difference, application of the uSTA method following assignment of resonances from the two forms allowed determination of binding surfaces simultaneously. Spike shows strong binding preference for the α anomers, as revealed by surfaces (**A**, **C**) even though its population is minor overall; both surfaces were highly similar for these two simpler monosaccharides but closely resemble those of extended trisaccharides **2** and **3** (Figure **3**). While the β form is dominant in terms of population and overall contribution to the 1D NMR spectra, its ability to bind spike (**B**, **D**), and hence its proportional contribution to the difference spectrum, was found to be significantly lower than the α form.

(**E**) For α and β anomers of **1** and **4**. While the 1D spectrum is dominated by the β form of both ligands, the STD spectrum is dominated by the α form. The uSTA surface shows a similar pattern for these, and ligands **2** and **3**, where the NAc from the methyl group and adjacent protons interact most strongly with the protein. Given the low signal intensities for the resonances from the β form, we cannot conclusive demonstrate any binding of the β form from these data.

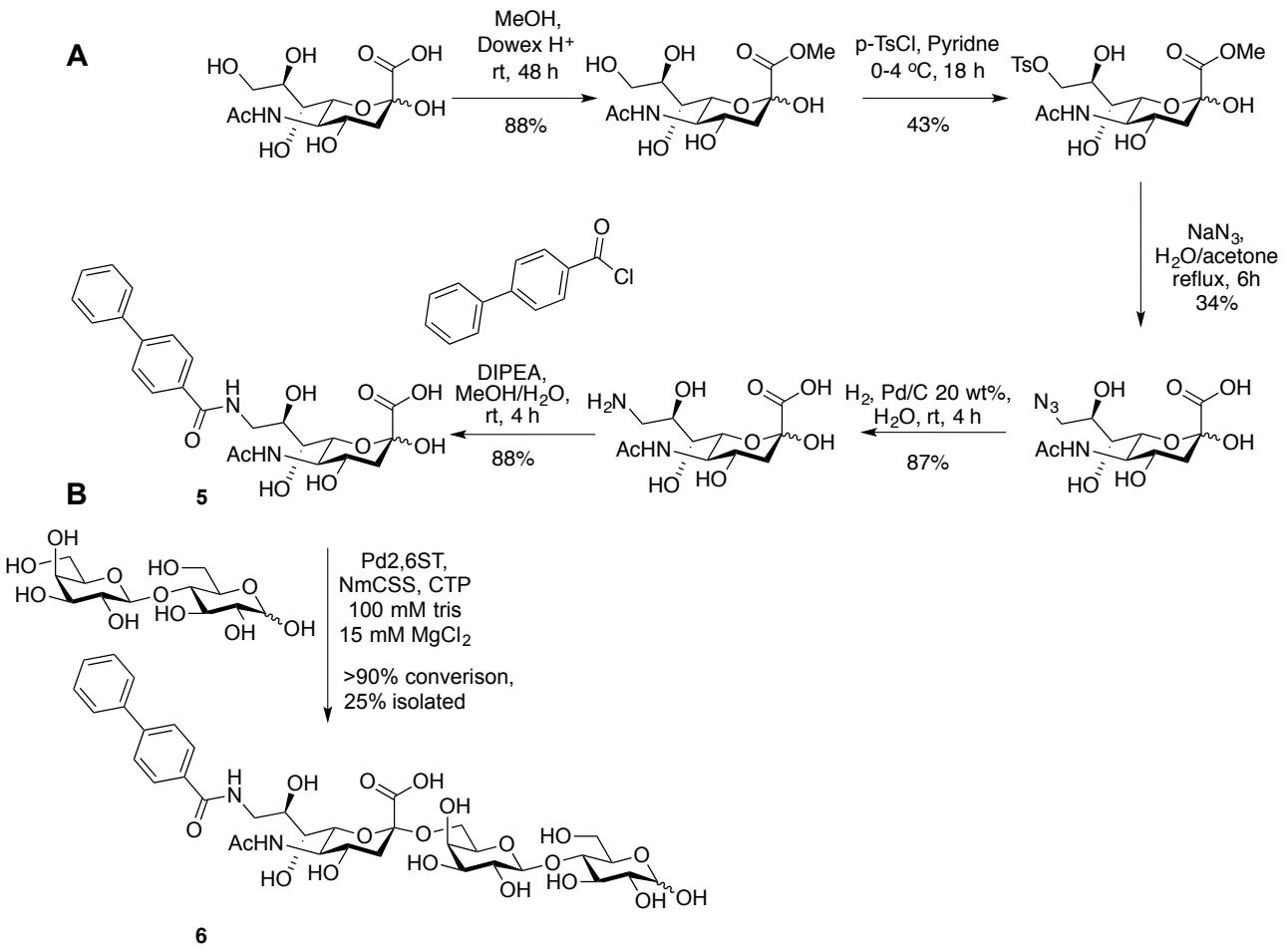

Supplementary Figure S12. Synthetic Routes for Hybrid Sugars 5 and 6. (**A**) Synthesis of BPC-Neu5Ac **5** over 5 steps from Neu5Ac. (**B**) Synthesis of **6** from **5**. See **Supplementary Methods** for full details.

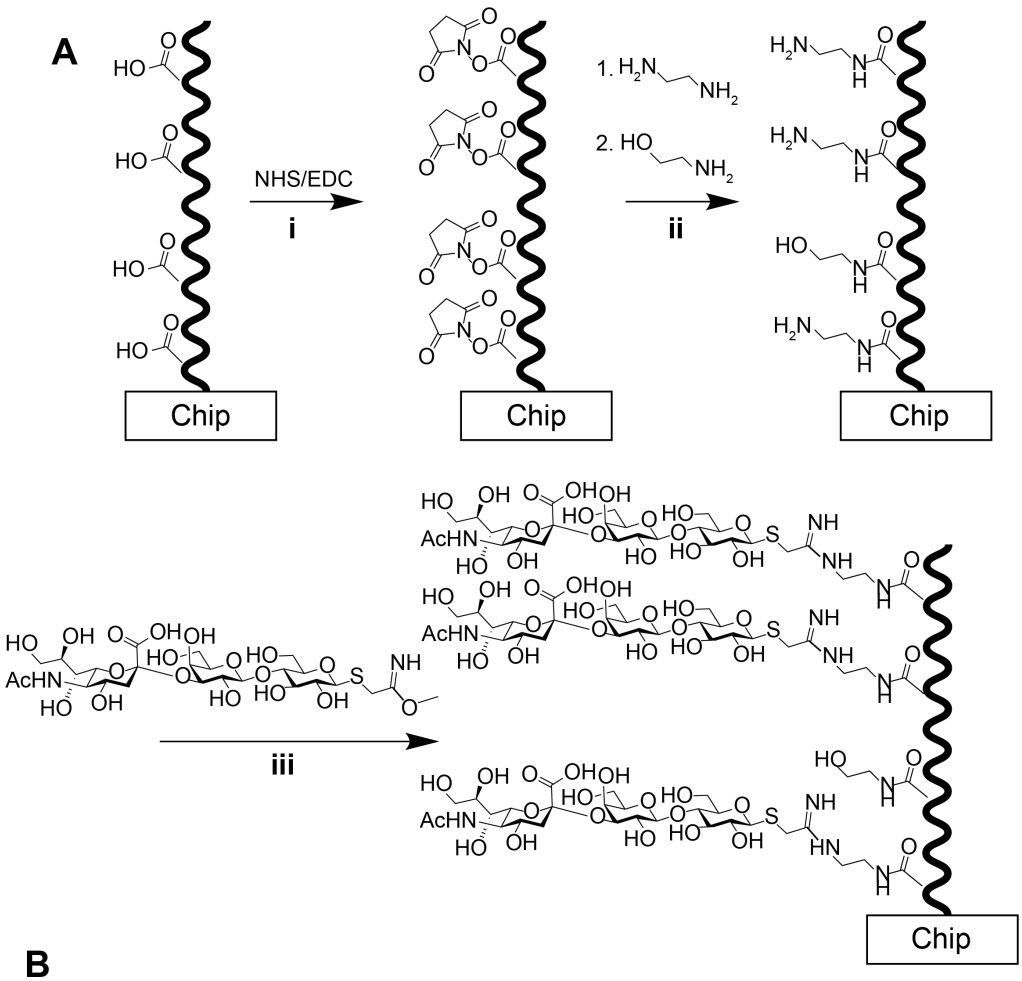
A
NHS/EDC
i
1. H2N NH2
2. HO NH2
ii
iii
Chip
Chip
Chip
Chip

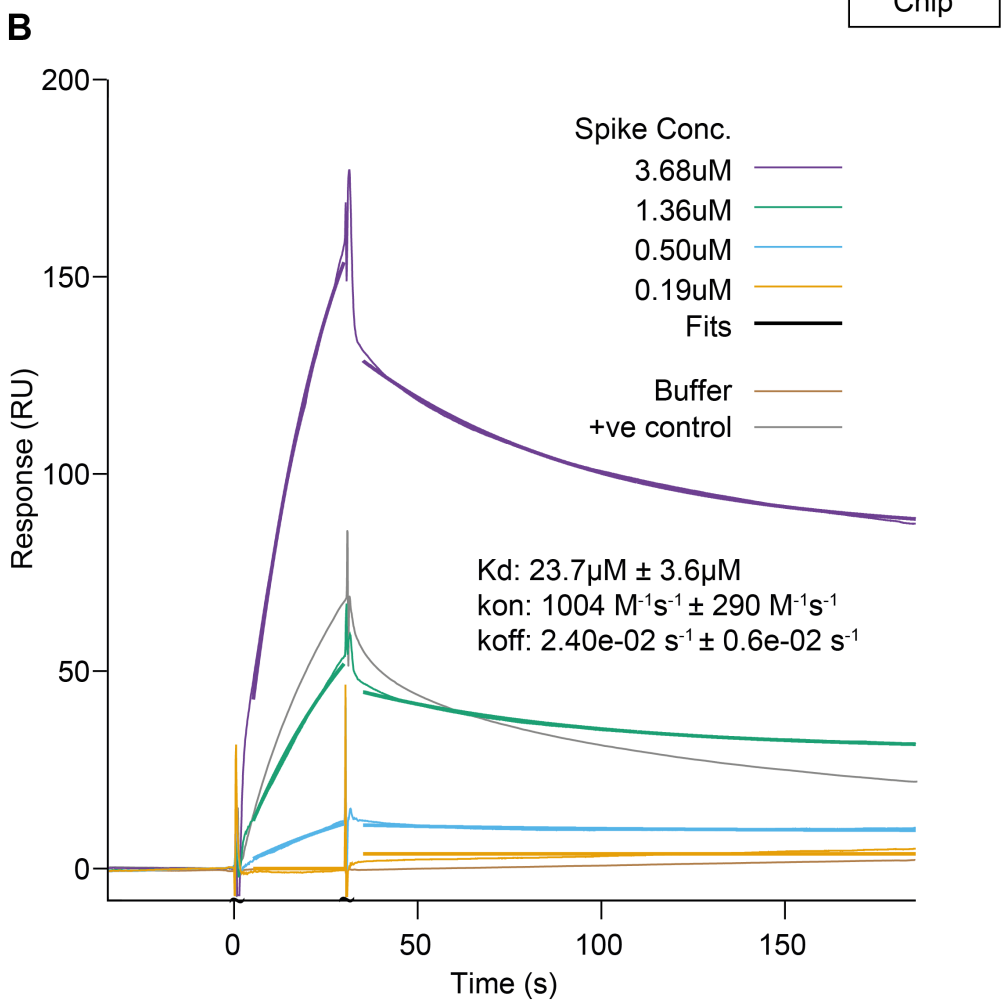
B
Response (RU)
Time (s)
Spike Conc.
3.68uM
1.36uM
0.50uM
0.19uM
Fits
Buffer
+ve control
Kd: 23.7μM ± 3.6μM
kon: 1004 M-1s-1 ± 290 M-1s-1
koff: 2.40e-02 s-1 ± 0.6e-02 s-1

Supplementary Figure S13. Preparation of SPR Chip and SPR Analysis. A) Immobilisation of **2** onto carboxymethylated SPR sensor chip. A carboxymethylated CM5 sensor chip was activated with N-hydroxysuuccinimide (NHS) and *N*-ethyl-N′-(3-dimethylaminopropyl)carbodiimide hydrochloride (EDC•HCl) and subsequently coupled to ethylenediamine followed by blocking of unreacted esters with ethanolamine. In order to introduce the sugar, a solution of SiaLac-IME was then injected into the flow cell, where it reacts with the surface bound free amines generating an amidine linkage to the glycan (SiaLac-Chip). Specifically, in step **i**, a CM5 chip activated with NHS (50 mM) and EDC (200 mM) 10 min at 10 µL/min. In step **ii**, ethylenediamine (1 M) was injected to functionalise chip with free amine groups for 7 min at 10 µL/min. Then ethanolamine (1 M) was injected over 10 min to block any unreacted NHS activated esters at 10 µL/min. In step **iii**, SiaLac-IME reagent **10** (5.6 mM) was injected over 10 min at 10 µL/mL followed by washing with HBP-EP buffer (wash steps with buffer between each step and during sensor equilibration).
B) Binding curves and fitted binding curves of spike at (3.68, 1.36, 0.50 and 0.19 µM) with 30 s association and 150 s dissociation at 16 ˚C, with a positive control (anti-SiaLac mouse serum) and corrected by subtracting BSA negative control. When accounting for background, the binding curves could be fitted to calculate apparent k_{on} and k_{off} rates at each spike concentration giving K_D = 23.7 µM ± 3.6 µM ; k_{on} = 1004 $M^{-1}s^{-1}$ ± 290 $M^{-1}s^{-1}$; k_{off} = 0.024 s^{-1} ± 0.06 s^{-1} from a global analysis of all 4 binding curves.

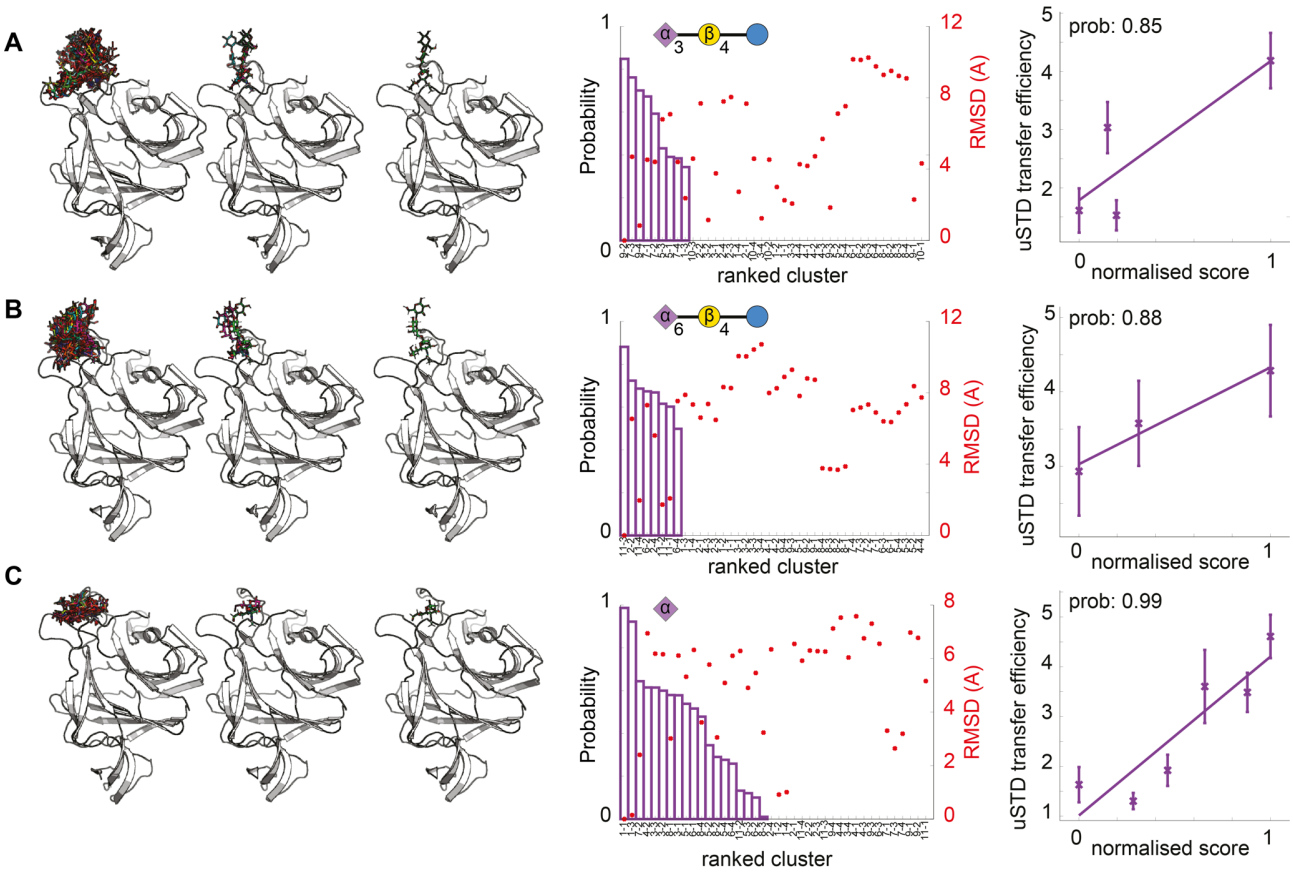

Supplementary Figure S14. Combination of uSTA with HADDOCK Allowed Ranking of Docked Model Ensembles. A) A series of models describing the interaction between relevant sugars and spike were calculated using HADDOCK2.4 following standard methods (see **Supplementary Methods**). The docking resulted in 13 clusters ranked by the score of their top four models (i). After comparison to the NMR data, the top 4 members of all clusters were scored based on uSTA data, which allowed selection of 3 very similar models showing excellent agreement with the data (ii) of which the top scorer is shown (iii, main text **Figure 5**). The interactions between Sia2,3Lac and the protein are highly similar for the sialic acid moiety for the top scoring models, with variation occurring predominantly in the flexible Glc residue that has relatively little interaction with the protein. **B)** For each proton in the ligand, the following score was calculated through summing all adjacent protons from the protein: $(\langle 1/r^6 \rangle)^{\wedge(1/6)}$. Thus any proton in close proximity to a large number of protons from the protein will receive a high score. This score is expected to correlate with the cross-relaxation rate between the protein and the ligand,(*99*) and so a high score should correlate with a high transfer efficiency, as measured using STD NMR spectroscopy. The Pearson 'R' correlation coefficient was calculated for each model for the correlation between the score for each atom in the ligand and converted to a probability that the correlation is not generated through random noise,(*100*) and the transfer efficiency, for the atoms with the highest transfer efficiencies (mapped to 5 heteroatoms, atoms 22,23,24 (Sia) 14 (Gal) and 42 (NAc)). The top-scoring model was an outlier, with a probability level of 98% making it statistically highly significant. The top three models form a cluster of models with a probability >90%, with all falling within 2Å all atom RMSD relative to the model with the highest R value (calculated with the proteins aligned). **C)** The correlation plots between a normalised score and the % transfer efficiency from the uSTA data for the best model (green, i, P(r)=98%), and two excluded models with P(r) values of 75% (blue, ii) and 39% (orange, iii) respectively. Qualitatively, the correlation line passes through the error bars of the selected models (P(r)>90%) and does not for the models that were excluded. Overall, all the top scoring models indicate highly similar interactions between the sialic acid and the protein, and they all predict that the NAc methyl group should be located in the vicinity of the highest proton density from the protein, in agreement with the measurements.

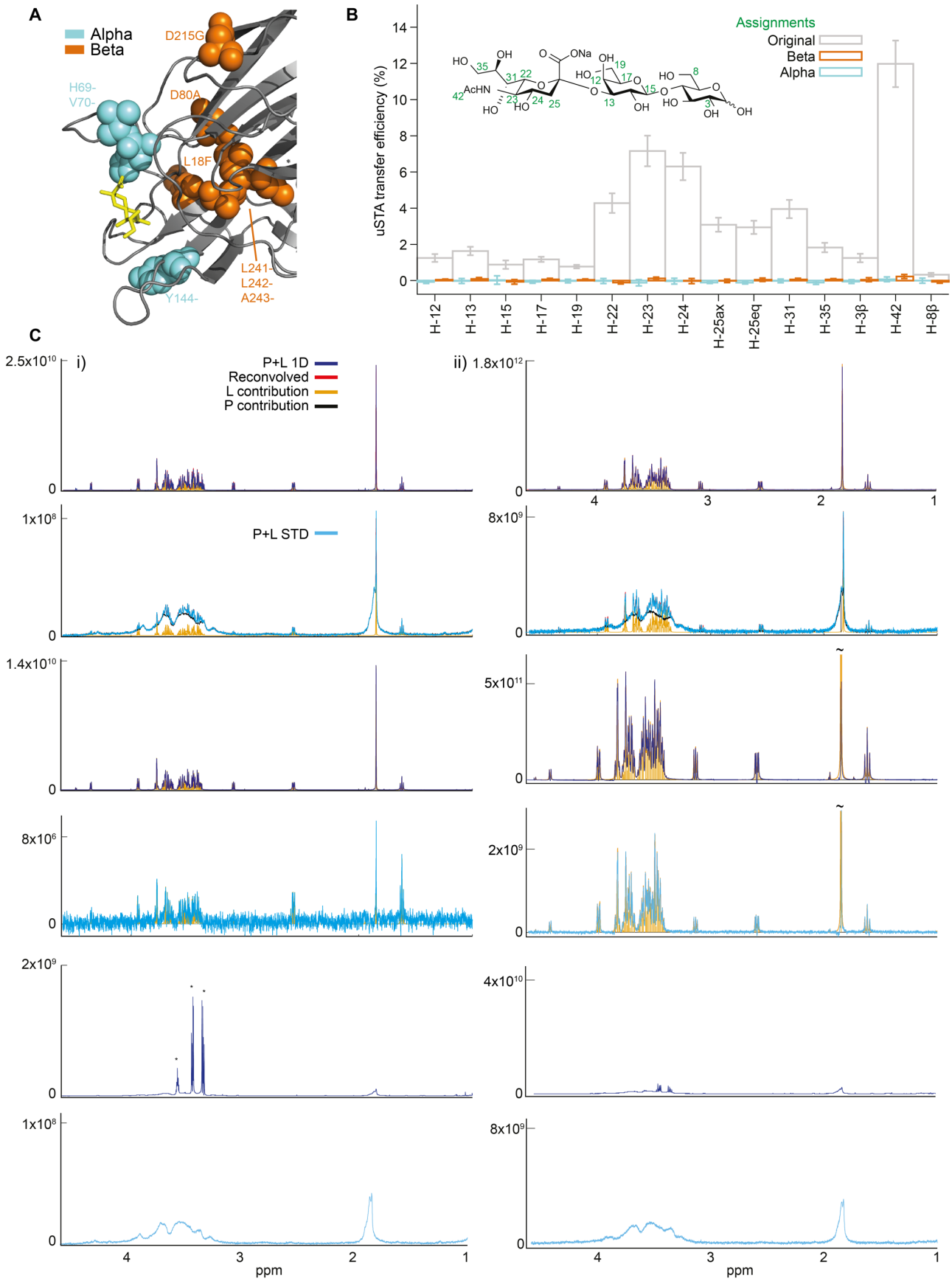

Supplementary Figure S15: uSTA Analysis of Spike from Variants of Concern. A) Sialic acid binding pocket indicating site of B.1.1.7 and B.1.351 mutations. **B**) atom specific binding comparison of the three variants showing greatly diminished binding in the B-lineage variants. **C**) raw data for B.1.351 (i) and B.1.1.7 (ii), showing mixture 1D, STD, ligand 1D, STD and protein 1D and STD.

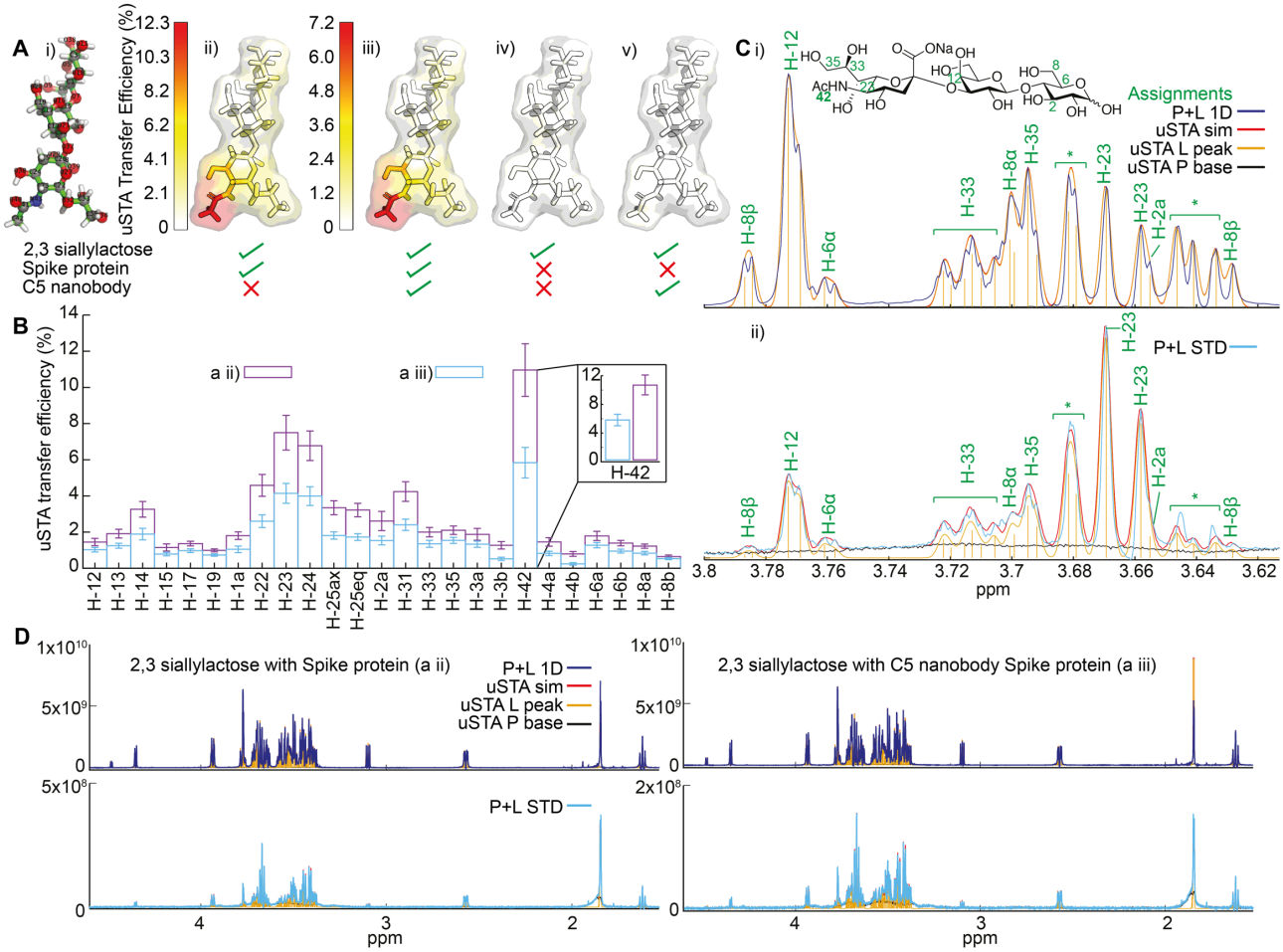

Supplementary Figure S16: Effects Upon Sialoside Binding of the RBD-Blocking Neutralizing C5 Antibody. A i) a wireframe with atom specific numbering **ii)** heatmap showing the uSTA binding of 2,3 sialyllactose to the SARS-CoV-2 Spike protein **iii)** heatmap showing an almost identical binding pose, but mediated transfer efficiency of the C5 nanobody-bound spike protein **iv)** heatmap showing essentially no uSTA response from 2,3 sialylactose without spike or C5 nanobody present, **v)** heatmap showing essentially no uSTA response from 2,3 sialyllactose with C5 nanobody present but no spike protein. **B**) the uSTA transfer efficiencies of 2,3-sialyllactose in spike and spike and nanobody systems. **C i)** a section of a 1-H spectrum of 2,3-sialyllactose with SARS-CoV-2 Spike protein. **C ii)** difference spectrum of 2,3-sialyllactose with SARS-CoV-2 Spike protein. The assignments are marked in green. * indicates a region with unassignable overlap. **D**) the reference spectra and difference spectra for mixtures without and with C5 nanobody

A

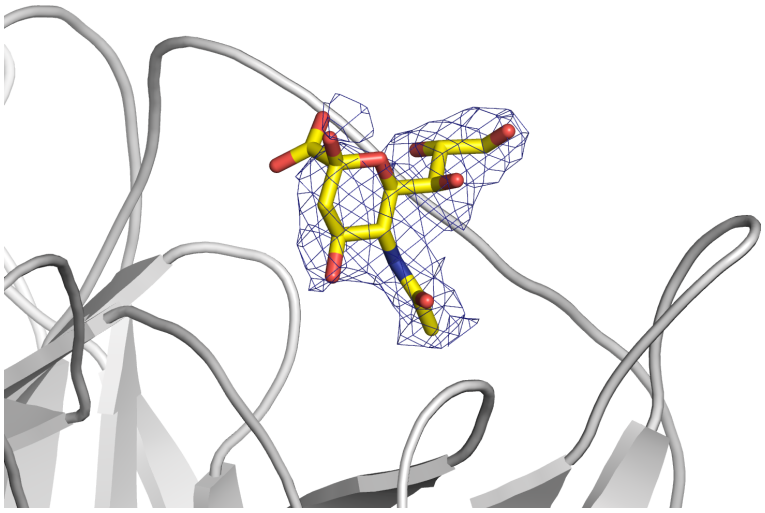

B

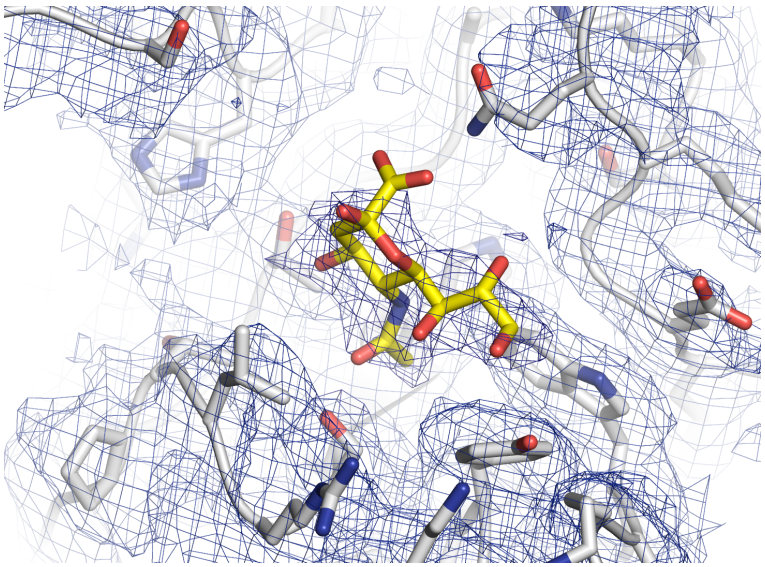

C

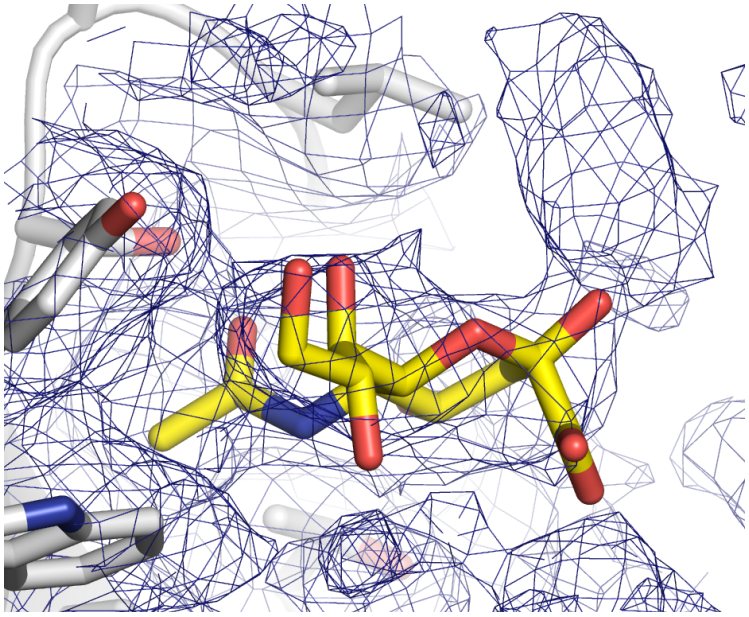

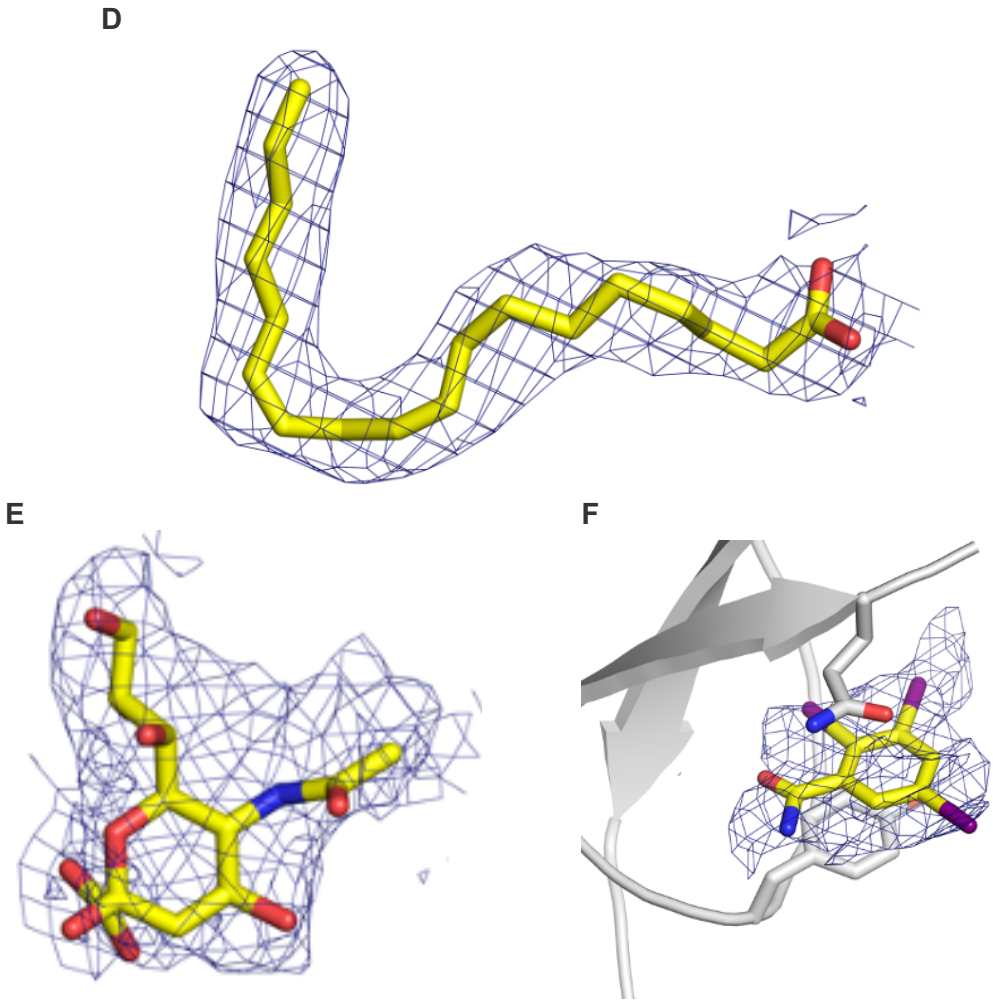

Supplementary Figure S17: Cryo-EM Coulombic Maps. A. Map for the sialoside acid portion, countered at 2.1 σ. **B.** Map at 2.6 σ showing the sugar is comparably ordered to the protein. **C.** Map for the sialic acid portion, countered at 1.6 σ, suggests evidence for galactoside moiety. **D.** Coloumbic map for the linoleic acid contoured at 4 σ. **E,F** Using EMDA(*101*) the map from the native structure was subtracted from the soaked structure. The result difference map has positive residual density where there is additional density in the map from the soaked molecule. **E**. The sialic acid molecule shown in its final place with the difference map contoured at 4 σ. **F**. The tri-iodo species shown in its final place with map contoured at 12 σ.

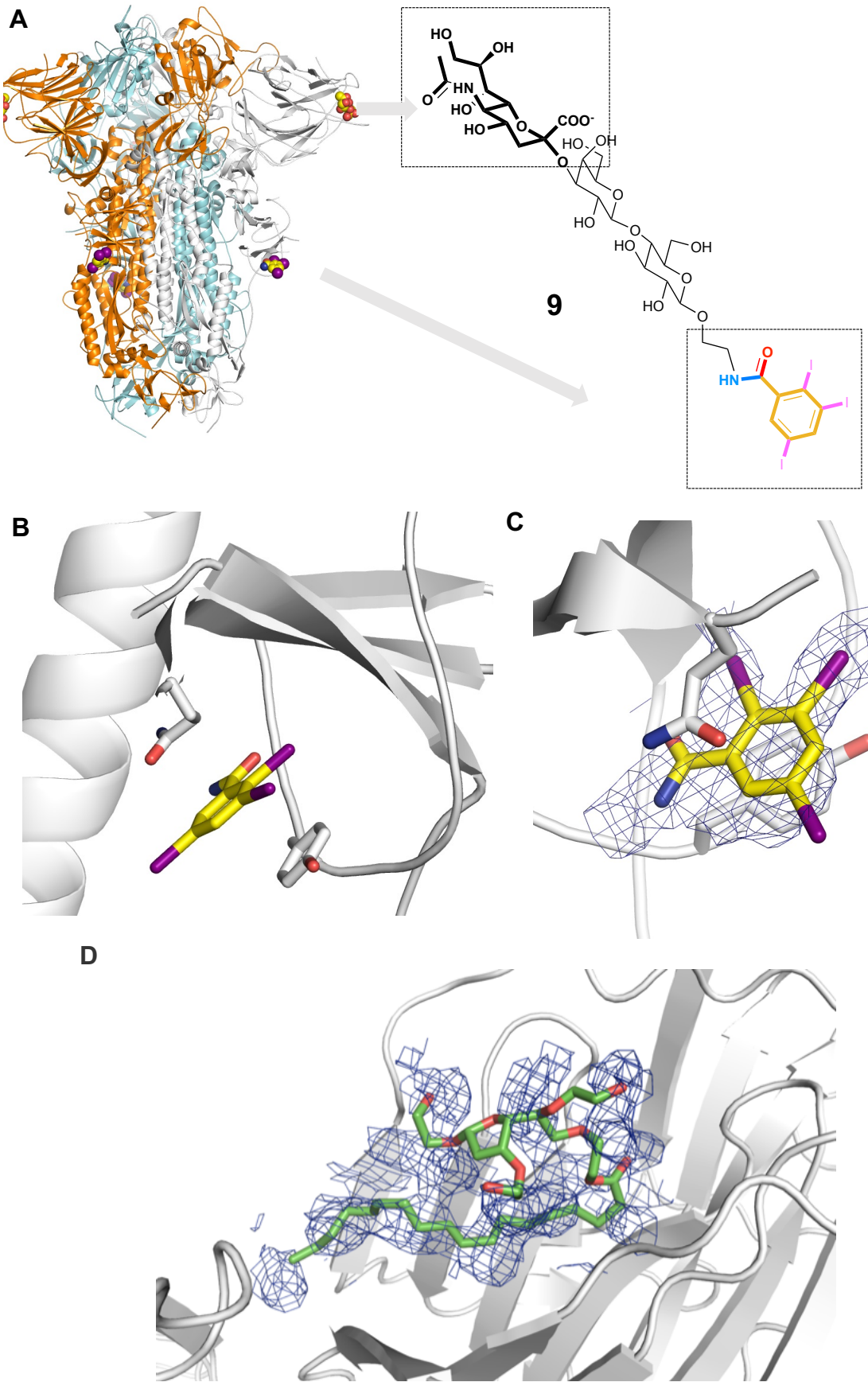

Supplementary Figure S18: Cryo-EM Confirms Additional Binding Mode for Aromatics in a Distinct Region of Spike. Location of the iodobenzamide moiety of **9** in comparison to the sialoside moiety of **9** in spike. **B.** Close-up view of the interactions of the iodobenzamide moiety

with protein. **C.** Coloumbic map for the ligand contoured at 4 σ. **D.** A previous study(*102*) showed clear density for polysorbate (RCSB 7jji) bound to a pocket in the N-terminal domain. A superposition of RCSB 7jji into the map we obtained from the soaked molecule, shows that polysorbate is not well fitted by the additional density that we have observed in this pocket. Consequently we did not include polysorbate in our model. The map is contoured at 4 σ. We have been unable to unambiguously identify the molecule(s) that gives rise to this density.

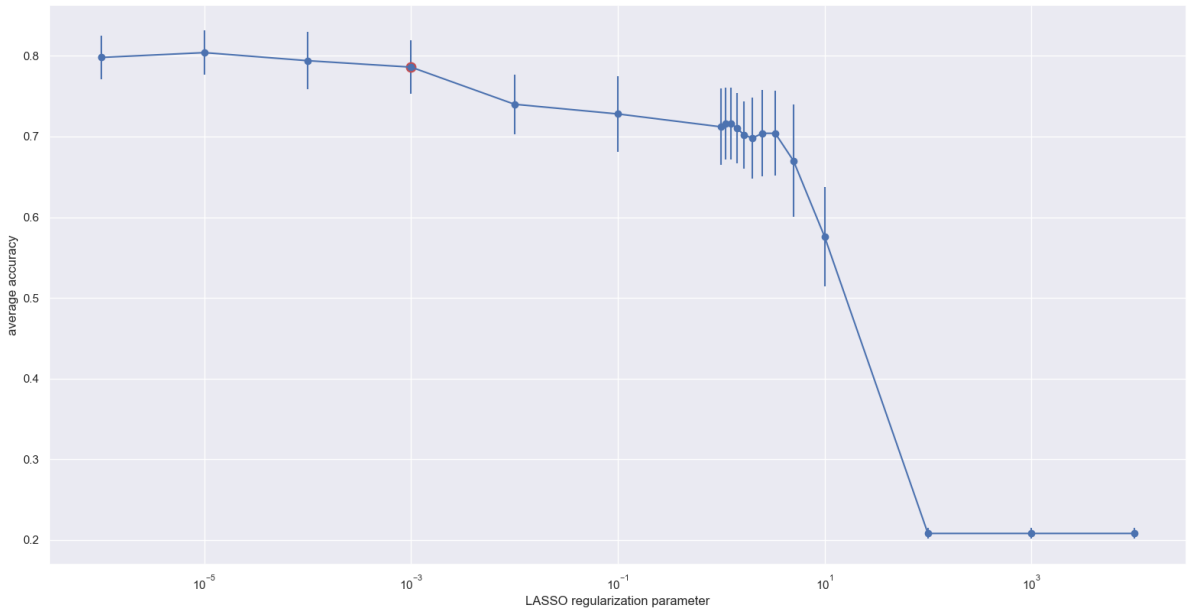

Supplementary Fig. S19. LASSO Regularization Profile of Clinical Data. Relevant genes for COVID-19 variability are discovered with a feature selection procedure based on the LASSO logistic regression model predicting the severity of the disease on the basis of the patient's genetic information. In the plot, the trade-off between the logistic regression model's accuracy (y-axis) and the model's simplicity (x-axis) are related to the number of input genes selected by the model. The data point highlighted in red corresponds to the optimal LASSO regularization parameter chosen for the fitting procedure. The parameter was selected as the most parsimonious value (low number of genes) providing an average score closer than one standard deviation from the highest score.

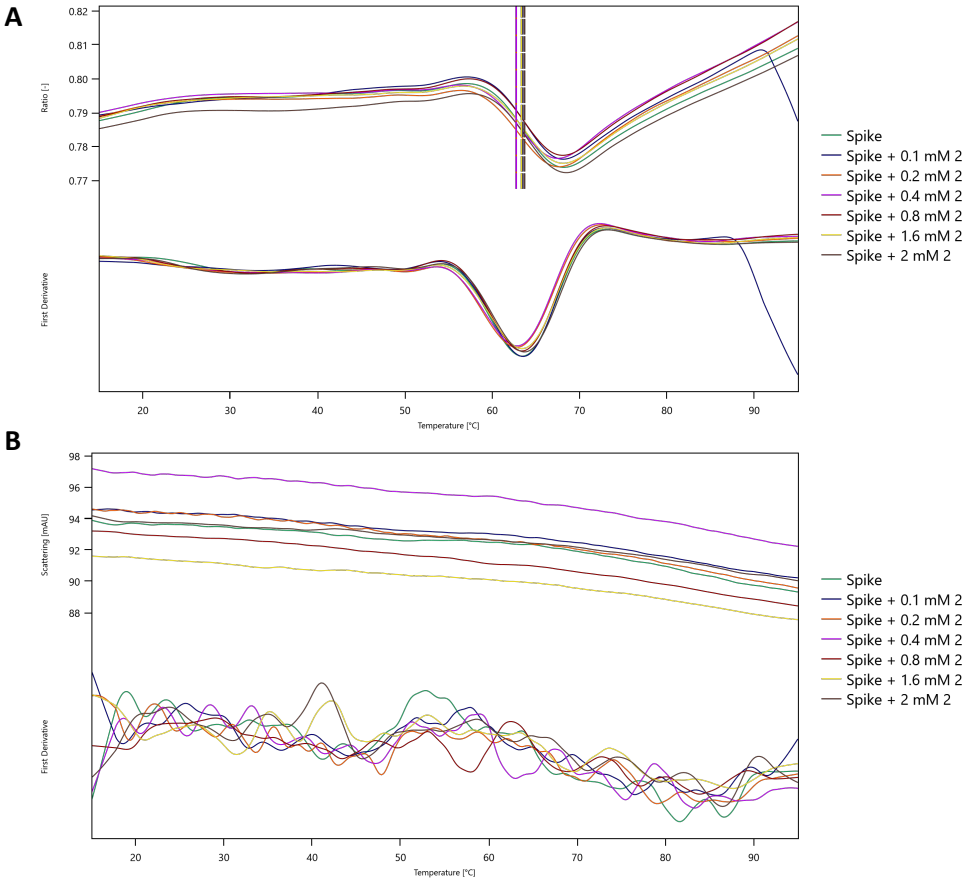

C

Sample	T_m (°C)
Spike	63.4
Spike + 0.1 mM 2	63.5
Spike + 0.2 mM 2	62.8
Spike + 0.4 mM 2	62.8
Spike + 0.8 mM 2	63.3
Spike + 1.6 mM 2	63.3
Spike + 2.0 mM 2	63.6

Supplementary Figure S20. **Thermal Denaturation Analysis.** Of SARS-CoV-2-spike in the presence of different concentrations of trisaccharide **2**. **A**: Fluorescence ratio at 330/350 nm, indicating the melting temperature of the protein. No significant change in melting temperature is seen in the presence of increasing concentration of trisaccharide **2**. **B**: Light scattering of Spike-BAP observed at increasing concentrations of trisaccharide **2**, used to give an indication of protein aggregation. No aggregation of Spike-BAP is seen at increasing concentrations of different concentrations of trisaccharide **2**. **C**: Melting temperatures of Spike-BAP in the presence and absence of different concentrations of trisaccharide **2**.

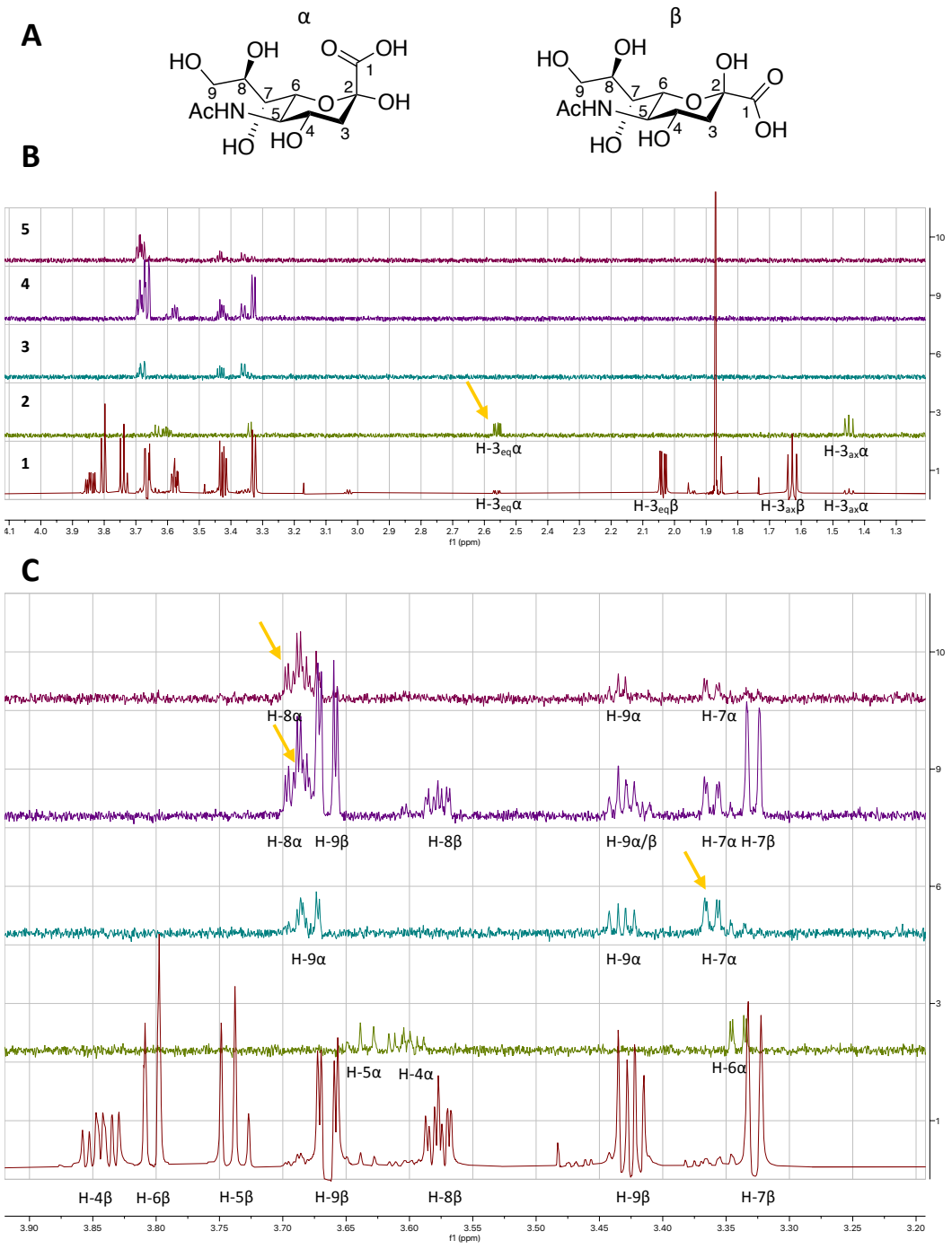

Supplementary Figure S21. Manual Assignment of Alpha Anomer of Neu5Ac. A) Alpha and beta anomers of Neu5Ac with atom numbers labelled. **B)** Overlays of proton and 1D TOCSY spectra indicating H-3 beta positions which can be observed easily in the ^{1}H proton (**1**) and H-3 alpha positions which can be seen in the 1D TOCSY (**2**). Irradiated frequencies- **2**= 2.550 ppm, **3**= 3.361 ppm, **4**= 3.680 ppm, **5**= 3.695 ppm (indicated as yellow arrows on spectra). **C)** Assigned peaks corresponding to alpha and beta anomers. Peaks were assigned by following coupling constants for each proton around the sugar ring.

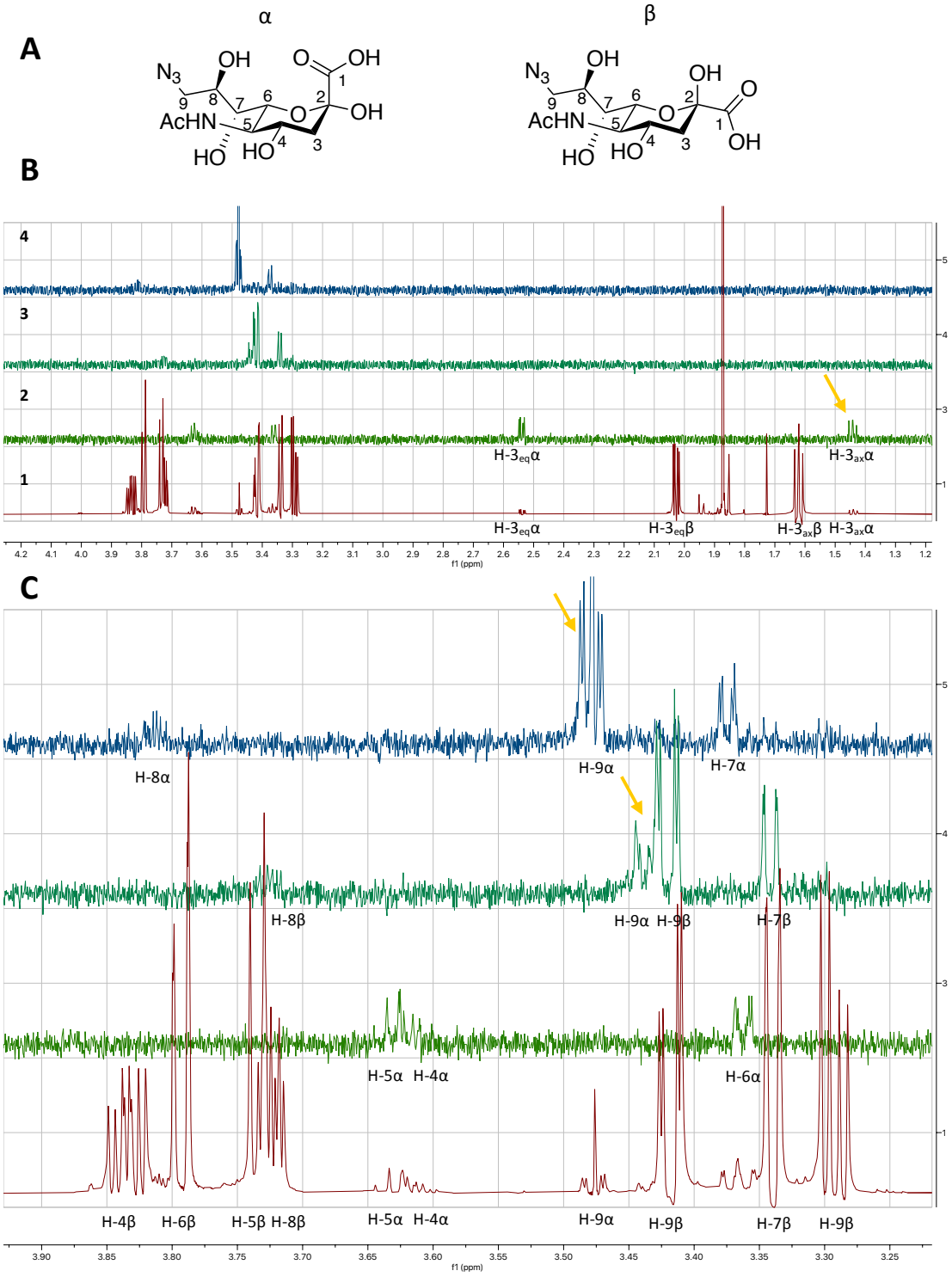

Supplementary Figure S22. Manual Assignment of Alpha Anomer of 9-azido-Neu5Ac. A) Alpha and beta anomers of 9-azido-Neu5Ac with atom numbers labeled. **B**) Overlays of proton and 1D TOCSY spectra indicating H-3 beta positions which can be observed easily in the ^{1}H proton (**1**) and H-3 alpha positions which can be seen in the 1D TOCSY (**2**). Irradiated frequencies- **2**= 1.438 ppm, **3**= 3.442 ppm, **4**= 3.477 ppm (indicated as yellow arrows on spectra). **C**) Assigned peaks corresponding to alpha and beta anomers. Peaks were assigned by following coupling constants for each proton around the sugar ring.

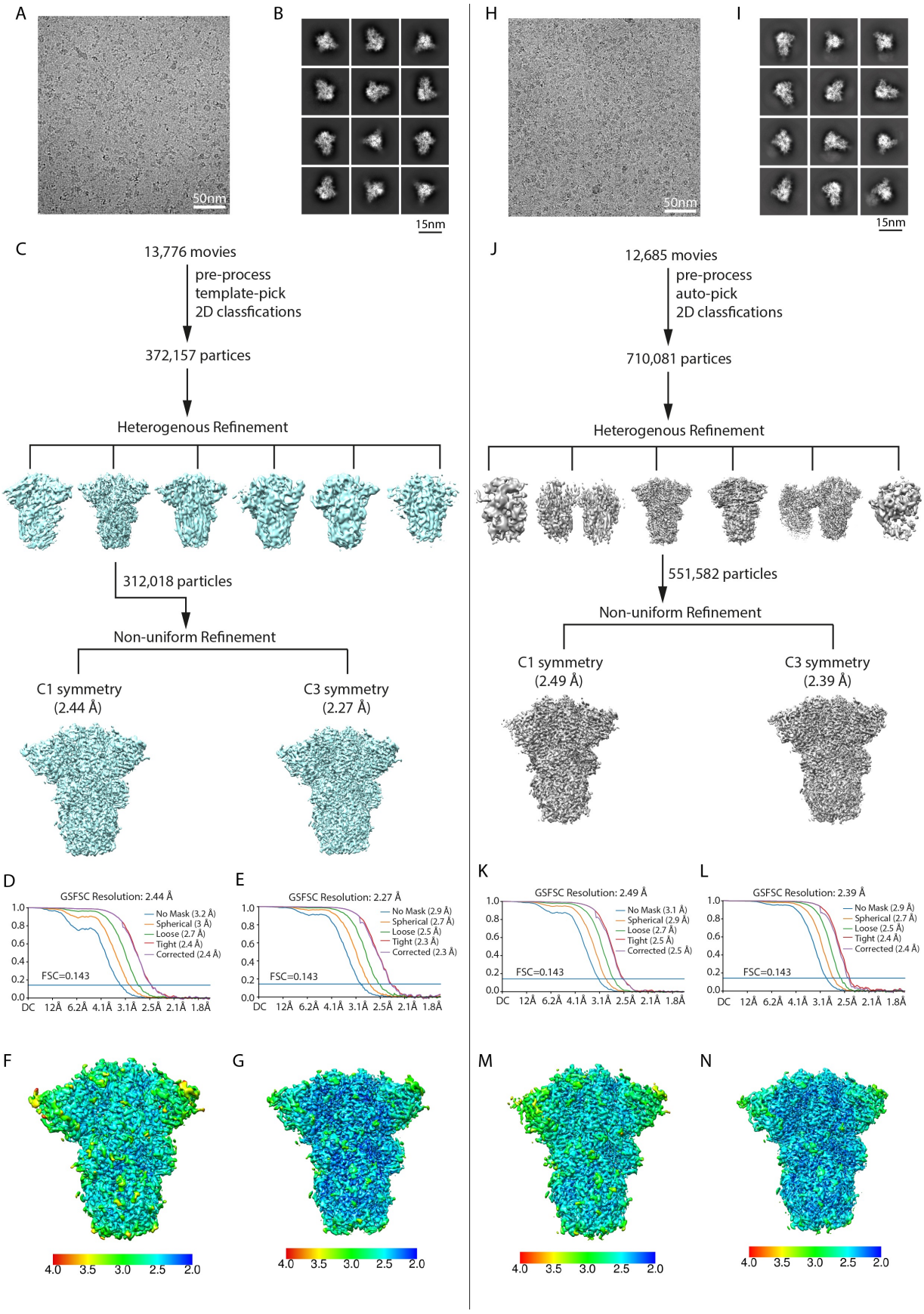

Supplementary Figure S23. Cryo-EM analysis of SARS-CoV-2 spike proteins.
(A-G) Cryo-EM analysis of SARS-CoV-2 spike with ethylbenzamide-triiodo siallyllactose. **A)** Representative micrograph recorded by K2 detector. Scale bar = 50 nm. **B)** Representative 2D

class averages. Scale bar = 15 nm. **C)** Overview of cryo-EM data collection and image processing workflow. **D-E)** FSC curves of SARS-CoV-2 spike with ethylbenzamide-triiodo siallyllactose at C1 **(D)** and C3 **(E)** symmetry. F-G) Local resolution estimation of SARS-CoV-2 spike with ethylbenzamide-triiodo siallyllactose at C1 **(F)** and C3 **(G)** symmetry.
(H-N) Cryo-EM analysis of native SARS-CoV-2 spike. **H)** Representative micrograph recorded by K2 detector. Scale bar = 50 nm. **I)** Representative 2D class averages. Scale bar = 15 nm. **J)** Overview of cryo-EM data collection and image processing workflow. **K-L)** FSC curves of native SARS-CoV-2 spike at C1 **(K)** and C3 **(L)** symmetry. **M-N)** Local resolution estimation of native SARS-CoV-2 spike at C1 **(M)** and C3 **(N)** symmetry.

Supplementary Tables

Supplementary Table S1. COVID-19 Cohort
Supplementary Table S2. *B3GNT8* and *LGALS3BP* genetic variants
Supplementary Table S3. *B3GNT8* chi-square five categories
Supplementary Table S4. *B3GNT8* chi-square 2x2
Supplementary Table S5. *LGALS3BP* chi-square five categories
Supplementary Table S6. *LGALS3BP* chi-square 2x2
Supplementary Table S7. Raw data and UniDecNMR fits used to calculate the uSTA surfaces shown in the manuscript.

[see also Methods section for **Supplementary Tables S8-12**]

As separate xlsx:

Supplementary Table S1. COVID-19 Cohort
Supplementary Table S2. *B3GNT8* and *LGALS3BP* genetic variants
S**upplementary Table S3.** *B3GNT8* chi-square five categories
Supplementary Table S4. *B3GNT8* chi-square 2x2
Supplementary Table S5. *LGALS3BP* chi-square five categories
Supplementary Table S6. *LGALS3BP* chi-square 2x2

Supplementary Table S7: a-i). Raw data and UniDecNMR fits used to calculate the uSTA surfaces shown in the manuscript. For each protein/ligand combination, the uSTA transfer efficiency surfaces were calculated from the protein only, ligand only and mixture STD datasets. A variety of impurities (*) were observed in the various spectra and were accounted for during analysis as described below. Small resonances coming from impurities are commonly detected in 1D ^{1}H NMR spectra. For the most part, these were of low intensity and did not overlap with the ligand resonances. In two cases, impurities were detected perhaps from cryoprotectants used during the protein preparation, and their concentration was sufficiently high that the underlying ligand resonances could not be resolved. In each spectrum, the symbol ~ indicates where intensity has been cut-off, in order to scale the spectrum so that resonances of low dynamic range can be clearly discerned.
The specific impurities encountered across the various spectra are tabulated below, together with a summary of their individual effects on the spectra.

	^{1}H chemical shift	**Features**	**Present in**
I1	1.71 ppm (s)	Negative STD when excited at 5.4 ppm or 8 ppm	a) mixture, protein b) mixture, protein only c) ligand only, mixture d) ligand only, mixture e) all f) all g) ligand only
I2	7.93 ppm (d)	Positive STD ligand only at 8 ppm, no STD when excited at 5.4 ppm	a) ligand only, mixture b) ligand only
I3	Glycerol intense peaks: 3.46 ppm (dd), 3.37 ppm (dd), 3.57-3.62 ppm (m)	Negligible STD when excited at 5.4 ppm	b) mixture
I4	2.02 ppm (s)	Negligible STD when excited at 5.4 ppm	a) protein only c) protein only d) protein only
I5	3.16 ppm (s)	Negative STD when excited at 5.4 ppm	c) mixture, ligand only
I6	3.536 ppm (s), 3.45-3.497 ppm (q)	Positive STD at 5.4 ppm	e) mixture
I7	3.42 ppm (dd), 3.26 ppm (dd)	No STD	g/h/i) protein only, mixture
I8	3.8 ppm (s)	No STD	g/h/i) ligand only
I9	0.98 ppm (d)	No STD	g/h/i) protein only, mixture

a) 2,3-sialyllactose and SARS-CoV-2 Spike Protein
Mixture 1 & 2, Ligand 2, Protein 1 & 4: no overlap with ligand, zero impact on analysis.
b) 2,6-sialyllactose and SARS-CoV-2 Spike Protein
Mixture 1, Ligand 2, Protein 1: no overlap with ligand, zero impact on analysis.
Mixture 3: Glycerol coming from protein batch used. Due to its high intensity (the intensity is 10x higher than the resonances from the ligand), the region was excluded.
Excluded atoms: 24, 31, 13, 14, 2β, 1β, 6β, 3α, 1α
We would expect an appreciable STD response for 24 and 31, and close to zero for the others. We can see evidence for this in the spectrum, but we can cannot accurately quantify due to the large glycerol resonance that covers this region. While we have no measurement of 24 and 31, we have

measurements of the surrounding protons which we can use to reasonably interpolate these values (see Methods).

c) Sialic acid and SARS-CoV-2 Spike Protein

Mixture 1 & 5, Ligand 1 & 5, Protein 4: no overlap with ligand, zero impact on analysis.

d) 9-azido-sialic acid and SARS-CoV-2 Spike Protein

Mixture 1, Ligand 1, Protein 4: no overlap with ligand, zero impact on analysis.

e) 9-BPC-2,6-sialyllactose and SARS-CoV-2 Spike Protein

Mixture 1, Ligand 1, Protein 1: no overlap with ligand, zero impact on analysis.

Mixture 6: coming from the ligand batch used. Due to its high intensity (the intensity is 10x higher than the resonances from the ligand), the region was excluded.

Excluded atoms: 24, 13

In the STD spectra, a modest STD response can be discerned for 24 and 13 whose magnitude is comparable to adjacent atoms. Although we cannot accurately measure the transfer efficiency, the interpolation will be accurate.

f) 9-BPC-sialic acid and SARS-CoV-2 Spike Protein

Mixture 1, Ligand 1, Protein 1: no overlap with ligand, zero impact on analysis.

g), h) and i) various concentrations of tryptophan and BSA

Mixture 7 & 9, Ligand 8, Protein 7 & 9: no overlap with ligand, zero impact on analysis.

a) 2,3-sialyllactose and SARS-CoV-2 Spike protein

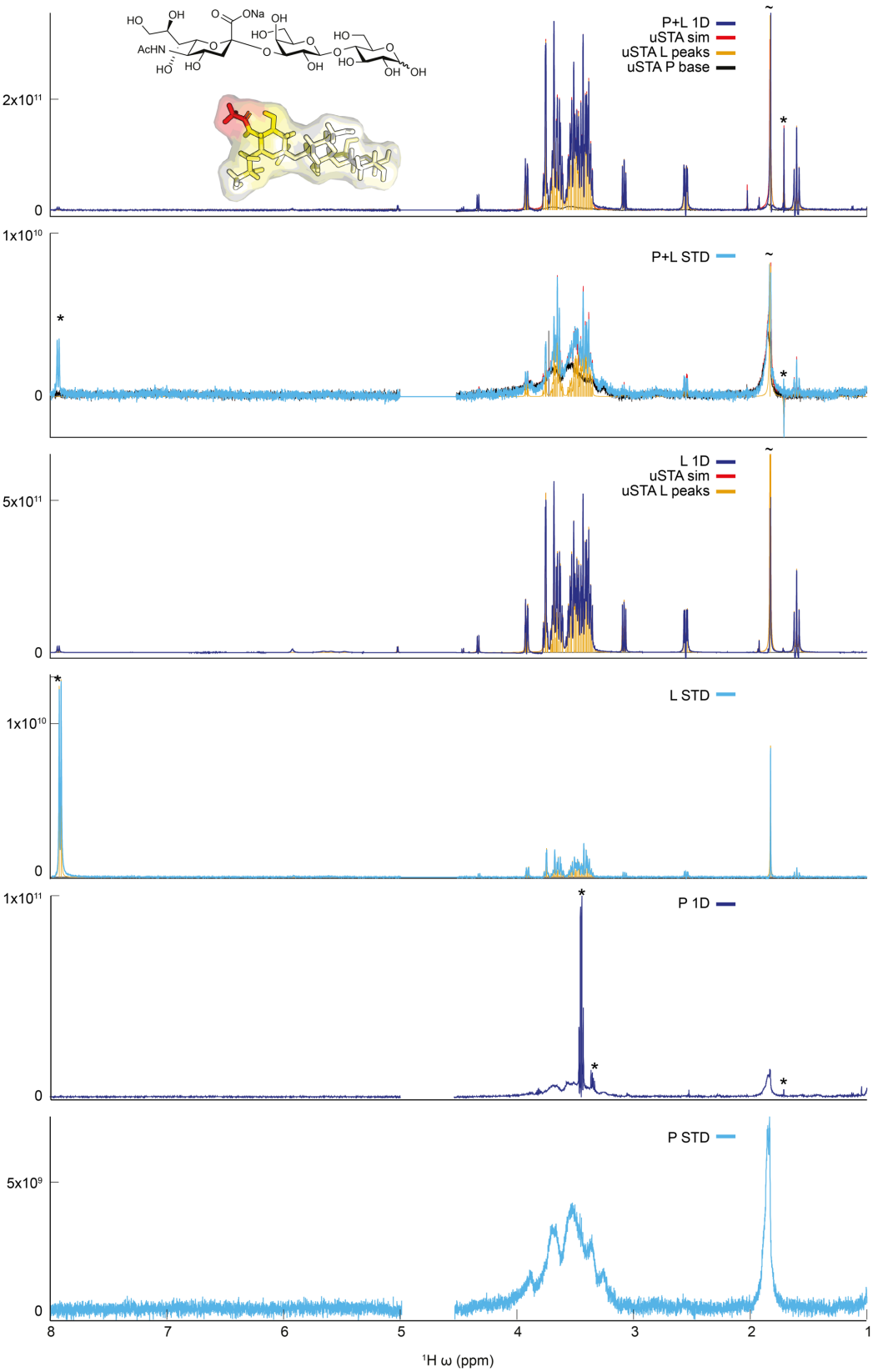

b) 2,6-sialyllactose and SARS-CoV-2 Spike protein

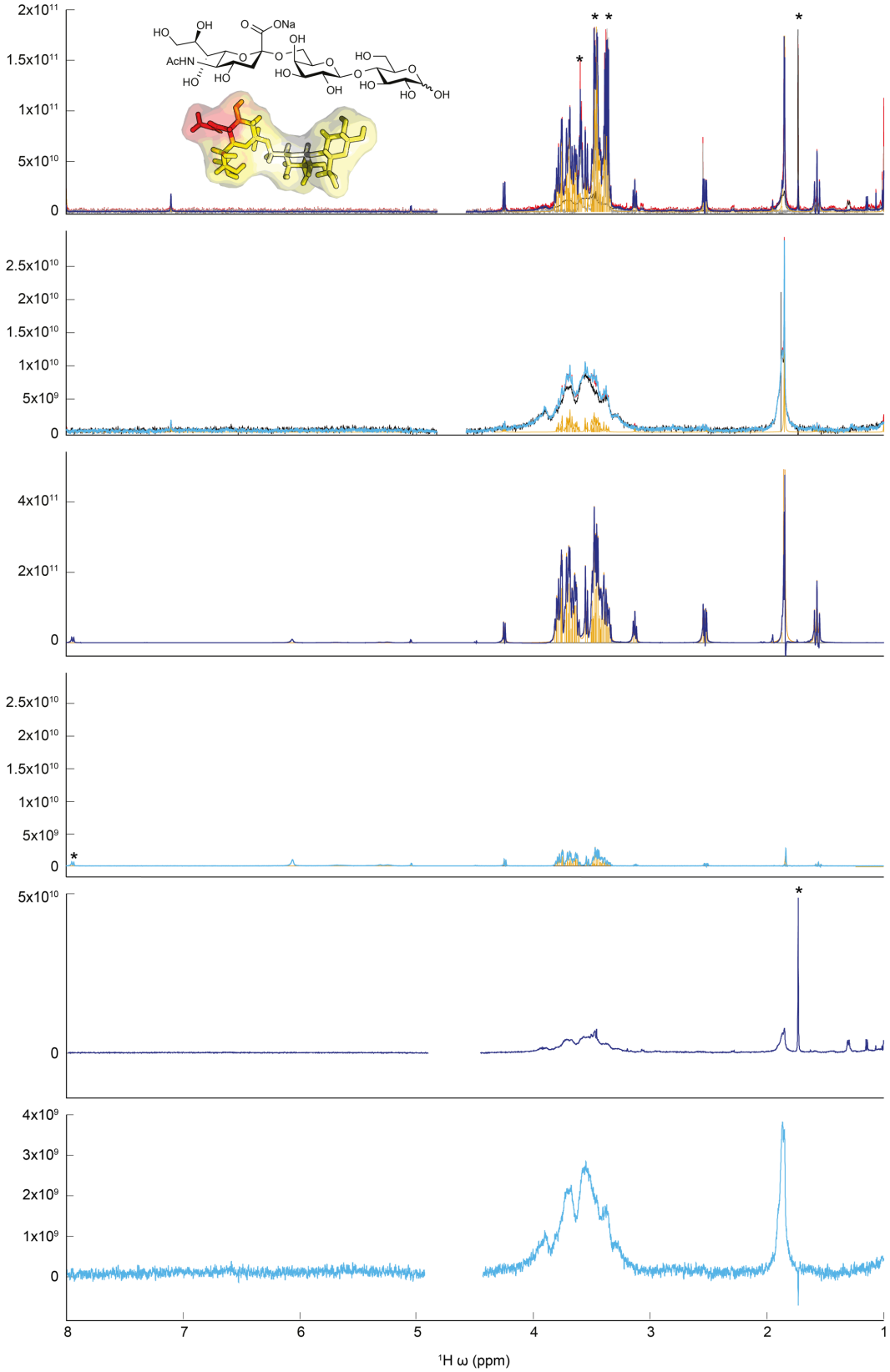

c) Sialic acid and SARS-CoV-2 Spike protein

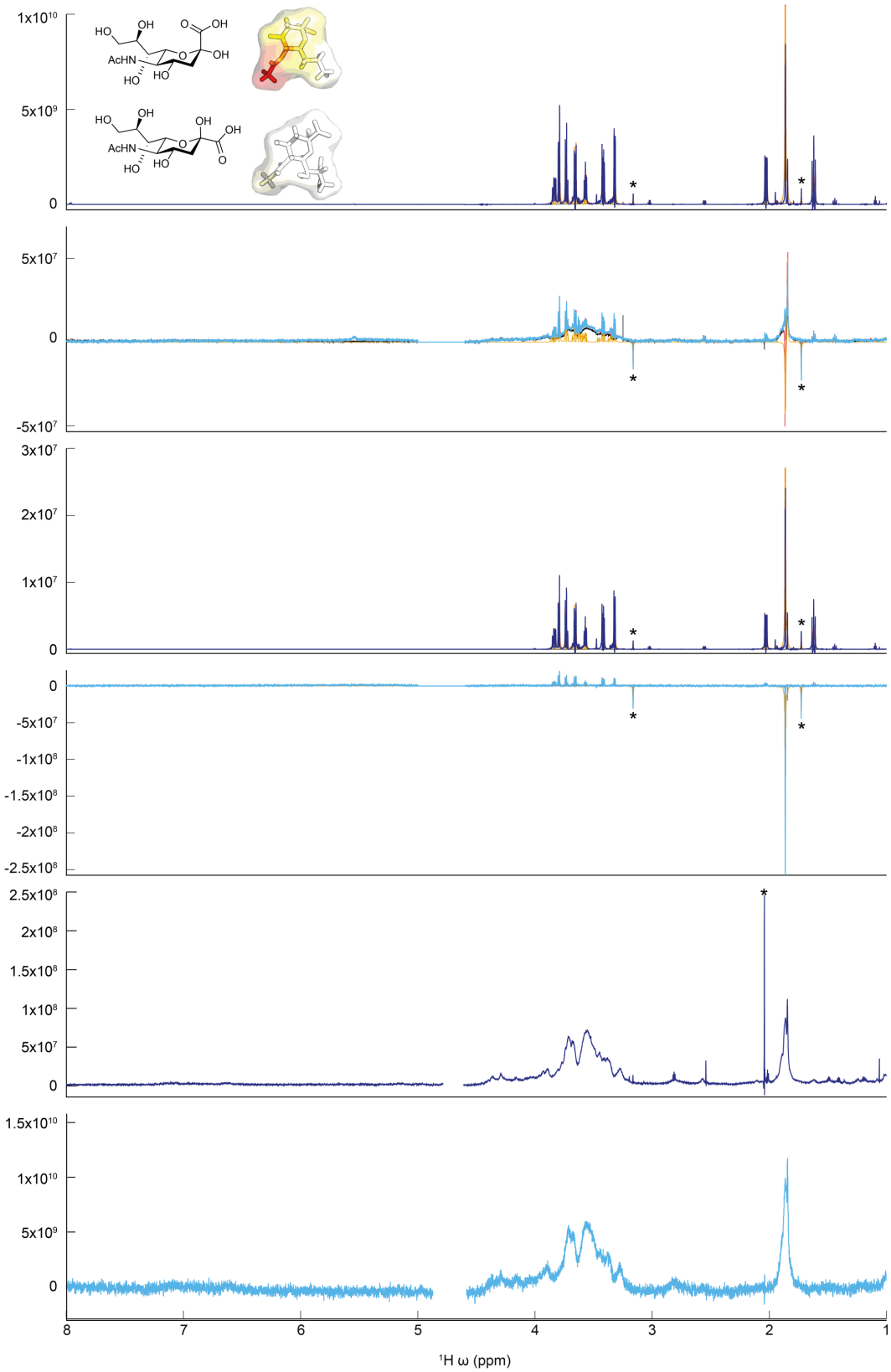

d) 9-azidosialic acid and SARS-CoV-2 Spike protein

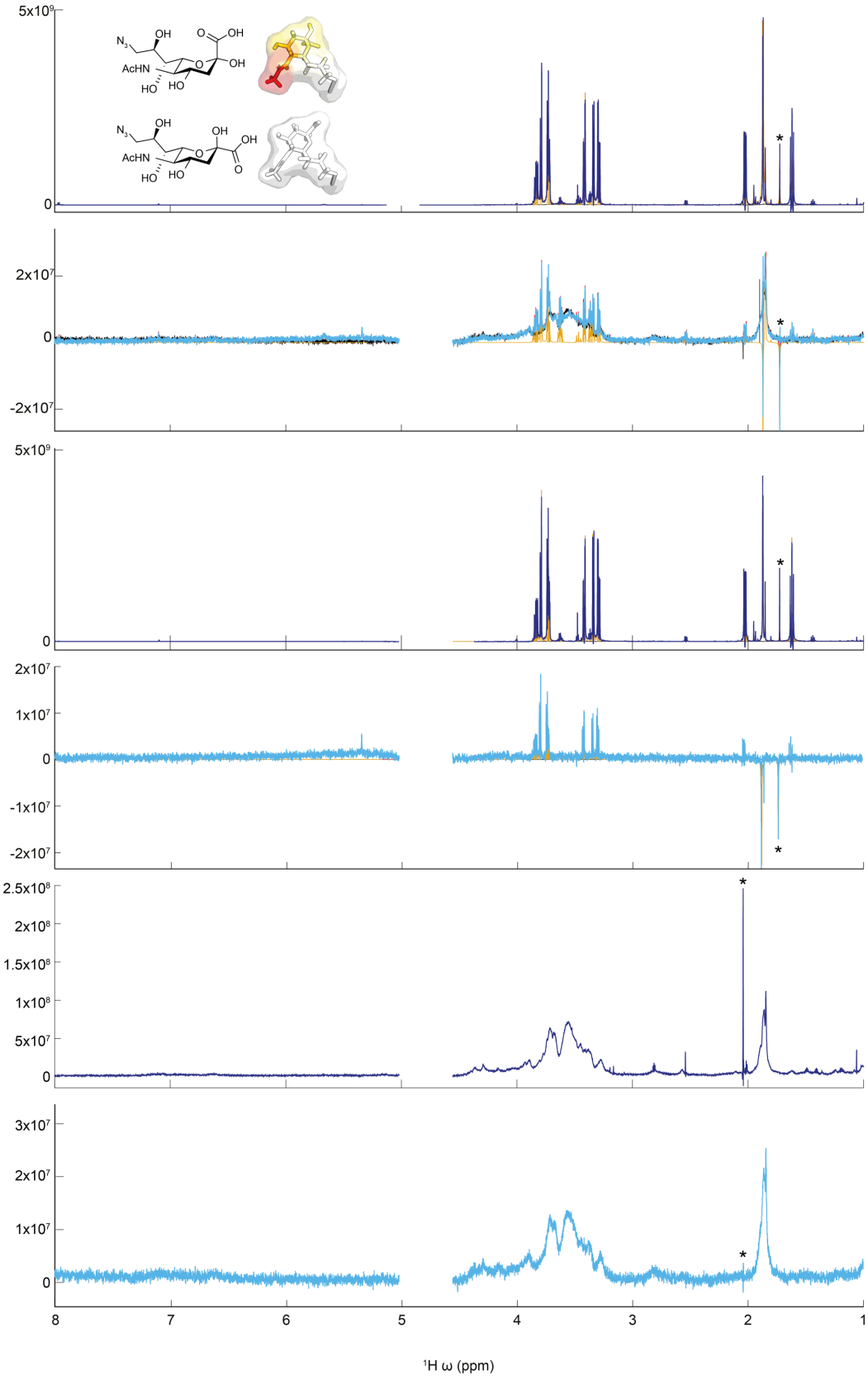

e) 9-BPC2,6-sialyllactose and SARS-CoV-2 Spike protein

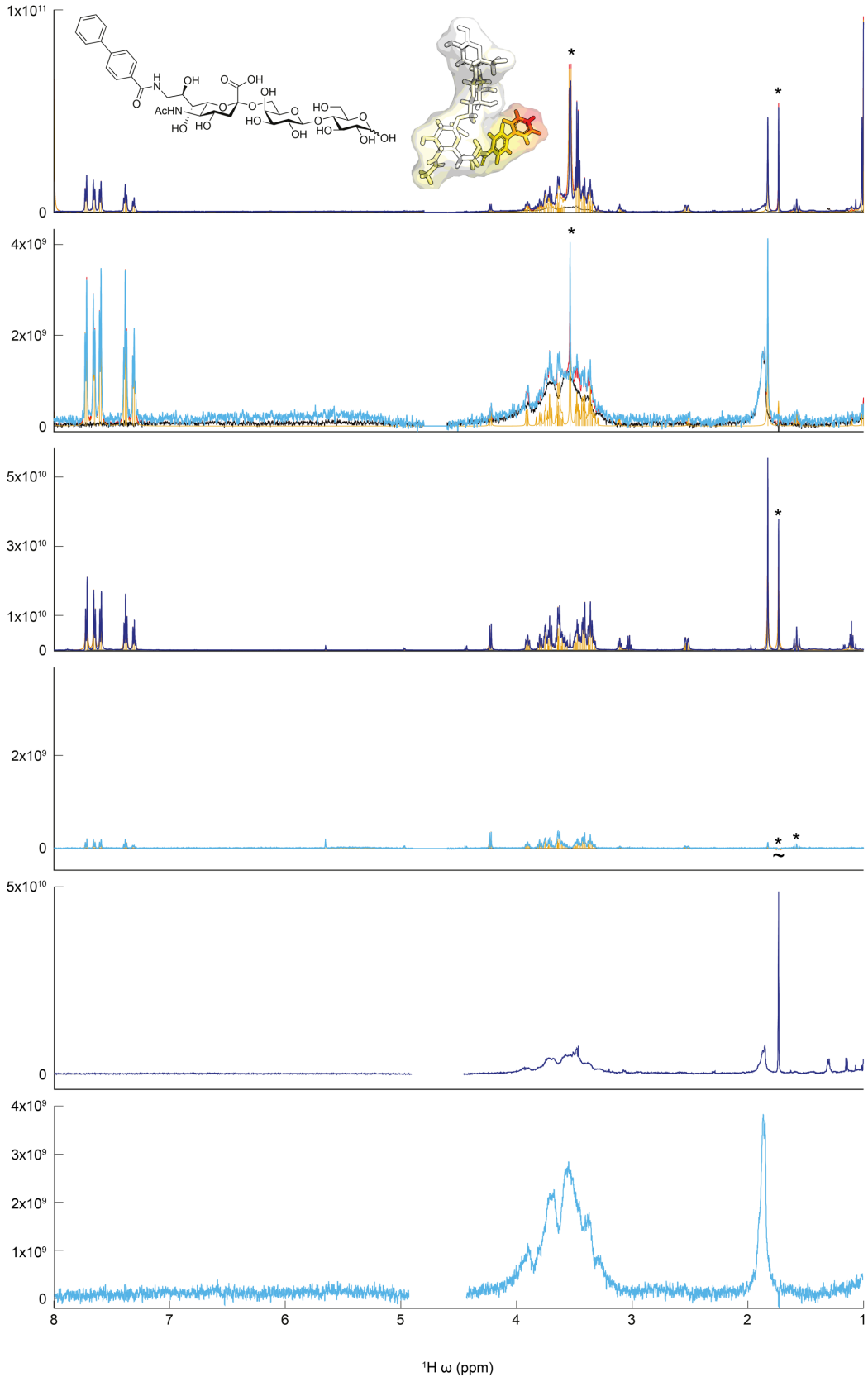

f) 9-BPCsialic acid and SARS-CoV-2 Spike protein

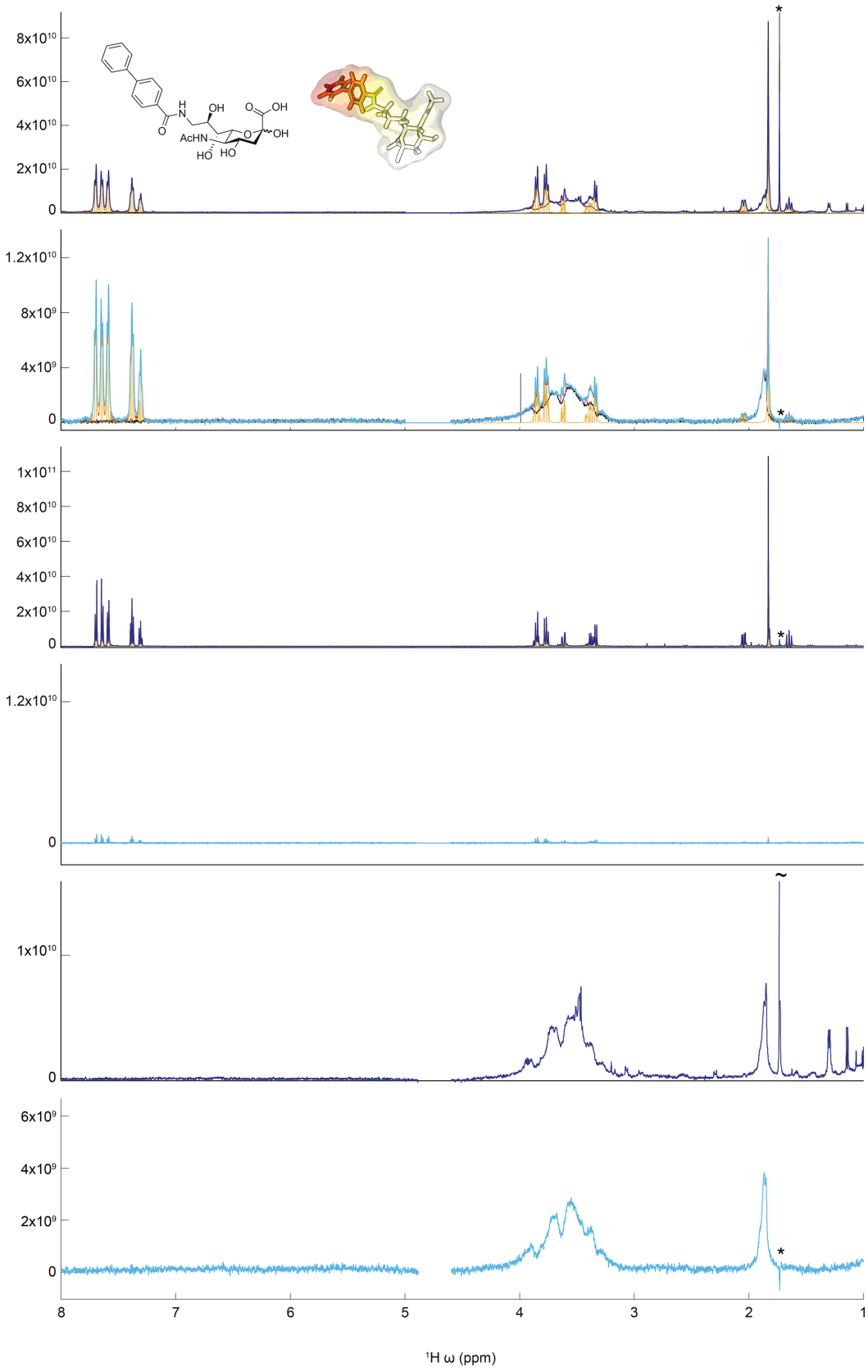

g) 40μM tryptophan and BSA

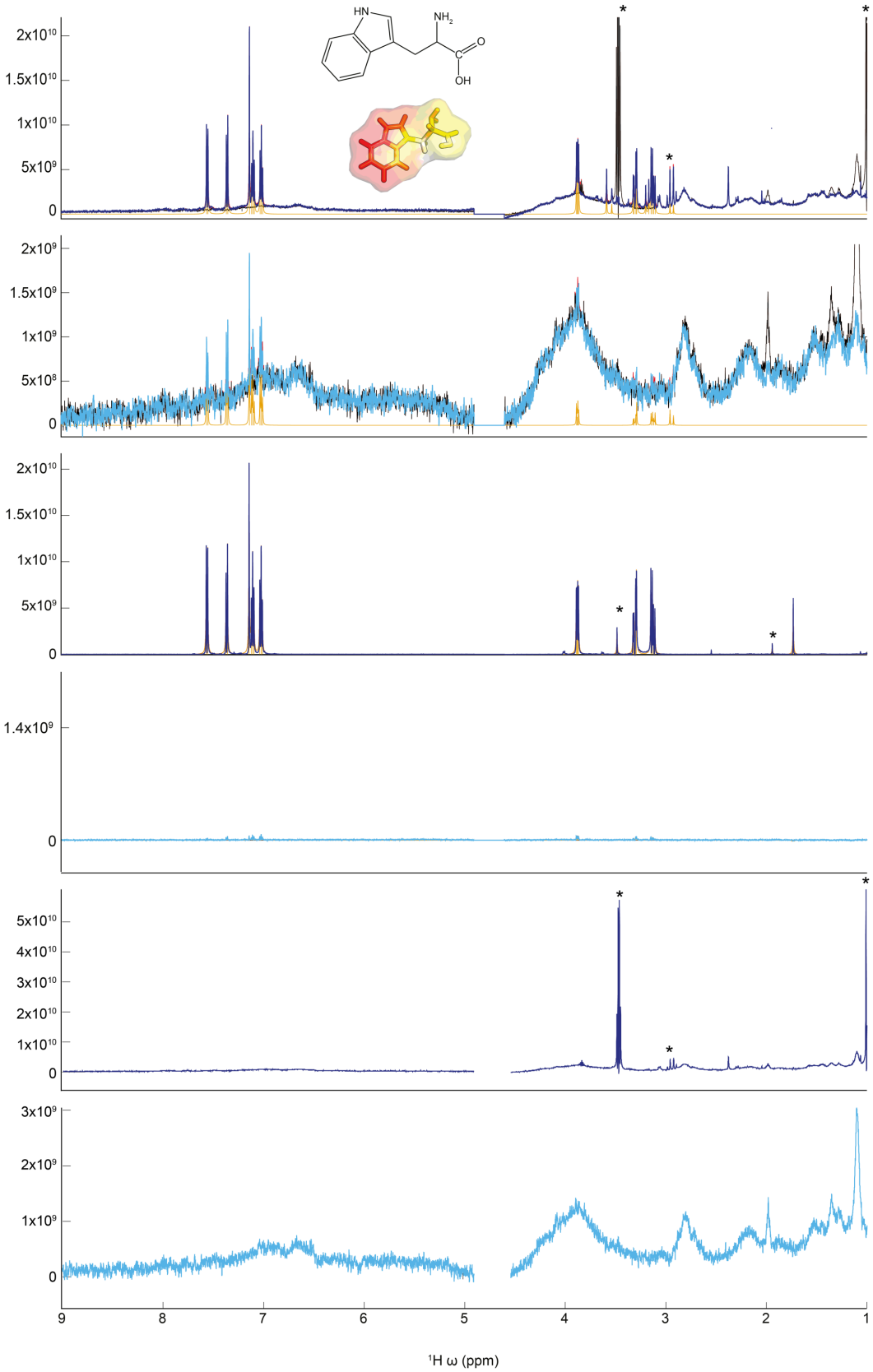

h) 200μM tryptophan and BSA

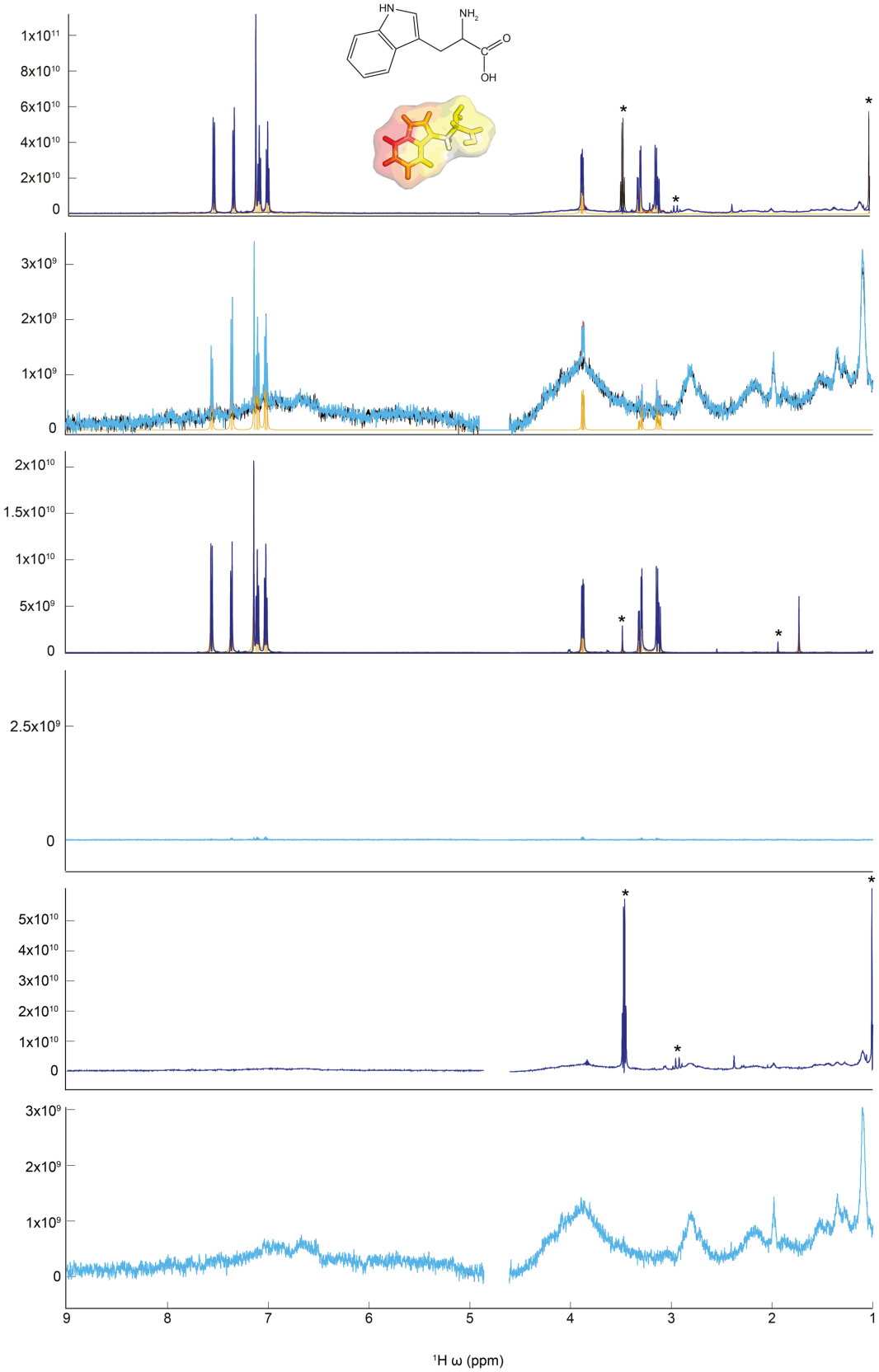

i) 1mM tryptophan and BSA

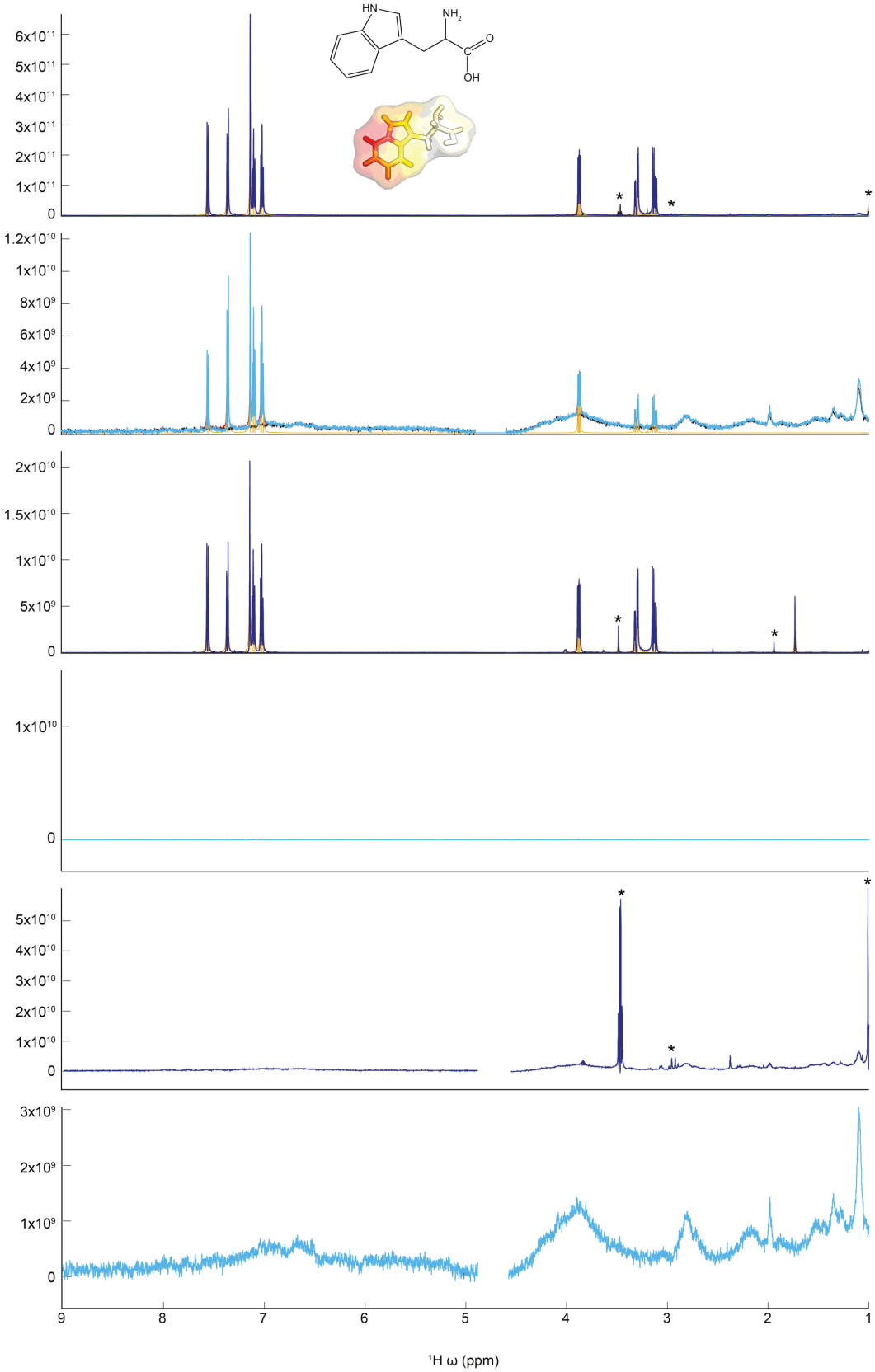

References and Notes

1. S. Yamada, Y. Suzuki, T. Suzuki, M. Q. Le, C. A. Nidom, Y. Sakai-Tagawa, Y. Muramoto, M. Ito, M. Kiso, T. Horimoto, K. Shinya, T. Sawada, M. Kiso, T. Usui, T. Murata, Y. Lin, A. Hay, L. F. Haire, D. J. Stevens, R. J. Russell, S. J. Gamblin, J. J. Skehel, Y. Kawaoka, Haemagglutinin mutations responsible for the binding of H5N1 influenza A viruses to human-type receptors. *Nature* **444**, 378–382 (2006). doi:10.1038/nature05264 Medline

2. W. Li, R. J. G. Hulswit, I. Widjaja, V. S. Raj, R. McBride, W. Peng, W. Widagdo, M. A. Tortorici, B. van Dieren, Y. Lang, J. W. M. van Lent, J. C. Paulson, C. A. M. de Haan, R. J. de Groot, F. J. M. van Kuppeveld, B. L. Haagmans, B.-J. Bosch, Identification of sialic acid-binding function for the Middle East respiratory syndrome coronavirus spike glycoprotein. *Proc. Natl. Acad. Sci. U.S.A.* **114**, E8508–E8517 (2017). doi:10.1073/pnas.1712592114 Medline

3. C. Schwegmann-Wessels, G. Herrler, Sialic acids as receptor determinants for coronaviruses. *Glycoconj. J.* **23**, 51–58 (2006). doi:10.1007/s10719-006-5437-9 Medline

4. R. J. G. Hulswit, Y. Lang, M. J. G. Bakkers, W. Li, Z. Li, A. Schouten, B. Ophorst, F. J. M. van Kuppeveld, G.-J. Boons, B.-J. Bosch, E. G. Huizinga, R. J. de Groot, Human coronaviruses OC43 and HKU1 bind to 9-*O*-acetylated sialic acids via a conserved receptor-binding site in spike protein domain A. *Proc. Natl. Acad. Sci. U.S.A.* **116**, 2681–2690 (2019). doi:10.1073/pnas.1809667116 Medline

5. Y.-J. Park, A. C. Walls, Z. Wang, M. M. Sauer, W. Li, M. A. Tortorici, B.-J. Bosch, F. DiMaio, D. Veesler, Structures of MERS-CoV spike glycoprotein in complex with sialoside attachment receptors. *Nat. Struct. Mol. Biol.* **26**, 1151–1157 (2019). doi:10.1038/s41594-019-0334-7 Medline

6. E. Qing, M. Hantak, S. Perlman, T. Gallagher, Distinct Roles for Sialoside and Protein Receptors in Coronavirus Infection. *mBio* **11**, e02764-19 (2020). doi:10.1128/mBio.02764-19 Medline

7. W. Li, M. J. Moore, N. Vasilieva, J. Sui, S. K. Wong, M. A. Berne, M. Somasundaran, J. L. Sullivan, K. Luzuriaga, T. C. Greenough, H. Choe, M. Farzan, Angiotensin-converting enzyme 2 is a functional receptor for the SARS coronavirus. *Nature* **426**, 450–454 (2003). doi:10.1038/nature02145 Medline

8. K. Kuba, Y. Imai, S. Rao, H. Gao, F. Guo, B. Guan, Y. Huan, P. Yang, Y. Zhang, W. Deng, L. Bao, B. Zhang, G. Liu, Z. Wang, M. Chappell, Y. Liu, D. Zheng, A. Leibbrandt, T. Wada, A. S. Slutsky, D. Liu, C. Qin, C. Jiang, J. M. Penninger, A crucial role of angiotensin converting enzyme 2 (ACE2) in SARS coronavirus-induced lung injury. *Nat. Med.* **11**, 875–879 (2005). doi:10.1038/nm1267 Medline

9. F. Li, W. Li, M. Farzan, S. C. Harrison, Structure of SARS coronavirus spike receptor-binding domain complexed with receptor. *Science* **309**, 1864–1868 (2005). doi:10.1126/science.1116480 Medline

10. D. Wrapp, N. Wang, K. S. Corbett, J. A. Goldsmith, C.-L. Hsieh, O. Abiona, B. S. Graham, J. S. McLellan, Cryo-EM structure of the 2019-nCoV spike in the prefusion conformation. *Science* **367**, 1260–1263 (2020). doi:10.1126/science.abb2507 Medline

11. R. Yan, Y. Zhang, Y. Li, L. Xia, Y. Guo, Q. Zhou, Structural basis for the recognition of SARS-CoV-2 by full-length human ACE2. *Science* **367**, 1444–1448 (2020). doi:10.1126/science.abb2762 Medline

12. D. Morniroli, M. L. Giannì, A. Consales, C. Pietrasanta, F. Mosca, Human Sialome and Coronavirus Disease-2019 (COVID-19) Pandemic: An Understated Correlation? *Front. Immunol.* **11**, 1480 (2020). doi:10.3389/fimmu.2020.01480 Medline

13. A. N. Baker, S.-J. Richards, C. S. Guy, T. R. Congdon, M. Hasan, A. J. Zwetsloot, A. Gallo, J. R. Lewandowski, P. J. Stansfeld, A. Straube, M. Walker, S. Chessa, G. Pergolizzi, S. Dedola, R. A. Field, M. I. Gibson, The SARS-COV-2 Spike Protein Binds Sialic Acids and Enables Rapid Detection in a Lateral Flow Point of Care Diagnostic Device. *ACS Cent. Sci.* **6**, 2046–2052 (2020). doi:10.1021/acscentsci.0c00855 Medline

14. W. Hao, B. Ma, Z. Li, X. Wang, X. Gao, Y. Li, B. Qin, S. Shang, S. Cui, Z. Tan, Binding of the SARS-CoV-2 spike protein to glycans. *Sci. Bull.* **66**, 1205–1214 (2021). doi:10.1016/j.scib.2021.01.010 Medline

15. L. Nguyen, K. A. McCord, D. T. Bui, K. M. Bouwman, E. N. Kitova, M. Elaish, D. Kumawat, G. C. Daskhan, I. Tomris, L. Han, P. Chopra, T.-J. Yang, S. D. Willows, A. L. Mason, L. K. Mahal, T. L. Lowary, L. J. West, S.-T. D. Hsu, T. Hobman, S. M. Tompkins, G.-J. Boons, R. P. de Vries, M. S. Macauley, J. S. Klassen, Sialic acid-containing glycolipids mediate binding and viral entry of SARS-CoV-2. *Nat. Chem. Biol.* **18**, 81–90 (2022). doi:10.1038/s41589-021-00924-1 Medline

16. W. Hao *et al*., Binding of the SARS-CoV-2 Spike Protein to Glycans. bioRxiv 2020.2005.2017.100537 (2020). doi: 10.1101/2020.05.17.100537

17. T. M. Clausen, D. R. Sandoval, C. B. Spliid, J. Pihl, H. R. Perrett, C. D. Painter, A. Narayanan, S. A. Majowicz, E. M. Kwong, R. N. McVicar, B. E. Thacker, C. A. Glass, Z. Yang, J. L. Torres, G. J. Golden, P. L. Bartels, R. N. Porell, A. F. Garretson, L. Laubach, J. Feldman, X. Yin, Y. Pu, B. M. Hauser, T. M. Caradonna, B. P. Kellman, C. Martino, P. L. S. M. Gordts, S. K. Chanda, A. G. Schmidt, K. Godula, S. L. Leibel, J. Jose, K. D. Corbett, A. B. Ward, A. F. Carlin, J. D. Esko, SARS-CoV-2 Infection Depends on Cellular Heparan Sulfate and ACE2. *Cell* **183**, 1043–1057.e15 (2020). doi:10.1016/j.cell.2020.09.033 Medline

18. N. Behloul, S. Baha, R. Shi, J. Meng, Role of the GTNGTKR motif in the N-terminal receptor-binding domain of the SARS-CoV-2 spike protein. *Virus Res.* **286**, 198058 (2020). doi:10.1016/j.virusres.2020.198058 Medline

19. X. Chi, R. Yan, J. Zhang, G. Zhang, Y. Zhang, M. Hao, Z. Zhang, P. Fan, Y. Dong, Y. Yang, Z. Chen, Y. Guo, J. Zhang, Y. Li, X. Song, Y. Chen, L. Xia, L. Fu, L. Hou, J. Xu, C. Yu, J. Li, Q. Zhou, W. Chen, A neutralizing human antibody binds to the N-terminal domain of the Spike protein of SARS-CoV-2. *Science* **369**, 650–655 (2020). doi:10.1126/science.abc6952 Medline

20. M. G. Rossmann, The canyon hypothesis. *J. Biol. Chem.* **264**, 14587–14590 (1989). doi:10.1016/S0021-9258(18)63732-9 Medline

21. Y. Watanabe, Z. T. Berndsen, J. Raghwani, G. E. Seabright, J. D. Allen, O. G. Pybus, J. S. McLellan, I. A. Wilson, T. A. Bowden, A. B. Ward, M. Crispin, Vulnerabilities in coronavirus glycan shields despite extensive glycosylation. *Nat. Commun.* **11**, 2688 (2020). doi:10.1038/s41467-020-16567-0 Medline

22. M. Mayer, B. Meyer, Characterization of Ligand Binding by Saturation Transfer Difference NMR Spectroscopy. *Angew. Chem. Int. Ed.* **38**, 1784–1788 (1999). doi:10.1002/(SICI)1521-3773(19990614)38:12<1784:AID-ANIE1784>3.0.CO;2-Q Medline

23. J. L. Wagstaff, S. L. Taylor, M. J. Howard, Recent developments and applications of saturation transfer difference nuclear magnetic resonance (STD NMR) spectroscopy. *Mol. Biosyst.* **9**, 571–577 (2013). doi:10.1039/C2MB25395J Medline

24. J. Angulo, P. M. Enríquez-Navas, P. M. Nieto, Ligand-receptor binding affinities from saturation transfer difference (STD) NMR spectroscopy: The binding isotherm of STD initial growth rates. *Chem. Eur. J.* **16**, 7803–7812 (2010). doi:10.1002/chem.200903528 Medline

25. R. H. McMenamy, J. L. Oncley, The specific binding of L-tryptophan to serum albumin. *J. Biol. Chem.* **233**, 1436–1447 (1958). doi:10.1016/S0021-9258(18)49353-2 Medline

26. P. Vallurupalli, G. Bouvignies, L. E. Kay, Studying “invisible” excited protein states in slow exchange with a major state conformation. *J. Am. Chem. Soc.* **134**, 8148–8161 (2012). doi:10.1021/ja3001419 Medline

27. T. Xie, T. Saleh, P. Rossi, C. G. Kalodimos, Conformational states dynamically populated by a kinase determine its function. *Science* **370**, eabc2754 (2020). doi:10.1126/science.abc2754 Medline

28. N. L. Fawzi, J. Ying, D. A. Torchia, G. M. Clore, Probing exchange kinetics and atomic resolution dynamics in high-molecular-weight complexes using dark-state exchange saturation transfer NMR spectroscopy. *Nat. Protoc.* **7**, 1523–1533 (2012). doi:10.1038/nprot.2012.077 Medline

29. G. Bouvignies, P. Vallurupalli, D. F. Hansen, B. E. Correia, O. Lange, A. Bah, R. M. Vernon, F. W. Dahlquist, D. Baker, L. E. Kay, Solution structure of a minor and transiently formed state of a T4 lysozyme mutant. *Nature* **477**, 111–114 (2011). doi:10.1038/nature10349

30. M. Mayer, B. Meyer, Group epitope mapping by saturation transfer difference NMR to identify segments of a ligand in direct contact with a protein receptor. *J. Am. Chem. Soc.* **123**, 6108–6117 (2001). doi:10.1021/ja0100120 Medline

31. M. T. Marty, A. J. Baldwin, E. G. Marklund, G. K. A. Hochberg, J. L. P. Benesch, C. V. Robinson, Bayesian deconvolution of mass and ion mobility spectra: From binary interactions to polydisperse ensembles. *Anal. Chem.* **87**, 4370–4376 (2015). doi:10.1021/acs.analchem.5b00140 Medline

32. L. Fielding, S. Rutherford, D. Fletcher, Determination of protein-ligand binding affinity by NMR: Observations from serum albumin model systems. *Magn. Reson. Chem.* **43**, 463–470 (2005). doi:10.1002/mrc.1574 Medline

33. A. Bujacz, K. Zielinski, B. Sekula, Structural studies of bovine, equine, and leporine serum albumin complexes with naproxen. *Proteins* **82**, 2199–2208 (2014). doi:10.1002/prot.24583 Medline

34. I. Pérez-Victoria, S. Kemper, M. K. Patel, J. M. Edwards, J. C. Errey, L. F. Primavesi, M. J. Paul, T. D. W. Claridge, B. G. Davis, Saturation transfer difference NMR reveals functionally essential kinetic differences for a sugar-binding repressor protein. *Chem. Commun.* **2009**, 5862–5864 (2009). doi:10.1039/b913489a Medline

35. U. Hars, R. Horlacher, W. Boos, W. Welte, K. Diederichs, Crystal structure of the effector-binding domain of the trehalose-repressor of Escherichia coli, a member of the LacI family, in its complexes with inducer trehalose-6-phosphate and noninducer trehalose. *Protein Sci.* **7**, 2511–2521 (1998). doi:10.1002/pro.5560071204 Medline

36. H. M. McConnell, Reaction Rates by Nuclear Magnetic Resonance. *J. Chem. Phys.* **28**, 430–431 (1958). doi:10.1063/1.1744152

37. J. E. Stencel-Baerenwald, K. Reiss, D. M. Reiter, T. Stehle, T. S. Dermody, The sweet spot: Defining virus-sialic acid interactions. *Nat. Rev. Microbiol.* **12**, 739–749 (2014). doi:10.1038/nrmicro3346 Medline

38. D. Lingwood, P. M. McTamney, H. M. Yassine, J. R. R. Whittle, X. Guo, J. C. Boyington, C.-J. Wei, G. J. Nabel, Structural and genetic basis for development of broadly neutralizing influenza antibodies. *Nature* **489**, 566–570 (2012). doi:10.1038/nature11371 Medline

39. H.-Y. Liao, C.-H. Hsu, S.-C. Wang, C.-H. Liang, H.-Y. Yen, C.-Y. Su, C.-H. Chen, J.-T. Jan, C.-T. Ren, C.-H. Chen, T.-J. R. Cheng, C.-Y. Wu, C.-H. Wong, Differential receptor binding affinities of influenza hemagglutinins on glycan arrays. *J. Am. Chem. Soc.* **132**, 14849–14856 (2010). doi:10.1021/ja104657b Medline

40. Y. Watanabe, J. D. Allen, D. Wrapp, J. S. McLellan, M. Crispin, Site-specific glycan analysis of the SARS-CoV-2 spike. *Science* **369**, 330–333 (2020). doi:10.1126/science.abb9983 Medline

41. M. P. Lenza, I. Oyenarte, T. Diercks, J. I. Quintana, A. Gimeno, H. Coelho, A. Diniz, F. Peccati, S. Delgado, A. Bosch, M. Valle, O. Millet, N. G. A. Abrescia, A. Palazón, F. Marcelo, G. Jiménez-Osés, J. Jiménez-Barbero, A. Ardá, J. Ereño-Orbea, Structural Characterization of N-Linked Glycans in the Receptor Binding Domain of the SARS-CoV-2 Spike Protein and their Interactions with Human Lectins. *Angew. Chem. Int. Ed.* **59**, 23763–23771 (2020). doi:10.1002/anie.202011015 Medline

42. C. Dominguez, R. Boelens, A. M. J. J. Bonvin, HADDOCK: A protein-protein docking approach based on biochemical or biophysical information. *J. Am. Chem. Soc.* **125**, 1731–1737 (2003). doi:10.1021/ja026939x Medline

43. G. C. P. van Zundert, J. P. G. L. M. Rodrigues, M. Trellet, C. Schmitz, P. L. Kastritis, E. Karaca, A. S. J. Melquiond, M. van Dijk, S. J. de Vries, A. M. J. J. Bonvin, The HADDOCK2.2 Web Server: User-Friendly Integrative Modeling of Biomolecular Complexes. *J. Mol. Biol.* **428**, 720–725 (2016). doi:10.1016/j.jmb.2015.09.014 Medline

44. A. Rambaut, E. C. Holmes, Á. O'Toole, V. Hill, J. T. McCrone, C. Ruis, L. du Plessis, O. G. Pybus, A dynamic nomenclature proposal for SARS-CoV-2 lineages to assist genomic epidemiology. *Nat. Microbiol.* **5**, 1403–1407 (2020). doi:10.1038/s41564-020-0770-5 Medline

45. J. Huo, A. Le Bas, R. R. Ruza, H. M. E. Duyvesteyn, H. Mikolajek, T. Malinauskas, T. K. Tan, P. Rijal, M. Dumoux, P. N. Ward, J. Ren, D. Zhou, P. J. Harrison, M. Weckener, D. K. Clare, V. K. Vogirala, J. Radecke, L. Moynié, Y. Zhao, J. Gilbert-Jaramillo, M. L. Knight, J. A. Tree, K. R. Buttigieg, N. Coombes, M. J. Elmore, M. W. Carroll, L. Carrique, P. N. M. Shah, W. James, A. R. Townsend, D. I. Stuart, R. J. Owens, J. H. Naismith, Neutralizing nanobodies bind SARS-CoV-2 spike RBD and block interaction with ACE2. *Nat. Struct. Mol. Biol.* **27**, 846–854 (2020). doi:10.1038/s41594-020-0469-6 Medline

46. J. Huo, H. Mikolajek, A. Le Bas, J. J. Clark, P. Sharma, A. Kipar, J. Dormon, C. Norman, M. Weckener, D. K. Clare, P. J. Harrison, J. A. Tree, K. R. Buttigieg, F. J. Salguero, R. Watson, D. Knott, O. Carnell, D. Ngabo, M. J. Elmore, S. Fotheringham, A. Harding, L. Moynié, P. N. Ward, M. Dumoux, T. Prince, Y. Hall, J. A. Hiscox, A. Owen, W. James, M. W. Carroll, J. P. Stewart, J. H. Naismith, R. J. Owens, A potent SARS-CoV-2 neutralising nanobody shows therapeutic efficacy in the Syrian golden hamster model of COVID-19. *Nat. Commun.* **12**, 5469 (2021). doi:10.1038/s41467-021-25480-z Medline

47. M. McCallum, A. C. Walls, J. E. Bowen, D. Corti, D. Veesler, Structure-guided covalent stabilization of coronavirus spike glycoprotein trimers in the closed conformation. *Nat. Struct. Mol. Biol.* **27**, 942–949 (2020). doi:10.1038/s41594-020-0483-8 Medline

48. C. Toelzer, K. Gupta, S. K. N. Yadav, U. Borucu, A. D. Davidson, M. Kavanagh Williamson, D. K. Shoemark, F. Garzoni, O. Staufer, R. Milligan, J. Capin, A. J. Mulholland, J. Spatz, D. Fitzgerald, I. Berger, C. Schaffitzel, Free fatty acid binding pocket in the locked structure of SARS-CoV-2 spike protein. *Science* **370**, 725–730 (2020). doi:10.1126/science.abd3255 Medline

49. R. Tibshirani, Regression Shrinkage and Selection Via the Lasso. *J. R. Stat. Soc. B* **58**, 267–288 (1996). doi:10.1111/j.2517-6161.1996.tb02080.x

50. K. Koths, E. Taylor, R. Halenbeck, C. Casipit, A. Wang, Cloning and characterization of a human Mac-2-binding protein, a new member of the superfamily defined by the macrophage scavenger receptor cysteine-rich domain. *J. Biol. Chem.* **268**, 14245–14249 (1993). doi:10.1016/S0021-9258(19)85233-X Medline

51. L. Johannes, R. Jacob, H. Leffler, Galectins at a glance. *J. Cell Sci.* **131**, jcs208884 (2018). doi:10.1242/jcs.208884 Medline

52. S. R. Stowell, C. M. Arthur, P. Mehta, K. A. Slanina, O. Blixt, H. Leffler, D. F. Smith, R. D. Cummings, Galectin-1, -2, and -3 exhibit differential recognition of sialylated glycans and blood group antigens. *J. Biol. Chem.* **283**, 10109–10123 (2008). doi:10.1074/jbc.M709545200 Medline

53. N. A. Kamili, C. M. Arthur, C. Gerner-Smidt, E. Tafesse, A. Blenda, M. Dias-Baruffi, S. R. Stowell, Key regulators of galectin-glycan interactions. *Proteomics* **16**, 3111–3125 (2016). doi:10.1002/pmic.201600116 Medline

54. A. Togayachi, Y. Kozono, A. Kuno, T. Ohkura, T. Sato, J. Hirabayashi, Y. Ikehara, H. Narimatsu, β3GnT2 (*B3GNT2*), a major polylactosamine synthase: Analysis of B3GNT2-deficient mice. *Methods Enzymol.* **479**, 185–204 (2010). doi:10.1016/s0076-6879(10)79011-x

55. M. Kanekiyo, C.-J. Wei, H. M. Yassine, P. M. McTamney, J. C. Boyington, J. R. R. Whittle, S. S. Rao, W.-P. Kong, L. Wang, G. J. Nabel, Self-assembling influenza nanoparticle vaccines elicit broadly neutralizing H1N1 antibodies. *Nature* **499**, 102–106 (2013). doi:10.1038/nature12202 Medline

56. M. Mammen, S.-K. Choi, G. M. Whitesides, Polyvalent Interactions in Biological Systems: Implications for Design and Use of Multivalent Ligands and Inhibitors. *Angew. Chem. Int. Ed.* **37**, 2754–2794 (1998). doi:10.1002/(SICI)1521-3773(19981102)37:20<2754:AID-ANIE2754>3.0.CO;2-3 Medline

57. R. T. Lee, Y. C. Lee, Affinity enhancement by multivalent lectin-carbohydrate interaction. *Glycoconj. J.* **17**, 543–551 (2000). doi:10.1023/A:1011070425430 Medline

58. N. Jia, L. Byrd-Leotis, Y. Matsumoto, C. Gao, A. N. Wein, J. L. Lobby, J. E. Kohlmeier, D. A. Steinhauer, R. D. Cummings, The Human Lung Glycome Reveals Novel Glycan Ligands for Influenza A Virus. *Sci. Rep.* **10**, 5320 (2020). doi:10.1038/s41598-020-62074-z Medline

59. M. A. Toscano, G. A. Bianco, J. M. Ilarregui, D. O. Croci, J. Correale, J. D. Hernandez, N. W. Zwirner, F. Poirier, E. M. Riley, L. G. Baum, G. A. Rabinovich, Differential glycosylation of TH1, TH2 and TH-17 effector cells selectively regulates susceptibility to cell death. *Nat. Immunol.* **8**, 825–834 (2007). doi:10.1038/ni1482 Medline

60. P. Tangvoranuntakul, P. Gagneux, S. Diaz, M. Bardor, N. Varki, A. Varki, E. Muchmore, Human uptake and incorporation of an immunogenic nonhuman dietary sialic acid. *Proc. Natl. Acad. Sci. U.S.A.* **100**, 12045–12050 (2003). doi:10.1073/pnas.2131556100 Medline

61. J. L. McAuley, B. P. Gilbertson, S. Trifkovic, L. E. Brown, J. L. McKimm-Breschkin, Influenza Virus Neuraminidase Structure and Functions. *Front. Microbiol.* **10**, 39 (2019). doi:10.3389/fmicb.2019.00039 Medline

62. J. Huo, Y. Zhao, J. Ren, D. Zhou, H. M. E. Duyvesteyn, H. M. Ginn, L. Carrique, T. Malinauskas, R. R. Ruza, P. N. M. Shah, T. K. Tan, P. Rijal, N. Coombes, K. R. Bewley, J. A. Tree, J. Radecke, N. G. Paterson, P. Supasa, J. Mongkolsapaya, G. R. Screaton, M. Carroll, A. Townsend, E. E. Fry, R. J. Owens, D. I. Stuart, Neutralization of SARS-CoV-2 by Destruction of the Prefusion Spike. *Cell Host Microbe* **28**, 445–454.e6 (2020). doi:10.1016/j.chom.2020.06.010 Medline

63. C.-L. Hsieh, J. A. Goldsmith, J. M. Schaub, A. M. DiVenere, H.-C. Kuo, K. Javanmardi, K. C. Le, D. Wrapp, A. G. Lee, Y. Liu, C.-W. Chou, P. O. Byrne, C. K. Hjorth, N. V. Johnson, J. Ludes-Meyers, A. W. Nguyen, J. Park, N. Wang, D. Amengor, J. J. Lavinder, G. C. Ippolito, J. A. Maynard, I. J. Finkelstein, J. S. McLellan, Structure-based design of prefusion-stabilized SARS-CoV-2 spikes. *Science* **369**, 1501–1505 (2020). doi:10.1126/science.abd0826 Medline

64. V. Jayalakshmi, N. R. Krishna, Complete relaxation and conformational exchange matrix (CORCEMA) analysis of intermolecular saturation transfer effects in reversibly forming

ligand-receptor complexes. *J. Magn. Reson.* **155**, 106–118 (2002). doi:10.1006/jmre.2001.2499 Medline

65. K. Nakamura, H. Sakagami, K. Asanuma-Date, N. Nagasawa, Y. Nakahara, H. Akiyama, H. Ogawa, Immobilized glycosylated Fmoc-amino acid for SPR: Comparative studies of lectin-binding to linear or biantennary diLacNAc structures. *Carbohydr. Res.* **382**, 77–85 (2013). doi:10.1016/j.carres.2013.10.003 Medline

66. A. Sali, Comparative protein modeling by satisfaction of spatial restraints. *Mol. Med. Today* **1**, 270–277 (1995). doi:10.1016/S1357-4310(95)91170-7 Medline

67. M. Y. Shen, A. Sali, Statistical potential for assessment and prediction of protein structures. *Protein Sci.* **15**, 2507–2524 (2006). doi:10.1110/ps.062416606 Medline

68. P. I. Koukos, L. C. Xue, A. M. J. J. Bonvin, Protein-ligand pose and affinity prediction: Lessons from D3R Grand Challenge 3. *J. Comput. Aided Mol. Des.* **33**, 83–91 (2019). doi:10.1007/s10822-018-0148-4 Medline

69. S. Q. Zheng, E. Palovcak, J.-P. Armache, K. A. Verba, Y. Cheng, D. A. Agard, MotionCor2: Anisotropic correction of beam-induced motion for improved cryo-electron microscopy. *Nat. Methods* **14**, 331–332 (2017). doi:10.1038/nmeth.4193 Medline

70. A. Punjani, J. L. Rubinstein, D. J. Fleet, M. A. Brubaker, cryoSPARC: Algorithms for rapid unsupervised cryo-EM structure determination. *Nat. Methods* **14**, 290–296 (2017). doi:10.1038/nmeth.4169 Medline

71. K. Zhang, Gctf: Real-time CTF determination and correction. *J. Struct. Biol.* **193**, 1–12 (2016). doi:10.1016/j.jsb.2015.11.003 Medline

72. S. H. W. Scheres, RELION: Implementation of a Bayesian approach to cryo-EM structure determination. *J. Struct. Biol.* **180**, 519–530 (2012). doi:10.1016/j.jsb.2012.09.006 Medline

73. J. Zivanov, T. Nakane, B. O. Forsberg, D. Kimanius, W. J. H. Hagen, E. Lindahl, S. H. W. Scheres, New tools for automated high-resolution cryo-EM structure determination in RELION-3. *eLife* **7**, e42166 (2018). doi:10.7554/eLife.42166 Medline

74. A. Punjani, H. Zhang, D. J. Fleet, Non-uniform refinement: Adaptive regularization improves single-particle cryo-EM reconstruction. *Nat. Methods* **17**, 1214–1221 (2020). doi:10.1038/s41592-020-00990-8 Medline

75. I. Guyon, J. Weston, S. Barnhill, V. Vapnik, Gene Selection for Cancer Classification using Support Vector Machines. *Mach. Learn.* **46**, 389–422 (2002). doi:10.1023/A:1012487302797

76. C. Buchanan *et al*., Pathogen-sugar interactions revealed by universal saturation transfer analysis. Zenodo, doi: 10.5281/zenodo.6299883 (2022).

77. P. I. Koukos, A. M. J. J. Bonvin, Modelling of the binding of various sialic acid-containing oligosaccharides to the NTD domain of the spike protein of SARS-CoV2. Zenodo, doi: 10.5281/zenodo.4271288 (2020).

78. C. J. Buchanan, A. J. Baldwin, Universal Saturation Transfer Analysis software. Zenodo, doi: 10.5281/zenodo.6303964 (2022).

79. N. Picchiotti, E. Benetti, C. Fallerini, S. Daga, M. Baldassarri, F. Fava, K. Zguro, F. Valentino, G. Doddato, A. Giliberti, R. Tita, S. Amitrano, M. Bruttini, L. Di Sarno, D. Alaverdian, G. Beligni, M. Palmieri, S. Croci, M. Lista, I. Meloni, A. Maria Pinto, C. Gabbi, S. Ceri, A. Esposito, P. Pinoli, F. P. Crawley, E. Frullanti, F. Mari, GEN-COVID Multicenter Study, M. Gori, A. Renieri, S. Furini, Post-Mendelian genetic model in COVID-19. *Cardiol. Cardiovasc. Med.* **5**, 673–694 (2021). doi:10.26502/fccm.92920232

80. C. Fallerini, N. Picchiotti, M. Baldassarri, K. Zguro, S. Daga, F. Fava, E. Benetti, S. Amitrano, M. Bruttini, M. Palmieri, S. Croci, M. Lista, G. Beligni, F. Valentino, I. Meloni, M. Tanfoni, F. Minnai, F. Colombo, E. Cabri, M. Fratelli, C. Gabbi, S. Mantovani, E. Frullanti, M. Gori, F. P. Crawley, G. Butler-Laporte, B. Richards, H. Zeberg, M. Lipcsey, M. Hultström, K. U. Ludwig, E. C. Schulte, E. Pairo-Castineira, J. K. Baillie, A. Schmidt, R. Frithiof, WES/WGS Working Group Within the HGI, GenOMICC Consortium, GEN-COVID Multicenter Study, F. Mari, A. Renieri, S. Furini, Common, low-frequency, rare, and ultra-rare coding variants contribute to COVID-19 severity. *Hum. Genet.* **141**, 147–173 (2022). doi:10.1007/s00439-021-02397-7 Medline

81. B. E. Collins, O. Blixt, S. Han, B. Duong, H. Li, J. K. Nathan, N. Bovin, J. C. Paulson, High-affinity ligand probes of CD22 overcome the threshold set by cis ligands to allow for binding, endocytosis, and killing of B cells. *J. Immunol.* **177**, 2994–3003 (2006). doi:10.4049/jimmunol.177.5.2994 Medline

82. M. S. Sandbhor, N. Soya, A. Albohy, R. B. Zheng, J. Cartmell, D. R. Bundle, J. S. Klassen, C. W. Cairo, Substrate recognition of the membrane-associated sialidase NEU3 requires a hydrophobic aglycone. *Biochemistry* **50**, 6753–6762 (2011). doi:10.1021/bi200449j Medline

83. Z. S. Chinoy, C. Bodineau, C. Favre, K. W. Moremen, R. V. Durán, F. Friscourt, Selective Engineering of Linkage-Specific α2,6-N-Linked Sialoproteins Using Sydnone-Modified Sialic Acid Bioorthogonal Reporters. *Angew. Chem. Int. Ed.* **58**, 4281–4285 (2019). doi:10.1002/anie.201814266 Medline

84. W.-L. Chuang, H. McAllister, L. Rabenstein, Chromatographic methods for product-profile analysis and isolation of oligosaccharides produced by heparinase-catalyzed depolymerization of heparin. *J. Chromatogr. A* **932**, 65–74 (2001). doi:10.1016/S0021-9673(01)01241-9 Medline

85. A. K. Powell, Y. A. Ahmed, E. A. Yates, J. E. Turnbull, Generating heparan sulfate saccharide libraries for glycomics applications. *Nat. Protoc.* **5**, 821–833 (2010). doi:10.1038/nprot.2010.17 Medline

86. K. J. Lee, S. Mao, C. Sun, C. Gao, O. Blixt, S. Arrues, L. G. Hom, G. F. Kaufmann, T. Z. Hoffman, A. R. Coyle, J. Paulson, B. Felding-Habermann, K. D. Janda, Phage-display selection of a human single-chain fv antibody highly specific for melanoma and breast cancer cells using a chemoenzymatically synthesized G(M3)-carbohydrate antigen. *J. Am. Chem. Soc.* **124**, 12439–12446 (2002). doi:10.1021/ja020737j Medline

87. Yissum Research Development Company of the Hebrew University of Jerusalem, patent application WO 2017/141251 A1 (2017).

88. S. R. Alexander, A. J. Fairbanks, Direct aqueous synthesis of cyanomethyl thioglycosides from reducing sugars; ready access to reagents for protein glycosylation. *Org. Biomol. Chem.* **14**, 6679–6682 (2016). doi:10.1039/C6OB01069E Medline

89. R. Huang, A. Bonnichon, T. D. W. Claridge, I. K. H. Leung, Protein-ligand binding affinity determination by the waterLOGSY method: An optimised approach considering ligand rebinding. *Sci. Rep.* **7**, 43727 (2017). doi:10.1038/srep43727 Medline

90. A. J. Baldwin, R. Bader, J. Christodoulou, C. E. MacPhee, C. M. Dobson, P. D. Barker, Cytochrome display on amyloid fibrils. *J. Am. Chem. Soc.* **128**, 2162–2163 (2006). doi:10.1021/ja0565673 Medline

91. J. A. Carver, J. A. Aquilina, R. J. W. Truscott, G. B. Ralston, Identification by 1H NMR spectroscopy of flexible C-terminal extensions in bovine lens α-crystallin. *FEBS Lett.* **311**, 143–149 (1992). doi:10.1016/0014-5793(92)81386-Z Medline

92. S.-T. D. Hsu, P. Fucini, L. D. Cabrita, H. Launay, C. M. Dobson, J. Christodoulou, Structure and dynamics of a ribosome-bound nascent chain by NMR spectroscopy. *Proc. Natl. Acad. Sci. U.S.A.* **104**, 16516–16521 (2007). doi:10.1073/pnas.0704664104 Medline

93. P. Allard, M. Helgstrand, T. Härd, The complete homogeneous master equation for a heteronuclear two-spin system in the basis of cartesian product operators. *J. Magn. Reson.* **134**, 7–16 (1998). doi:10.1006/jmre.1998.1509 Medline

94. W. H. Richardson, Bayesian-Based Iterative Method of Image Restoration. *J. Opt. Soc. Am.* **62**, 55–59 (1972). doi:10.1364/JOSA.62.000055

95. L. B. Lucy, An iterative technique for the rectification of observed distributions. *Astron. J.* **79**, 745 (1974). doi:10.1086/111605

96. S. J. Bergeron, I. D. Henry, R. E. Santini, A. Aghdasi, D. Raftery, Saturation transfer double-difference NMR spectroscopy using a dual solenoid microcoil difference probe. *Magn. Reson. Chem.* **46**, 925–929 (2008). doi:10.1002/mrc.2275 Medline

97. C. A. Lepre, J. M. Moore, J. W. Peng, Theory and applications of NMR-based screening in pharmaceutical research. *Chem. Rev.* **104**, 3641–3676 (2004). doi:10.1021/cr030409h Medline

98. A. Viegas, J. Manso, F. L. Nobrega, E. J. Cabrita, Saturation-Transfer Difference (STD) NMR: A Simple and Fast Method for Ligand Screening and Characterization of Protein Binding. *J. Chem. Educ.* **88**, 990–994 (2011). doi:10.1021/ed101169t

99. A. Abragam, *The Principles of Nuclear Magnetism* (Clarendon, 1961).

100. J. R. Taylor, *Introduction To Error Analysis: The Study of Uncertainties in Physical Measurements* (University Science, 1997).

101. R. Warshamanage, K. Yamashita, G. N. Murshudov, EMDA: A Python package for Electron Microscopy Data Analysis. *J. Struct. Biol.* **214**, 107826 (2022). doi:10.1016/j.jsb.2021.107826 Medline

102. S. Bangaru, G. Ozorowski, H. L. Turner, A. Antanasijevic, D. Huang, X. Wang, J. L. Torres, J. K. Diedrich, J.-H. Tian, A. D. Portnoff, N. Patel, M. J. Massare, J. R. Yates 3rd, D. Nemazee, J. C. Paulson, G. Glenn, G. Smith, A. B. Ward, Structural analysis of full-length SARS-CoV-2 spike protein from an advanced vaccine candidate. *Science* **370**, 1089–1094 (2020). doi:10.1126/science.abe1502 Medline